Summer 2017

Geology and Geochemistry of the Uvas Volcanic Field and Rubio Peak Formation of South-Central New Mexico, USA

Max Logan Hoffman
Missouri State University, Max1991@live.missouristate.edu

GEOLOGY AND GEOCHEMISTRY OF THE UVAS VOLCANIC FIELD AND RUBIO PEAK FORMATION OF SOUTH-CENTRAL NEW MEXICO, USA

A Masters Thesis

Presented to

The Graduate College of

Missouri State University

In Partial Fulfillment

Of the Requirements for the Degree

Masters of Science, Geospatial Sciences in Geography, Geology, and Planning

By

Max Logan Hoffman

August 2017

GEOLOGY AND GEOCHEMISTRY OF THE UVAS VOLCANIC FIELD AND RUBIO PEAK FORMATION OF SOUTH-CENTRAL NEW MEXICO, USA

Geology, Geography, and Planning

Missouri State University, August 2017

Master of Science

Max Logan Hoffman

ABSTRACT

South-central New Mexico is characterized by many Cenozoic volcanic and tectonic events that produced a complex system of magma sources. These mechanisms are responsible for the diverse volcanic activity and magmatic evolution in New Mexico. To understand the growth and development of the mantle sources associated with these events, geochemical, petrographic, structural and spatial distribution data were collected from the Uvas volcanic field (UVF) and the Rubio Peak Formation of the Mogollon-Datil volcanic field (MDVF). Volcanic rocks from these volcanic fields were chosen based on their importance to relative timing of magmatic and tectonic transitioning events. The structural and spatial data from the UVF infer that magma migration relied on tensional fractures trending NW/SE, to progressively become magma-feed fractures. The emplacement of these dikes are explained by the mechanism of stretching, allowing discontinuous echelon dike segments to cross-cut adjacent to the extensional stress. The relationships and differences of UVF and MDVF magma sources are explained by the combination of geochemical and petrologic data. Results from oxygen isotope and radiogenic ratios suggest the UVF volcanic rocks are heavily contaminated by high and low $\delta^{18}O$ values, while Rubio Peak rocks reflect a homogenous mantle source relative to the differential mantle array.

KEYWORDS: basaltic andesites, geochemistry, magma-feed fractures, New Mexico, spatial analyst, Uvas Volcanic Field

This abstract is approved as to form and content

_____

Gary S. Michelfelder
Chairperson, Advisory Committee
Missouri State University

GEOLOGY AND GEOCEHMISTRY OF THE UVAS VOLCANIC FIELD AND RUBIO PEAK FORMATION OF SOUTH-CENTRAL NEW MEXICO, USA

By

Max Logan Hoffman

A Masters Thesis
Submitted to the Graduate College
Of Missouri State University
In Partial Fulfillment of the Requirements
For the Degree of Master of Science, Masters of Science, Geospatial Sciences in Geography, Geology, and Planning

August 2017

Approved:

_____
Gary S. Michelfelder, PhD

_____
Kevin L. Mickus, PhD

_____
Xin Miao, PhD

_____
Julie Masterson, PhD: Dean, Graduate College

ACKNOWLEDGEMENTS

I would like to thank the people involved in this research project for their help and their support. First, I would like to thank my committee members Dr. Gary Michelfelder (Chairperson), Dr. Kevin Mickus, and Dr. Xin Miao for their leadership and support in developing and completion of this project. A much deserved thanks to Emily Salings, Shannon Rentz, Grant Spoering, Amber Akers, and Brandie Oehring, whom helped with in the field and laboratory. Special thanks is much appreciated from Dr. Peter Larson of Washington State University and Dr. Frank Ramos of New Mexico State University their professional analytical and laboratory assistance.

I would like to thank the Graduate College of Missouri State University for their funding assistance to help cover the cost of travel, field work, laboratory test, and attend professional conferences. I would also like to thank the Department of Geography, Geology, and Planning and the College of Natural and Applied Sciences for providing the analytical software and tools necessary to produce the results of this research. A final thanks goes out to all of my family and friends who provided the encouragement to help me through this journey.

TABLE OF CONTENTS

TABLE OF CONTENTS (CONTINUED)

LIST OF TABLES

LIST OF FIGURES

LIST OF FIGURES (CONTINUED)

CHAPTER 1 - INTRODUCTION

The wide distribution of volcanism, shifting tectonics, and evolving magma sources in New Mexico has made it a popular region of interest for understanding complex changes and development of both heterogeneous and homogenous igneous systems (Johnson et al., 1990; Mack, 2004; Ramos and Reid, 2005; Annen et al., 2006; Best et al., 2016). Previous studies (Dungan et al., 1986; Perry et al., 1987; Duncker et al., 1991; McMillan et al., 2000) have described the geologic record in southern New Mexico and have determined implications of three mantle sources associated with these igneous systems: lithosphere, asthenosphere, and ocean-island basalts (OIB). Though previous research has distinguished these mantle sources to local volcanic fields, there is uncertainty understanding the evolving magmatic processes and implications of crustal contamination without constraining the assimilating factors.

The objective of this project is to characterize the petrogenesis and magmatic evolution of the Sierra de las Uvas volcanic field (UVF) and the Rubio Peak formation of the Mogollon-Datil volcanic field (MDVF) in southern New Mexico (Fig. 1.1). The following chapters examine geochemical, petrographic, structural, and geomorphologic data associated with the UVF and the Rubio Peak formation of the MDVF to examine the magmatic implications involved with these extrusive records of magmatism during two time periods of tectonic transition: (1) continental arc magmatism and (2) early Rio Grande rifting. The specific goals of this project address three questions: (1) What are the primary sources of magma associated with the Uvas basaltic andesites and the intermediate composition rocks of the Rubio Peak Formation? (2) What are the processes

involved in the differentiation of these magmas? (3) What does the magmatic plumbing system look like and is there a structural control on the magma reservoir feeding the Uvas Volcanic Field cinder cones?

This study examines the deep magma genesis of the Rubio Peak formation and Uvas lavas in addition to understand the magmatic implications of a shallow crustal environment on controlling magma compositions during changes in the tectonic regime. The question of understanding the shallow magmatic plumbing system can help understand the deep magmatic reservoir. The relationships between shallow and deep magmatic reservoir growth and development is vital to understanding the tectonic implications that cause the immense calc-alkaline volcanism in south-central New Mexico (45-24 Ma; McMillan et al., 2000).

Manuscript 1

The first manuscript titled "Structural and surface analysis of the Sierra de las Uvas volcanic field, New Mexico: Implications for magma migration" has recently been submitted to the Bulletin of Volcanology and awaits comments from the reviewers. This manuscript presents a study using publicly available geospatial and remote sensing data and geometric classifications to provide insight on the magma migration pathways in the UVF. The manuscript seeks to determine if structural controls and geomorphic analyses suggest a relationship to the known tectonic and volcanic history in the area.

The goal of this manuscript was to look at a poorly studied volcanic field and determine the evolution of this volcanic field. This manuscript uses geospatial and remote sensing analyses to identify known and unknown volcanic centers and structures of the

UVF and determine controlling structural trends. The analytical procedure includes using sets of spatial analyst and data management tools to provide statistical and surface results on the UVF and its structures. These were comprised of creating geologic maps, identifying known and suggested volcanic centers, creating drainage networks and rose diagrams of faults and dikes, cone analyses, and relating information to suggested magmatic implications. These methods correlate to similar research (Adlyaman et al., 1998; Corazzato and Tibaldi, 2006; Grosse et al., 2012; Bolós et al., 2014; Muirhead et al., 2016) in which determined the relationships between volcanic structures and patterns. In this study, I propose three research questions: (1) Through remote sensing and geospatial analyses, can volcanic centers and distribution be characterized? (2) Is there a dominant trending relationship between faults and volcanic centers? (3) Through structural and spatial analyses, can the trend of magma feed structures in the shallow crust be determined?

Manuscript 2

The second manuscript "Oxygen Isotopes and Geochemistry of Volcanic Rocks in South-Central New Mexico: Insight on Crustal Contamination and Magmatic Evolution", is undergoing completion and will be submitted to the Journal of Petrology. This manuscript presents a study that used whole-rock and mineral separate geochemical analyses combined petrological, and stratigraphic analysis of the UVF and the Rubio Peak Formation of the MDVF. This study examined the effects of crustal contaminants on primary magmas in south-central New Mexico. Particularly, the study focused on basalt and basaltic andesites from the UVF and the Rubio Peak Formation of the MDVF

(Fig. 1.1). The goal of this study was to determine quantitatively the amount of crustal contamination in magmas through time by single crystal and whole rock analyses.

Oxygen isotope analyses were compared with former published (McMillan et al., 2000) and new radiogenic isotope data. These analyses were performed on phenocryst separates from obtained rock samples to look at individual phase $^{18}\delta O$ variations. Careful interpretation of oxygen isotope analyses of individual phases were important in this study to distinguish differences between fractional crystallization and partial melting/assimilation processes within open crustal magmatic systems (Feeley et al., 1995; Feeley et al., 2008; Bohrson and Spera, 2001). Although radiogenic isotope signatures are helpful in identifying mantle sources compositions and crustal components, these isotopic signatures and exchanged in magmatic processes between sources and crustal contaminants during crustal hybridization (Bohrson and Spera, 2001; Dufek & Bergantz, 2005; Annen et al., 2006; Feeley et al., 2008; France et al., 2016). Oxygen isotopes however, are indicative products of their source and do not interchange between sources, allowing them to quantitatively describe the evolution of these magmas (Feeley and Sharp, 1995; Eiler 2001; Bindeman, 2008). Therefore, interpreting radiogenic isotopes with oxygen isotope data provide a better understanding between the associated magma source and crustal contaminants. (Freund et al., 2013; Loewen and Bindeman, 2016; Underwood and Clynne, 2017). Oxygen isotope analyses of mineral separates with radiogenic isotopes were used to address three proposed questions: (1) What are the magmatic sources in southern New Mexico and how did these sources change with time? (2) Through detailed oxygen isotope analysis, can a source or contaminant be determined

to see how it has changed at the local scale? (3) Can the effect of crustal contamination on magmatism and volcanism in southern New Mexico be determined?

References

Adıyaman, O., Chorowicz J., and Köse, O., 1998, Relationships between volcanic patterns and neotectonics in Eastern Anatolia analysis of satellite images and DEM: Journal of Volcanology Geothermal Research. v. 85, p.17–32.

Annen, C., Blundy, J and Sparks, R., 2006, The genesis of intermediate and silicic magmas in deep crustal hot zones: Journal of Petrology, v. 47, p. 505-539.

Best, G. M, Christiansen, E.H., de Silva, S., and Lipman, P. L., 2016, Slab-rollback ignimbrite flareups in the southern Great Basin and other Cenozoic American arcs: A distinct style of arc volcanism: Geological Society of America, v. 12, p. 1097-1135, doi: 10.1130/GES01285.1.

Bindeman, I., 2008, Oxygen isotope in mantle and crustal magmas as revealed by single crystal analysis: Mineralogical Society of America, v. 69, p. 445-478, doi:10.2138/rmg.2008.69.12.

Bohrson, W. A. & Spera, F. J., 2001, Energy-constrained open-system magmatic processes II: application of energy-constrained assimilation–fractional crystallization (EC-AFC) model to magmatic systems: Journal of Petrology, v.42, p. 1019–1041.

Bolós, X., Barde-Cabusson, S., Pedrazzi, D., Martí, J., Casas, A., Lovera, R., and Nadal-Sala, D., 2014, Geophysical exploration on the subsurface geology of La Garrotxa monogenetic volcanic field (NE Iberian Peninsula): International Journal Earth Science (Geol Rundsch). doi:10.1007/s005531-014-1044-3.

Corazzato, C., and Tibaldi, A., 2006, Fracture control on type, morphology and distribution of parasitic volcanic cones: An example from Mt. Etna, Italy: Journal of Volcanology and Geothermal Research, v. 158, p. 177-194. doi: 10.1016/j.volgeores.2006.04.018.

Dufek, J. and Bergantz, G.W., 2005, Lower crustal magma genesis and preservation: A stochastic framework for the evaluation of basalt–crust interaction: Journal of Petrology, v. 46, p. 2167-2195, doi: https://doi.org/10.1093/petrology/egi049.

Duncker, K. E., Wolff, J. A., Harmon, S. R., Leat, P. T., Dickin, A. P., and Thompson, R. N., 1991, Diverse mantle and crustal components in lavas of the NW Cerros del Rio volcanic field, Rio Grande Rift, New Mexico: Contributions to Mineralogy and Petrology, v. 108, p. 331-345. doi:10.1007/BF00285941.

Dungan, M.A., Lindstrom, M.M., McMillan, N.J., Moorbath, S., Hoefs, J., and Haskin, L.A., 1986, Open system magmatic evolution of the Taos Plateau volcanic field, northern New Mexico: 1, The petrology and geochemistry of the Servilleta Basalt: Journal of Geophysical Research, v. 91, p. 5999–6028.

Eiler, J.M., 2001, Oxygen Isotope Variations of Basaltic Lavas and Upper Mantle Rocks: Reviews in Mineralogy and Geochemistry, v. 43, p. 319-364, doi: 10.2138/gsrmg.43.1.319.

Feeley, T.C., and Sharp, Z.D., 1995, 18O/16O isotope geochemistry of silicic lava flows erupted from Volcan Ollagüe, Andean Central Volcanic Zone: Earth and Planetary Science Letters, v. 133, p. 239-254.

Feeley, T.C., Clynne, M.A., Winer, G.S., and Grice W.C., 2008, Oxygen isotope geochemistry of the Lassen Volcanic Center, California: Resolving crustal and mantle contributions to continental arc magmatism: Journal of Petrology, v. 49, p. 971-997.

France, L., Demacon, M., Gurenko, A.A., and Briot, D., 2016, Oxygen isotopes reveal crustal contamination and a large, still partially molten magma chamber in Chaîne des Puys (French Massif Central): Lithos, v. 260 p. 328-338.

Freund S. Beier C. Krumm S. Haase K. M., 2013, Oxygen isotope evidence for the formation of andesitic–dacitic magmas from the fast-spreading Pacific–Antarctic Rise by assimilation–fractional crystallization: Chemical Geology, v. 347, p. 271–283.

Grosse, P. B., Van Wyk de Vries, Euillades, P. A., Kervyn, M., and Petrinovic, I. A., 2012, Systematic morphometric characterization of volcanic edifices using digital elevation models: Geomorphology, v. 136, p.114–131, doi:10.1016/j.geomorph.2011.06.001.

Johnson, C.M., Lipman, P.W., and Czamanske, G.K., 1990, H, O, Sr, Nd, and Pb isotope geochemistry of the Latir volcanic field and cogenetic intrusion, New Mexico, and relations between evolution of a continental magmatic center and modifications of the lithosphere: Contributions to Mineralogy and Petrology, v. 104, p. 99–124, doi:10.1007/BF00310649.

Loewen, M.W., Bindeman, I.N., 2016. Oxygen isotope thermometry reveals high magmatic temperatures and short residence times in Yellowstone and other hot-dry rhyolites compared to cold-wet systems: American Mineralogist, v. 101, p. 1222-1227, doi: 10.2138/am-2016-5591.

Mack, G.H., 2004, Middle and late Cenozoic crustal extension, sedimentation, and volcanism in the southern Rio Grande rift, Basin and Range, and southern Transition Zone of southwestern New Mexico, in Mack G.H and Giles, K.A., eds, The Geology of New Mexico: A Geologic History. New Mexico Geological Society, Special Publication v. 11, p. 389-406.

McMillan, N.J., Dickin, A.P., and Haag, D., 2000, Evolution of magma source regions in the Rio Grande rift, southern New Mexico: Geological Society of America Bulletin, v. 112, p. 1582-1593.

Muirhead J.D., Van Eaton, A.R., Re G., White, J.D.L., Ort, M.H., 2016, Monogenetic volcanoes fed by interconnected dikes and sills in the Hopi Buttes volcanic field, Navajo Nation, USA: Bulletin of Volcanology v. 78, p. 1-16.

Perry, F.V., Baldridge, W.S., and Depaolo, D.J., 1987, Role of asthenosphere and lithosphere in the genesis of Late Cenozoic basaltic rocks from the Rio Grande Rift and adjacent regions of the southwestern United States: Journal of Geophysical Research v. 92 p. 9193-9213, doi:10.1029/JB092iB09p09193.

Ramos, F.C., and Reid, M.R., 2005, Distinguishing melting of heterogeneous mantle sources from crustal contamination: Insights from Sr isotopes at the phenocryst scale, Pisgah Crater, California: Journal of Petrology v. 46, p. 999-1012, https://doi.org/10.1093/petrology/egi008.

Underwood, S.J. and Clynne, M.A., 2017, Oxygen isotope geochemistry of mafic phenocrysts in primitive mafic lavas from the southernmost Cascade Range, California: Mineralogical Society of America, v. 102, p.252-261. doi: https://doi.org/10.2138/am-2017-5588.

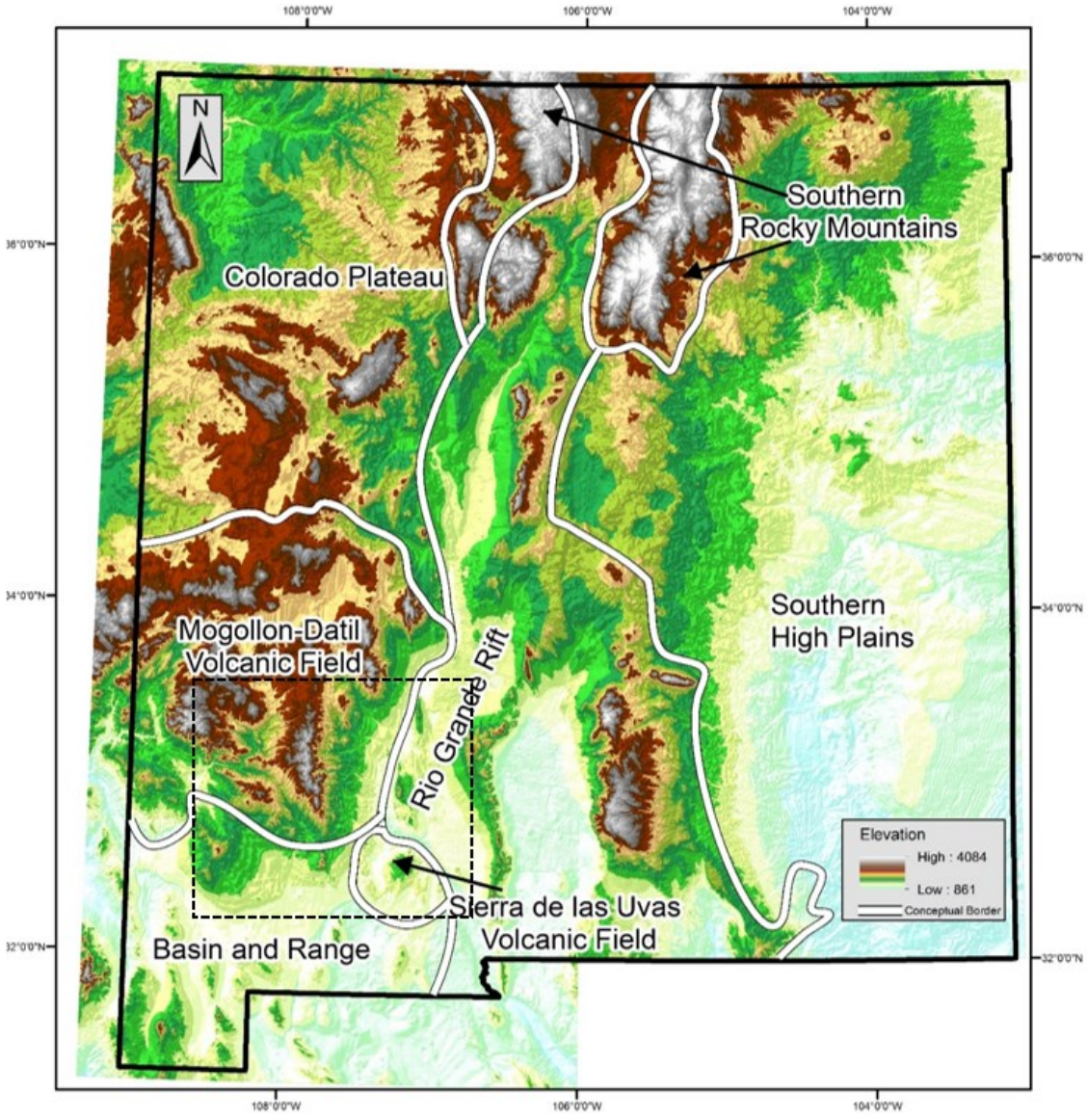

Figure 1.1: Digital Elevation Model (DEM) of New Mexico. Significant physiographic provinces are outlined to show boundaries of landforms and tectonic regimes. These provinces include: Southern Rocky Mountains (1.6-1.7 Ga), Colorado Plateau (1.6 Ga), Southern High Plains, Rio Grande Rift, Basin and Range (17 Ma), MDVF (40-24 Ma), and UVF (28-24 Ma). The study area consists of the UVF and the southern half of the MDVF.

CHAPTER 2 - BACKGROUND GEOLOGY OF SOUTH-CENTRAL NEW MEXICO

South-central New Mexico is characterized by numerous Cenozoic tectonic events that produced a complex system of magmatic sources and crustal contaminates responsible for diverse magma compositions associated with volcanic activity throughout New Mexico (McIntosh, 1989; Cather 1990; Chapin et al., 2004; Mack et al., 2004; Annen et al., 2006; Best et al., 2016). The dominant phase of magmatism is associated with the development of continental arc (45-36 Ma) related to the subduction of the Farallon Plate, followed by an ignimbrite flare-up between 36-28 Ma (Davis et al., 1993; Lipman and Bachmann, 2015; Best et al., 2016). Around 36 Ma, slab rollback/slab break-off allowed inflow of asthenospheric mantle, changing the style of volcanism from intermediate magmatism to bimodal magma (Davis and Hawkesworth 1994; 1995; Chapin et al., 2004). Geochemical and isotopic signatures of volcanic rocks from this period suggest crustal modification and hybridization by mafic magmas derived from the subduction of the Farallon Plate; shifting mantle source from a subduction-modified lithospheric mantle signature between 45-28 Ma to a more enriched or OIB-like mantle signature around 28 Ma (Livaccari and Perry, 1993; Chapin et al,. 2004). Continental basalts and andesites derived with lithospheric mantle signatures are interpreted to have low concentrations of Nb and Ta and high concentrations of Ba, Sr, Rb and low and variable ε_{Nd} values (+2 to -8) compared to ocean island basalts (OIB) sources (Fitton et al., 1991; Kempton et al., 1991). However, asthenospheric signatures from some upper Cenozoic basalts in the area suggest they are products from partial melting within the

upwelling and decompressing asthenosphere (Fitton et al., 1991; McMillan et al., 2000). These asthenospheric magmas have high Nb and Ta concentrations and ε_{Nd} values between +7 and +4, which are similar to concentrations and isotope ratios of other North American OIBs (McMillan et al., 2000). The question of magmatic development through a period of tectonic transition is important in understanding the magma genesis of the area.

Rubio Peak Formation

The Rubio Peak Formation (Eocene, 46.3 ± 0.3 to 37.6 ± 2 Ma; McMillan et al., 2000) is found throughout southern New Mexico (Fig. 2.1). This formation is a thick sequence of basalt to dacite lava flows, interbedded volcaniclastic sediments, and small volume ash flows (Clemons, 1982). This calc-alkaline volcanic suite predominantly consist of plagioclase and hornblende bearing andesites. (58-62% SiO_2; 1982; Davis et al., 1993; Davis and Hawkesworth 1994; 1995; McMillan, 1998; McMillan et al., 2000). Thickness of the unit varies from less than a 100 m to around 900 m but is suggested by Seager (1975) to be around 1980 m at the type section near the town of Deming, New Mexico. The Rubio Peak Fm. along with the Palm Park Fm., and the Orejon andesites are correlated with the construction of Eocene composite cones in the region (McMillan et al., 2000). Evidence of "arc-like" geochemical signatures in Rubio Peak rocks suggest this unit represents a lithospheric mantle source from the Laramide continental arc magmatism in New Mexico (Davis et al., 1993; Davis and Hawkesworth, 1994, 1995; McMillan et al., 2000; Chapin et al., 2004).

Uvas Basalt-Basaltic Andesites

The Uvas Basalts (Oligocene, 28-24 Ma) of the UVF, located northwest of Las Cruces near the town of Hatch. The lavas from the Uvas volcanic field are calc-alkalic (moderate to high K_2O) basaltic andesites, andesites, and tholeiitic basalts (Seager and Cleamons, 1975). These greyish black lavas have a fine to coarse scoracious texture with basal flows being heavily abundant in calcite and quartz amygdules. Uvas basaltic andesites and andesites predominately consist of hornblende and plagioclase phenocryst with occasional pyroxene and olivine. Geophysical characteristics of these lavas suggest that this volcanic suite was derived from the heating of the lithosphere from convecting asthenosphere (Davis et al., 1993; Davis and Hawkesworth, 1994). These characteristics are based on similar major and trace element data, $^{87}Sr/^{86}Sr$ (0.704404 to 0.707085) ratios, and ε_{Nd} (-4.5 to 0.8), that correlate with the Rubio Peak Formation and Bell Top Formation (McMillan et al., 2000). It is suggested that these volcanic rocks erupted during extension and that the subduction-modified lithospheric mantle was melting during the earliest period of Rio Grande rifting (McMillan et al., 2000).

References

Annen, C., Blundy, J and Sparks, R., 2006, The genesis of intermediate and silicic magmas in deep crustal hot zones: Journal of Petrology, v. 47, p. 505-539.

Best, G.M., Christiansen, E.H., de Silva, S., and Lipman, P. L., 2016, Slab-rollback ignimbrite flare-ups in the southern Great Basin and other Cenozoic American arcs: A distinct style of arc volcanism: Geological Society of America, v. 12, p. 1097-1135, doi: 10.1130/GES01285.1.

Cather, S.M., 1990. Stress and volcanism in the northern Mogollon-Datil volcanic field, New Mexico: Effects of post-Laramide tectonic transition: Geological Society of America Bulletin, v. 102, p. 1447–1458.

Chapin, C.E., McIntosh, W. C., and Chamberlin, R. M., 2004, The late Eocene-Oligocene peak of Cenozoic volcanism in southwestern New Mexico, in Mack, G. H., and Giles, K. A., eds., The geology of New Mexico: A geologic history: New Mexico Geological Society Special Publication, v. 11, p. 271-293.

Clemons, R.E., 1982, Geology of Massacre Peak quadrangle, Luna County, New Mexico: New Mexico Bureau of Mines and Mineral Resources, Geologic Map 51, scale 1:24,000.

Davis, J.M., Elston, W.E., and Hawkesworth, C.J., 1993, Basic and intermediate volcanism of the Mogollon-Datil volcanic field: Implications for mid-Tertiary tectonic transitions in southwestern New Mexico, USA: , in Prichard, H.M., Alabaster, T., Harris, N.B.W., and Neary C. R., eds., Magmatic processes and plate tectonics: Geological Society [London] Special Publication, v. 76, p. 469-488.

Davis, J.M., and C.J., Hawkesworth, 1994, Early calc-alkaline magmatism in the Mogollon-Datil Volcanic Field, New Mexico, USA: Journal of the Geological Society, v. 151 p. 825-843.

Davis, J.M., and C.J., Hawkesworth, 1995, Geochemical and tectonic transitions in the evolution of the Mogollon-Datil Volcanic Field, New-Mexico, USA: Chemical Geology, v. 119, p. 31-53.

Fitton, J.G., and James, D., 1991, Basic magmatism associated with late Cenozoic extension in the western United States: Compositional variations in space and time: Journal of Geophysical Research, v. 96, p. 693-711.

Kempton, P.D., Fitton, J.D., Hawkesworth, C.J., and Ormerod, D.S., 1991, Isotopic and trace element constraints on the composition and evolution of the lithosphere beneath the southwestern United States: Journal of Geophysical Research, v. 96, p. 13713–13735.

Lipman, P.W., and Bachmann, O., 2015, Ignimbrites to batholiths: Integrating perspectives from geological, geophysical, and geochronological data: Geosphere, v. 11, p. 705–743.

Livaccari, R.F., and Perry, F.V., 1993, Isotopic evidence for preservation of Cordilleran lithospheric mantle during the Sevier-Laramide orogeny, western United States: Geology, v. 21, p. 719–722.

Mack, G.H., 2004, Middle and late Cenozoic crustal extension, sedimentation, and volcanism in the southern Rio Grande rift, Basin and Range, and southern Transition Zone of southwestern New Mexico, in Mack G.H and Giles, K.A., eds, The Geology of New Mexico: A Geologic History: New Mexico Geological Society, Special Publication v. 11, p. 389-406.

McIntosh, W.C., 1989, Timing and distribution of ignimbrite volcanism in the Eocene–Miocene Mogollon-Datil volcanic field, in Chapin, C.E., and Zidek, J., eds., Eocene–Miocene Mogollon-Datil volcanic field, New Mexico, Excursion 6A: IAVCEI Field Excursions, New Mexico Bureau of Mines and Mineral Resources, Memoir v. 46, p. 58-59.

McMillan, N., 1998, Temporal and spatial magmatic evolution of the Rio Grande rift: New Mexico Geological Society Guidebook, v. 49, p. 107-116.

McMillan, N.J., Dickin, A.P., and Haag, D., 2000, Evolution of magma source regions in the Rio Grande rift, southern New Mexico: Geological Society of America Bulletin, v. 112, p. 1582-1593.

Seager, W.R., 1975, Cenozoic tectonic evolution of the Las Cruces area, New Mexico: New Mexico Geological Society 26th Annual Fall Field Conference Guidebook, v. 26, p. 241-250.

Seager, W.R., and Clemons, R.E., 1975, Middle to late Tertiary geology of the Cedar Hills–Selden Hills area, New Mexico: New Mexico Bureau of Mines and Mineral Resources Circular, v. 133, p. 1-24

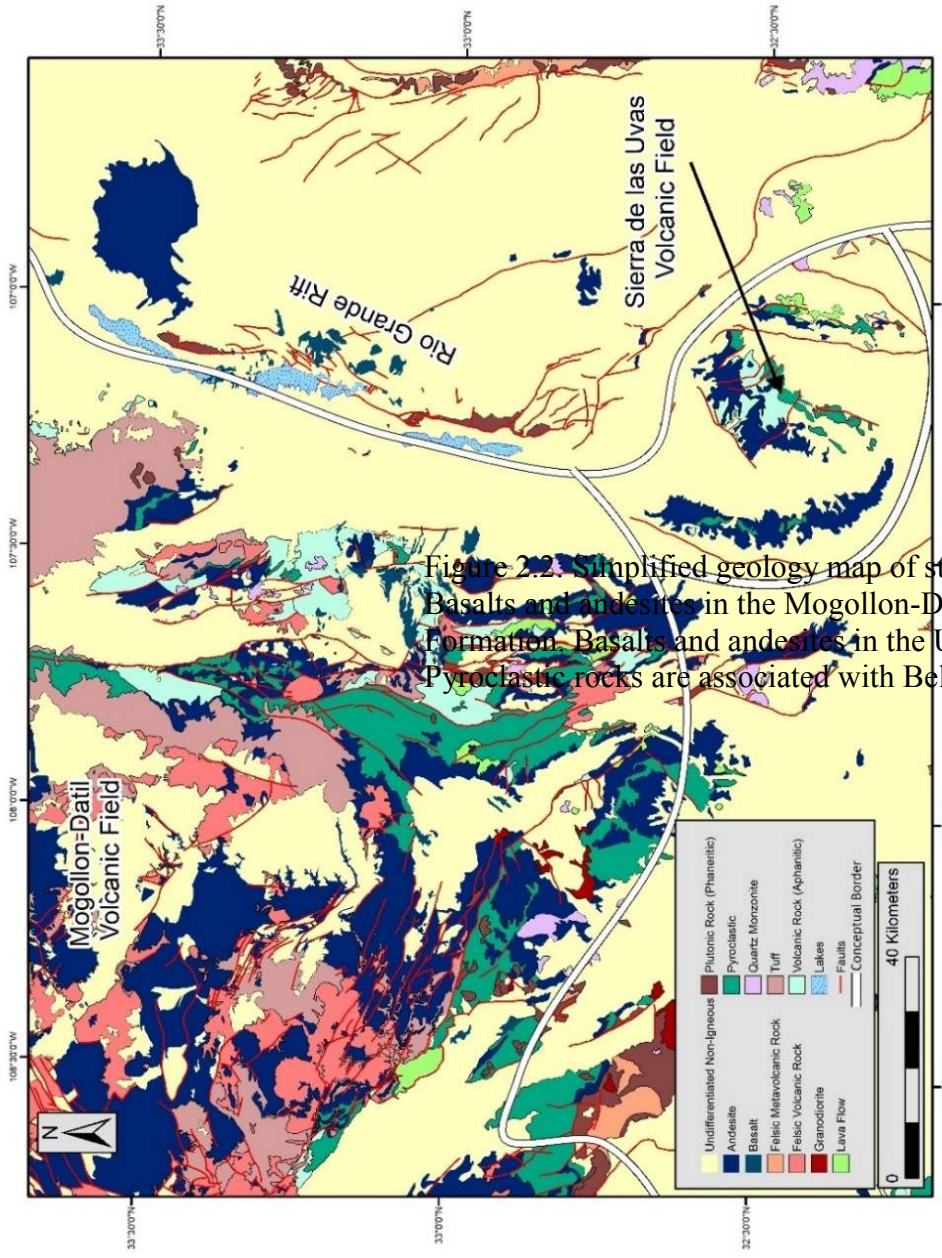

Figure 2.2. Simplified geology map of study area in southern New Me
Basalts and andesites in the Mogollon-Datil Field and associated with
Formation. Basalts and andesites in the UVF are associated with the U
Pyroclastic rocks are associated with Bell Top aged units.

CHAPTER 3 - METHODS

In order to address the questions discussed above in both manuscript chapters this study includes a combination of geochemical, petrographic, and structural data and geospatial analyses to characterize the magma plumbing system associated with the UVF and the Rubio Peak Formation of the MDVF. These data are combined with existing major and trace element data and radiogenic isotope data from McMillan et al., (2000).

Oxygen Isotope Geochemistry

In order to better understand the magmatic processes and crustal contamination brought into the primary mantle sources, it is critical to differentiate between the sources and the consisting mineral phases. Discriminating between mantle and crustal sources can be often difficult due to small isotope fractionations at high temperatures, but high precision of oxygen isotope analysis is helpful in this discrimination and understanding magma genesis and evolution. (Bindeman, 2008). Oxygen isotope geochemistry is also utilized in environments where low-temperature weathering and water-rock interactions with crustal rock sources that make their isotopic fractions strongly vary from mantle source rocks that have continuously resided in the mantle with same oxygen signature over time (Eiler, 2001).

Advantages of oxygen isotopes include but are not limited to: (1) help constrain the roles of magma sources based off of the homogeneity of primary mantle-derived basalts (5.7 ± 0.2‰), (2) relative to mantle sources, enriched or depleted $\delta^{18}O$ crustal rocks are independent of age, (3) small isotopic fractionations exist between silicate

minerals and melt at high temperatures, (4) mass balancing allows for simplification and discrimination between rock types and magmatic sources (5) mineral phases containing oxygen in their chemical structure may be used for analyses, and (6) single-crystal oxygen isotope analysis provides more precision than whole-rock and allows individual phase fractionations to be observed (Bindeman, 2008; Feeley et al., 2008). From these advantages, insight on crustal and mantle basalt interaction at subducted levels can be observed looking at contaminants from the lithosphere. Although oxygen isotope studies have been performed for over half a century, much of the former analyses focused on whole rock analysis and lacked in single crystal precision (Bindeman, 2008).

Geospatial Structural and Volcanic Analysis

The characterization of the volcanic centers and cones in the UVF was implemented using geospatial information science (GIS) software, ArcMap 10.4.1, in combination with remote-sensed imagery and new and prior geologic information. Structural and surface analyses were performed on the study area using spatial analyst tools to quantify and provide interpretations. These tools utilized include the surface, zonal, hydrology, features and raster calculator.

Hydrology tools consisting (fill, flow accumulation, and flow direction) were combined with digital elevated models (DEM) and geologic shapefiles to determine surface patterns to help interpret the development of the UVF from the geomorphic influences of weathering. Interpreted mass lava flows were outlined based on evidence from volcanic centers, geologic record, and structural patterns.

Structural analyses of the study area include a cross-section of the interpreted shallow upper crust, suggesting the magma migration and structural deformation; mapping and lineation analyses of fault and dike trends. Rose diagrams were used to represent fault and dike trends. Bonali et al. (2011), Grosse et al. (2012), Bolós et al. (2014), and Norini et al. (2015) have performed related structural analyses in published studies.

Volcanic center and cone analyses were performed in ArcMap, using spatial analyst tools to interpret the degree and style of volcanism from magma pathways. Remote-sensed images were imported from EarthExplorer's database and were used to provide sketches of volcanic centers and cones. These analyses include individual characterization of volcanic centers and cones to quantify and qualify relationships in combination with structural implications. Parameters for these eruptive points consisted of ellipticity, contour, height, and volume measurements. Contours were used to determine interpreted approximate base and summit elevations to contribute to morphometric characteristics. Adlyaman et al. (1998), Corazzato and Tibaldi (2006), and Muirhead et al. (2016) have performed related volcanic analyses in published studies.

References

Adıyaman, O., Chorowicz J., and Köse, O., 1998, Relationships between volcanic patterns and neotectonics in Eastern Anatolia analysis of satellite images and DEM: Journal of Volcanology Geothermal Research. v. 85, p.17–32.

Bindeman, I., 2008, Oxygen isotope in mantle and crustal magmas as revealed by single crystal analysis: Mineralogical Society of America, v. 69, p. 445-478, doi:10.2138/rmg.2008.69.12.

Bolós, X., Barde-Cabusson, S., Pedrazzi, D., Martí, J., Casas, A., Lovera, R., and Nadal-Sala, D., 2014, Geophysical exploration on the subsurface geology of La Garrotxa monogenetic volcanic field (NE Iberian Peninsula): International Journal Earth, v. 103, p. 2255-2269, doi:10.1007/s005531-014-1044-3.

Bonali, F.L., Corazzato, C., and Tibaldi, A., 2011, Identifying rift zones on volcanoes: An example from La Réunion Island, Indian Ocean: Bulletin of Volcanology, v. 73, p. 347–366.

Corazzato, C. and Tibaldi, A., 2006, Fracture control on type, morphology and distribution of parasitic volcanic cones: An example from Mt. Etna, Italy. Journal of Volcanology and Geothermal Research, v. 158, p. 177-194, doi: 10.1016/j.volgeores.2006.04.018.

Eiler, J.M., 2001, Oxygen Isotope Variations of Basaltic Lavas and Upper Mantle Rocks: Reviews in Mineralogy and Geochemistry, v. 43, p. 319-364, doi: 10.2138/gsrmg.43.1.319.

Feeley, T.C., Clynne, M.A., Winer, G.S., and Grice, W.C., 2008, Oxygen isotope geochemistry of the Lassen Volcanic Center, California: Resolving crustal and mantle contributions to continental arc magmatism: Journal of Petrology, v. 49, p. 971-997.

Grosse, P. B., Van Wyk de Vries, Euillades, P. A., Kervyn, M., and Petrinovic, I. A., 2012, Systematic morphometric characterization of volcanic edifices using digital elevation models: Geomorphology, v. 136, p.114–131, doi: 10.1016/j.geomorph.2011.06.001.

McMillan, N.J., Dickin, A.P., and Haag, D., 2000, Evolution of magma source regions in the Rio Grande rift, southern New Mexico: Geological Society of America Bulletin, v. 112, p. 1582-1593.

Muirhead J.D., Van Eaton A.R., Re G., White, J.D.L., Ort M.H., 2016, Monogenetic volcanoes fed by interconnected dikes and sills in the Hopi Buttes volcanic field, Navajo Nation, USA: Bulletin of Volcanology, v. 78, p. 1-16 .

Norini, G., Groppelli, G., Sulppizio, R., Nunez, G.C., and De Franco, R., 2015, Structural analysis and thermal remote sensing of the Los Humeros Volcanic Complex: Implications for volcano structure and geothermal exploration: Journal of Volcanology and Geothermal Research, v. 301 p. 221-237.

CHAPTER 4 – STRUCTURAL AND SURFACE ANALYSIS OF THE SIERRA DE LAS UVAS VOLCANIC FIELD, NEW MEXICO

Abstract

The Sierra de las Uvas volcanic field, located in south-central New Mexico, consist primarily of Oligocene lava flows known as the Uvas Basaltic Andesites (28-24Ma). These lavas successively overlay Eocene (Palm Park and Rubio Peak Formation) and early Oligocene ash-beds (Bell Top Formation). Much of the geologic mapping in this area dates back nearly half a century using traditional mapping techniques. Detailed mapping of the quadrangles provides a detailed look at the Uvas Volcanic Field, I reappraise the terrain and look at it from a statistical and quantitative characterization approach using remote-sensing imagery and surface analysis in a GIS domain (ESRI© ArcGIS 10) to look for relationships between volcanic structures and fault orientations. Using advanced imagery and geospatial tools, I illustrate the structural and spatial patterns between faults, dikes, and volcanic centers to characterize the volcanic development of the Uvas Volcanic Field. Here I see that tensional fractures of the Uvas follow along the minor domal axis of the field in a NW/SE trend, while dikes propagate in a nearly N/S trend along the major axis. Volcanic centers and cones are identified, quantified, and characterized to help understand the orientation of magma-feed fractures. Understanding these emplacements of volcanic cones and centers allows us to suggest the volcanic field growth and development was strongly influenced by NW/SE trending dikes that favored as magma conduits along the minor axis which established multiple complex eruptive centers in the central area of the Uvas Volcanic Field.

KEYWORDS*:* magma-feed fractures, remote-sensing, Sierra de Las Uvas, structural analyses, volcanic centers

Introduction

The use of remote-sensing data, geometric information and structural analyses of volcanic terrains in the past decade has shed light on buried magmatic-feed fractures, and linear trends in magmatic systems (Corazzato and Tibaldi, 2006; Muirhead et al., 2016). These methods provide insight into the spatial distribution relationships of magmatic intrusions based on the controlling stress factors in the region; ultimately demonstrating magma mobility on the surface (Adlyaman et al., 1998; Corazzato and Tibaldi 2006).

Buried magmatic plumbing systems are coincidentally the result of upwelling and propagating magma forcing its way through a rigid crustal environment. However, fractures and structural orientation plays a vital role in the rise of magma through the substrate (Corazzato and Tibaldi, 2006; Kereszturi and Németh, 2012). Interpreting these magma feed-fractures can provide information on a combination of many factors including; magmatic composition and viscosity, spatial distribution and morphology of volcanic features, and geometry of terrain (drainage networks, fault and dike orientations, structural implications).

The Sierra de las Uvas volcanic field (UVF), located in south-central New Mexico, consist of Oligocene basalt to andesite volcanic centers and lavas flows (Seager, 1975). The volcanic activity is suggested to be associated with Laramide uplift/relaxation and domal uplift of the volcanic field (Seager, 1975). A lithospheric mantle source has been identified for the supply of magmas responsible for the development of the UVF (McMillan, 1998; McMillan et al., 2000) but the distribution of volcanic centers, monogenic cones, and structural relationships are poorly understood. Understanding this distribution of volcanic cones allows the stresses and fracture orientations to be constrained to define the volcanic field development and magma-feed fractures.

Complications in determining the magmatic ascent and pathways through the subsurface in monogenetic volcanic fields is primarily due to multiple interfingered lava flows from different volcanic centers (Gürer et al., 2015). In the UVF, not only are multiple volcanic centers buried, but the number of flows and total thickness of each flow decrease radially away from the domal axi (Fig. 4.1; Clemons and Seager, 1973). To quantitatively characterize these lava flows and associated volcanic centers,

geomorphometric parameters and structural analysis can provide insight on evolving magmatic pathways (Corazzato and Tibaldi, 2006; Grosse et al., 2012;). As resolution and accuracy have increased for digital elevated models (DEM's), spatial resolution and land-surface analysis, geomorphic and volcanic hazard assessments, they have become more successful in providing detailed information on volcanic characteristics (Grosse et al., 2012). Understanding the spatial distribution of the centers and the volcanic-structural relationships, lava flow stratigraphy, and regional structural features can help discriminate the magmatic pathways and plumbing system architecture in the subsurface. In the characterization of the structural and volcanic relationship in the UVF I present three proposed questions: (1) Through a remote sensing analysis can I characterize volcanic centers and distribution? (2) Is there a dominant trending relationship between faults and volcanic centers? and (3) Through structural and spatial analysis can I determine the trends of magma feed fractures in the shallow crust?

Here I present a remote-sensing and structural analysis of the UVF in order to identify volcanic centers and stratigraphic-structural relationships within the volcanic field. I provide constraints on the volcanic-structural relationships through a combination of spatial analyst tools, stratigraphic and petrographic data, aerial photography, reflective imagery of land cover and DEM (digital elevated models). These combined methods present and interpret suspected volcanic centers, the eruptive source of lava flows, relationship between centers, and present a model for structural control over vent location and the relationship of the plumbing systems for each center.

Regional Setting

Southern New Mexico is an area of geologically complex with transitions between a variety of magmatic and crustal sources (McMillan, 1998). Much of this complexity is due to the local source variations from shifting Laramide arc magmatism (80 Ma) to Rio Grande rift extension (30 Ma; Chapin et al., 2004). Laramide magmatism and structural deformation accounts for much of the western half of New Mexico (Yonkee and Weil, 2015). In the Las Cruces area, south-central New Mexico, these Laramide structures and magmatism are represented by two volcanic phases. A late Eocene phase is represented as predominately calc-alkaline orogenic intermediate rocks (basaltic-andesites to dacites). An Oligocene phase is represented as widespread intermediate to felsic rocks with local basalts and ash-flow tuffs (Seager, 1975; McMillan et al., 2000). This large array of magmatic variations are distinguished by eruption ages and folded structures (Seager, 1975; Cather, 1990; Davis and Hawkesworth, 1994; 1995).

Volcanic rocks and centers in extensional tectonic environments are geochemically defined by upwelling asthenospheric mantle, but are defined in southern New Mexico, by lithospheric mantle and lower and upper continental crust during magma genesis, differentiation, and migration (Davis et al., 1993; Davis and Hawkesworth, 1994; 1995; McMillan, 1998). This is significant as it relates to magmatic and volcanic infrastructure, but also when defining the components of geochemical and geodynamical sources, such as varying radiogenic isotope ratios and volcanic eruptive styles. Radiogenic isotope ratios, major and trace element concentration and ratios (low Nb/Ba, Ta/Ba ratios, and ε_{Nd} values, and moderate $^{87}Sr/^{86}Sr$ ratios) presented by McMillan (1998) suggest that magmas in the UVF erupted during the initiation of

extension and are primary magmas sourced from the subduction-modified lithospheric mantle.

Uvas volcanic field. The UVF is located in south-central New Mexico, just south of the town of Hatch (Fig. 4.1). The volcanic field is expressed by a sequence of basalt-basaltic andesite lava flows and ash-flow tuffs erupted from buried Oligocene cinder (tephra) cones and vents throughout the field (Seager, 1975). Significance of this volcanic system is related to the initiation of the Rio Grande Rift and the tectonic regime shifting from subduction to extension allowing for wide spread volcanism in southern New Mexico (Seager, 1975; Davis et al., 1993; Davis and Hawkesworth, 1994; Best et al., 2016). Previous studies suggest that as the lithospheric magmatic sources were pushing through the deep Earth they had evolved over a course of time from a felsic Eocene suite to an Oligocene intermediate-mafic suite (Kempton et al., 1991; Davis and Hawkesworth, 1995; McMillan et al., 2000; Chapin et al., 2004; Mack, 2004). Volcanic rocks from the UVF are suspected to be partial mantle melts resulting from "slab-rollback" of the subduction-modified lithospheric mantle (McMillan et al., 2000). Geochemically these volcanic rocks are to be the result of early rifting (Clemons and Seager, 1973; McMillan, 1998).

Uvas basaltic andesites. The Uvas Basaltic Andesites (~28-24 Ma) are greyish-black, calc-alkaline basalt and basaltic andesite lava flows with interbedded scoria and basaltic tuff (Kottlowski, 1953b; Mack, 2004). Majority of these rocks are fine-grained hypocrystalline with a predominantly plagioclase matrix. Pyroclastic and interstitial textures are both prominent. Phenocryst phases include pyroxene and hornblende with trace amounts of olivine and iron oxides. Plagioclase compositions are mostly andesine

and are subhedral to euhedral. Plagioclase phenocryst range from 500μm to 1mm. Hornblendes are prevalent in some lavas and minor in others, with subhedral to anhedral grains ranging from approximately 10μm to 1mm. Olivine are primarily anhedral approximately 10μm to 150μm. Pyroxenes are anhedral to subhedral approximately 10μm to 0.75mm. Iron oxides are mostly anhedral and approximately 10μm to 0.5mm Most of the lava flows are typically micro-vesicular to vesicular while basal flows contain large amounts of calcite amygdules. Some of these amygdules include olivine and pyroxene grains that have been secondary replaced by calcite and quartz.

Structure. The general structural feature of the UVF is interpreted to have originally been a circular or elongated shield-like structure (Sierra de las Uvas Dome) that extended approximately 19 kilometers in length trending NE-SW and approximately 12-16 kilometers in width trending NW-SE (Clemons and Seager, 1973). A lobe of the UVF (~19 Km) extends to the southwest and curves into a northwest trending topographic high that connects with the Goodsight Mountains (Fig. 4.1 and 4.2). However, due to uplifting of the dome, prior to late Tertiary block faulting, movement along Sierra de las Uvas fault zone left the structure broken and separated (Clemons and Seager, 1973). Timing of the uplift is not clearly defined, but magmatism suggests it predates most major rift faults in the region and post-date the volcanic activity of the Uvas basaltic andesite lavas (Seager, 1975).

Faulting in the UVF suggest a complex structural array that is difficult to interpret due to the uncertainty of reactivation of faults existing prior to domal uplift. Nevertheless, the broken and bounded grabens suggest fault orientations and alignments show a northwest fault trend (Seager, 1975). Evidence of tuffaceous sandstone overlying

basaltic andesite lava flows in the moats of synclines indicate that domal uplift and moat subsidence occurred shortly after or during the Uvas volcanic activity (Seager, 1973; Cather, 1990). Seager (1975) suggested that Sierra de las Uvas dome formed from a resurgent magma, indicated by the axial graben system and geometry that relates to processes of other typical resurgent domes. It is unclear if resurgence was caused by injection of silicic magma or the presence of a stock or batholith lies below the dome (Seager, 1975). Though no clear source has been identified, aeromagnetic data correlates a circular 200 gamma low anomaly with the dome (Seager, 1975; Keller and Cather 1994a).

The Sierra de las Uvas volcanic centers were primarily erupted from local-relief vents and cinder cones (Seager, 1973). One of the largest volcanic centers, Little White Gap, in the UVF is located just north of White Gap tank (Fig. 4.3), and lies just to the north of the Big White Gap Fault. The center is encompassed with large volumes of basaltic lapilli tuff, agglomerate, and blocks ash-flow tuffs (Clemons and Seager, 1973). A second prominent volcanic center is located near Escondido Ranch, in the northeast section of the UVF. This volcanic center is recognized as an intrusive plug (approximately 1.5 km in diameter) of a dissected cinder cone that is linked with the composition of dikes that merge into basal Uvas flows (Clemons and Seager, 1973). North of this cinder marks several small dikes in a nearly N-S trending orientation. A third suspected buried vent lies near the Augustine Tanks, which has been suggested to be along the Sierra de las Uvas domal axis from the presence of course-crystalline dome-like mass of hypersthene andesite and thickening of lava flows (Clemons and Seager, 1973).

Away from the main axial trend of volcanic centers is a minor trend of Oligocene vents recognized on the eastern margin of the volcanic field in the Cedar-Hills Vent Zone (Fig. 4.1). It is interpreted that this vent zone marks a major zone of subsidence on the eastern margin regarding the volcanic activity of the Goodsight-Cedar Hills Depression (Seager et al., 1975). Here, Uvas cinder cones present along with Oligocene Bell Top group vents erupting rhyolitic ignimbrite and lava flows, and a diatreme are associated with the tuff sequence (Seager, 1975). Ring fractures enclosing pyroclastic and basaltic andesite plugs suggest the plugs were once at higher elevations and subsided into upper Bell Top Formation vents. Clemons and Seager (1973) suggest that the occurrence of vent zones are along the axial grabens and that the intrusions exploited in tensional fractures during domal uplift.

Methodology

This study uses combination statistical and quantitative characterization of volcanic centers with previous studies of the UVF (Corazzato and Tibaldi, 2006; Seager et al., 1975; Gürer et al., 2015), including geologic mapping of volcanic features and distinguishing structural profiles (Seager and Clemons, 1975). Quantitative methods include remote sensing analyses performed using a GIS domain (ESRI© ArcGIS 10.4.1) at an 1:125,000 scale and advanced image processing software (ENVI© Classic (64-bit)). These methods were used to identify and measure the volcano-structural features, such as vents, dike, eruptive fissures and faults. Publicly available Digital Elevated Models (DEM; 30x30m resolution) and aerial photographs (1:40,000) from the United States Geological Survey (USGS) Earth Explorer (107°17’0” W to 107°0’0” W and 32°37’0” N

to 32°25’0” N) database were used as base layers for analysis. Geologic maps from Clemons and Seager (1973); and Seager and Clemons (1975) were digitized, georeferenced and overlain on the DEM to support statistical analyses. Spatial references of data were projected in the datum 1984 WGS UTM zone 13N and raster cells from reflective imagery value (30x30) with 8-bit pixel depth. Regions of interest were determined by location of Uvas lavas, ash beds, and sedimentary units. These units were distinguished based on their different reflectance imagery and compared to mapped lithologic units. Due to limitations of remote sensing resolution, many of the Uvas vents could only be recognized by close proximity to the source in person to determine Uvas basaltic lapilli and cinder bed agglomerates.

The hydrology toolbox in ArcMap 10.4.1 was used to analyze drainage patterns and landforms for several major and minor flow features to determine a preferred orientation of structural features. The drainage network was composed using the series of steps: Fill tool→Flow Direction→Flow Accumulation on the DEM. Once the new surface was generated, features were identified to the best of the resolution extent; and compared to previous mapping. From the drainage network, inferred mass lava flows were determined based on orientation of unidirectional patterns.

Determining lava volumes in volcanic fields are vital in understanding volcanic development, volcanic hazards, and effusive activity (Naranjo et al., 2016). To calculate the estimated volume for the UVF cones and volcanic centers a series of steps and ArcMap tools were utilized. In ArcMap, I used spatial analyst tools: contour, extraction by mask, zonal statistics, raster calculator and the features to polygon tool from data management tools. To compute the volume of individual volcanic cones a corrected

DEM was used as a basemap and a reference plane at 1,550m above sea level for the base of the volcanic dome. This elevation is considered a rough estimate for the volcanic lava flow plane and does not refer to the lava and/or domal uplift extent. To focus on the region of interest (ROI) for elevations above the reference plane, a "Feature to Polygon" tool was utilized. This polygon was then used as a "mask" help delineate the pixels inside and outside of the ROI, ultimately allowing the integration of pixels inside the area of interest. The "Extract by Mask" tool was then applied, using the DEM as the input value and the polygon (previously created) as the mask value. Elevation values above this reference plane are then generated and represented as a new DEM (extraction) for the particular polygon. The elevation values in the DEM extraction for the ROI were converted into delta Z values to represent the actual height between the reference elevation and the surface. This was calculated in the raster calculator as: ["Extracted.file" - "reference plane elevation"], generating a DEM representing delta Z values. Next, a zonal statistics table was derived from the delta Z DEM. From this table, looking at the main feature row, the area value (247.65 Km^2) was multiplied by the mean value (515), providing an approximate volume value of 127, 292.1 Km^3 at a 1,550m elevation. This estimated UVF volume pertains to the mass within the bulk of the volcanic field, and does not reflect the volume of lava flows due to additional domal uplifted sedimentary members.

In addition to calculating the estimated volume of UVF, cinders and cones, finding the size and shape parameters have an importance in assessing the geomorphometric analysis of volcanic fields (Grosse et al., 2012). To calculate these dimensions, a series of steps were utilized to acquire certain parameters. Simply using the

measurment tool on remote sensed images and ArcMap layouts provided heights and widths (of summits and bases), ellipticity, and shape. These parameters combined allowed for the UVF and the volcanic centers to be quantified and classified to summarize their profile shape and volcanic dimensions using the guidelines of Corazzato and Tibaldi (2006). These features were then characterized in relationship to their spatial distribution from other volcanic centers and underlying fractures.

Further structural analyses included the comparison of fault and dike trend relationships transecting through the UVF study area. This procedure consisted of using geographically mapped faults and dikes from previous field mapping. Here, geologic maps from Seager and Clemons (1975) were georeferenced in ArcMap and used as a basemap. Next, a DEM of the area was overlain on this map. From here, faults and dikes were traced and azimuths were identified. Once an azimuth collection for both faults and dikes obtained, their data was formatted into rose diagrams to statistically analyze and further interpret their preferred orientation and pattern if relevant.

Results

This section presents the findings from field work, and surface and structural analysis for the study area in the UVF. Field work and volcanic stratigraphy show that lava flows in the UVF are relatively horizontal and dips < 15º except in the Cedar Hills Vent Zone where the dip angle reach 20-45º in some areas. There is an evident change in the geomorphology and drainage pattern at the flanks of the UVF in the reflectance imagery (Fig. 4.3 and 4.4) and drainage network map (Fig. 4.6). Perhaps the most obvious feature is the strong radial patterns from the fluvial system found on the eastern

half of the Sierra de las Uvas Dome. Most faults here are downthrown to the west and point towards the domal axis (Seager et al., 1975).

DEM Analysis. The DEM of the UVF shows an ideal of a typical volcanic dome with elevated highs near the center and lower elevations outward on the flanks (Fig. 4.2). This DEM outlines the topographic highs and depressions to provide reasonable candidate features for further description in the analyses (Fig. 4.2). The drainage network map calculated from the DEM and overlain on a simplified geology layer added a spatial component to show orientations and sloping directions of elevated surfaces. From this drainage network, parallel semi-unidirectional patterns and can be seen within the UVF suggesting where mass lava flows could have been produced, but still leaving their outline on the drainage network (Fig. 4.6).

In the UVF, three drainage patterns are evident from the drainage network analysis (Fig. 4.6), radial, fan, and parallel. Radial patterns reflect domal or basin features characteristics, with hydraulic flow merging into or dispersing from a central uplift or central depression. (Ritter, 2006). Fan drainage patterns are similar to radial patterns but do not exist or show complete flow direction around a feature. The parallel drainage patterns resemble steep slopes with unidirectional hydraulic flow. These stream tributaries are seen as very straight throughout decreasing vertical relief.

Mass lava flow 1 shows the most complete and evident extent of a potential lava flow (Fig. 4.6). This fan drainage network suggests volcanic intrusions propagated from the central area of the volcanic field and migrated in a northwestern direction. Mass lava flow 2 resembles a similar fan drainage network to mass lava flow 1, but extends nearly half the distance. Mass lava flow 4 and 6 show prominent radial drainage patterns from a

central uplifted elevation. While mass lava flow 4 is comparatively smaller than mass lava flow 6 it shows a much clear circular feature while mass lava flow 6 is more elongated in the NW/SE direction. Mass lava flow 3 and 4 are much more difficult to distinguish between lava flow extents and possible volcanic centers based on no major drainage patterns and eroded lava bedding planes. However, parallel drainage networks can be seen in these mass lava flows in N/S and NE/SW trends.

Structural Analysis. Structural analyses of fault and dike trends and orientations (Fig 4.5) show that patterns between the two components analyzed. A total of 31 major faults and 11 dike trends were identified in the analysis of the DEM, satellite images and geology maps. Faults follow two general trends. The first trend is at 280º NW and the second is at 0º N. Dikes follow a nearly N/S trend between 0ºN to 30ºNE (Fig. 4.5). Faults trending in this direction coincide with the direction of the minor domal axis of the volcanic field (Fig. 4.1). Dikes trending in a N/S alignment coincide with the major domal axis along the suggested major tensional fracture stress force. These alignments are indicative of structural evolution of the UVF. Although not all faults, dikes and volcanic centers are included in these analyses, an overall representation of the major components define a clear relationship and support the main structural features of the area.

Structural interpretation of the substrate by illustrative cross-section A-A' (Fig. 4.7) reflects fault orientations based upon suggested magma migration. Lavas and tuffs associated with the UVF are mostly horizontal (0-17º). Faulting in these units consist of orientations directed towards volcanic centers and dikes. Normal faults observed in the

UVF suggest a concave upward trend with increasing depth and continue as listric faults towards volcanic intrusions.

Cone Analysis. Determining suitable and identifiable volcanic cones for cone analysis was crucial to provide a representative classification for individual volcanic centers. Finding volcanic cones was determined by combination of geologic maps and remote sensing analysis. Remote sensing imagery was used to distinguish between Uvas basalt, sedimentary, and ash bed units (Fig. 4.3 and 4.4). In the false color multispectral image (Fig. 4.3), RBG bandwidths were used to distinguish the particular wavelength ranges for these three classified units. Volcanic cones were delineated based on Uvas basalt reflectance wavelength, topographic circular or ellipsoidal structures, and elevated centers. Seven cones and centers easily identified on the satellite image were selected for this analysis: Massacre Peak, Sugar Loaf Peak, Peconcillo Peak, Escondido Ranch cinder cone, Little White Gap Peak, and an unnamed cone in the southern region. Other possible cones are based on these centers. Figures 4.8 and 4.9 present these trends comparing each center's geometric dimensions.

Cone analysis for peaks and volcanic centers categorize these features based on volume, ellipticity and base width/summit width ratio. Cones and peaks in the southern portion of the study area are consistent with each other in volume, size, and ellipticity, while volcanic centers located in center of the UVF are higher and wider summits with a lesser pattern in following trends. The Escondido Ranch cinder cone and the Little White Gap cone (Fig. 4.8) have a particular distinction in the analyses that offsets them from the others analyzed cones. Both of these cones with the largest volume (approximately 0.75 Km^3 and 2.6 Km^3, respectively) developed within the center of the region of the volcanic

field. The Escondido Ranch cone is a cinder cone that appears to be dissected and has an ellipticity (1.18 θ) similar to the southern cone and the Sugar Loaf. However, what distinguishes the Escondido Ranch in the analyses, is the volume of 2.6 km^3, which is more than twice that of other cones. The Little White Gap cone is not as clear to what its geometric origin was pertained due to geomorphology, but it is evident that the ellipticity (1.84 θ) is much greater than the other UVF cones (Fig. 4.9). The Escondido Ranch and Little White Gap cones large ellipticity and volume may be explained by their emplacement and their close fractures breaching out.

Advantages and Limitations of Surface Analyses. Advantages of surface analyses chosen, provide a generalized concept for the UVF and show ideal patterns for drainage networks and fault and dike orientations. Profiles for calculated cones and volcanic centers can be determined and classified based on suggested eruption points and volcanic structures. However, detailed resolution for these centers would provide a better input on the geologic evolution between volcanic centers. Concept of surface analysis is constrained to just surficial extents versus knowing extended and bisecting magmatic migration patterns. In this, regards further geophysical assessment is needed to understand the magmatic migration through the subsurface of these eruptive vents to speculate concentrations of ascending magma.

Discussion

The following sections discuss the qualitative and quantitative characterization of identified volcanic cones in the UVF regarding their morphology and volcanic processes. I classify the cones based on size, shape, volume, base and summit widths and heights,

ellipticity, and mean slopes of volcanic cones. Structural analysis interpretations regarding volcanic propagation patterns and characterization, tensional fractures and implied stress directions are discussed to explore the complexity of this volcanic center distribution. The parameters utilized to depict and differentiate the volcanic cones and structural parameters were considered and recognized by previous work from Corazzato and Tibaldi (2006) and Bolós et al., (2014).

Drainage Network Analysis Interpretation: Identification of Cone and Lava Flow Morphology. Drainage network patterns of the UVF combined with DEM and structural analysis of volcanic cones show trends of structures that suggest the orientation of volcanic features (Fig. 4.6). These patterns consist of three trends; parallel, fan, and radial. Radial trends of UVF volcanic structures are present as cones, cinders, and peaks. Parallel patterns in the UVF are identified as ridges and saddle features. Fan drainage patterns in the UVF are identified as orientations following a similar direction radiating from a center. These drainage patterns may be a smaller piece of a radial pattern but buried by other structure trends.

In mass lava flows 1 and 2 I associate a fan drainage network pattern to these regions. Mass lava flow 1 is recognized by a prominent drainage network radiating in the NW direction. It is likely that the volcanic center for this flow is based from the Little White Gap center, due to the apex of this fan structure located here. Mass lava flow 2 shows a similar drainage network but does not appear to share the same volcanic center. I suggest that the center for this lava flow is located and buried as the marked point on Fig. 4.6. This point is determined based on the fan pattern drainage network changing flow direction further eastward. Mass lava flows 4 and 6 are recognized as clear radial

drainage networks. Mass lava flow 6 occurs as an elongated saddle like feature while mass lava flow 4 occurs as a distinguishable cone. In both cases I suggest that the volcanic centers are found in the center of this structures. Mass lava flows 3 and 5 do not show a clear direction of flow direction, but areas with parallel patterns can be identified. These parallel patterns correlate to areas with steep gradient allowing unidirectional flow. It is difficult to determine volcanic centers in these areas based on this chaotic drainage network, however a volcanic center by the Augustine Tanks is recognized by a small Uvas dike and lapilli material.

Distinguishing between these drainage network patterns allows for interpretations of volcanic structures, structural orientations, and volcanic edifices. In principal, flows of considerably size may allow a structural element to be determined even with known geomorphometric events, as suggested in Dohrenwend et al. (1987).

Cone Classification. Cone analysis of the many peaks in the UVF vary in locality and size as well as breaching directions. Majority of cones in the UVF and in the southern region are smaller than the dissected cones in the center of the field. The cones in the southern region represent simple cones, this are indicated on Figure 4 as the southern cones, Sugar Loaf Peak, Massacre Peak, and Peloncillo Peak. While the southern cones have similar in ellipticity to Sugar Loaf and the Escondido Cinder, the Peloncillo Peak and Massacre Peak share a relative ellipticity and summit width/ base width ratio (Fig. 4.9), but are respectively far in distance. Cones like the Escondido Ranch cinder cone are more representative of a multiple-rifted cone, where the propagating lava developed along a magma-feed fracture and the cone is strongly elongated (1.18 θ; Fig. 8; Corazzato and Tibaldi, 2006). The elongated major axi of this

cone coincides with the suggested σ_3 stress of the UVF (Fig. 4.10). This σ_3 stress field correlates to the migrated dike trending patterns, traveling from the SE to the NW. Lava flow breaching of this Escondido cone occurs to the NE, and not parallel to the magma feed fracture, suggesting that the substrate was not relatively horizontal but rather dipping to the NE. Cones like the Little White Gap are not as easily distinguishable by their shape and size and correspond to mixed-type cones. This classification is given by its superimposed edifices and multiple interfering eruptive points (Corazzato and Tibaldi, 2006). This cone is strongly elliptical (1.84 θ) and composed of ejected lapilli and volcanic agglomerate from its nearby center. These elongated cones are suggested to form along closer spaced eruptive points and share a common conduit (Corazzato and Tibaldi, 2006). Where the cones become more elongated in multiple rifted settings, behaviors are related to a high magma pressure or a relatively low confining stress both favoring an eruptive fracture opening (Corazzato and Tibaldi, 2006). The simple cones of more circular behavior result either from a lower magma pressure or higher confining pressure, but regardless belong to a localized eruptive conduit (Corazzato and Tibaldi, 2006). These simple cones include Massacre Peak, Peloncillo Peak, southern cone, and the Sugarloaf Peak. For other morphologies of cone development, variations of magma pressure, magnitude of confining stresses, and locality of eruptive conduits explain the growth of these structures. These different structures provide insight on their relationships to the underlying fractures in their substrate (Corazzato and Tibaldi, 2006; Le Corvec et al., 2013a; Muirhead et al., 2016; Tadini et al., 2014).

When taking into account the structural orientations of the fault and dike trends in the UVF I suggest parameters on how magmatic feed fractures are propagating. A strong

N/S alignment of dikes are detected crossing the paths of faults along the surface with NW/SE trends as σ^3 stresses. Southern areas of the UVF are more typical simple cones while the centralized and northern volcanic centers are more elongated. This geometry of more simple and circular cones further south in the UVF suggest the idea that localized conduits migrated further in this direction away from more complex and compact eruptive centers in the central area of the UVF (Corazzato and Tibaldi, 2006). Growth from the central region extending into the southern areas along a significant sharing fracture is quite possible but this is difficult to evaluate when faults are not clustered in this alignment.

Relationship of Fault Structure and Volcanic Distribution. Relationships between volcanic center distribution and fault structures has been proven to determine magma migration pathways through shallow crustal zones (Bonali et al., 2011; Le Corvec et al., 2013a, Muirhead et al., 2016). My analyses of structural and surface features in the UVF explains and provides new information on the development of the UVF, including calculations of individual cones and volcanic centers, and insight on magmatic migration in the shallow crust. These findings tribute other publications regarding using fault structure and volcanic distribution to interpret magma pathways (Bolós et al., 2014), tectonic variations (Adlyaman et al., 1998), and volcanic distribution (Corazzato and Tibaldi, 2006; Becerril et al., 2013).

The orientation of the UVF faults strike mostly NW/SE (280º NW to 0º N) and indicate that the stress field from this resurgent field was mostly homogenous. Most of these fractures are from 1-2 km in length and I suggest are shallow crustal faults that associated with upwelling volcanic intrusions. Because dikes often infill extensional

fractures, they often indicate the field mechanisms of shortening or stretching (Muirhead et al., 2016). In the UVF the direction of fault trends are nearly perpendicular with dike trends. This suggests the UVF dike segments may have perpendicularly cut across the major domal axi (σ_1) and protruded through extensional σ_3 stresses with most major faulting. This is illustrated by the relationship between volcanic center distribution and the major faults within the UVF (Fig. 4.10). The orientation of UVF centers follows a NE/SW trending orientation along the major axis, which is interpreted to be the σ_1 stress direction. Along this horizontal stress, echelon dike migration occurred in a N/S trend (0ºN to 30ºNE). This migration suggests that a link between the upwelling dikes along tensional fractures mobilized perpendicular to the σ_1 stress regime and the relationship of distanced volcanic centers from the dikes. However, due to erosion and basin fill I cannot determine if volcanic centers in the central UVF area, such as the Little White Gap vent, were rooted from tension fractures.

Seager (1975) described the Sierra de las Uvas Dome to being a complexly faulted axial graben system. This is evident by established fault geometry; however, structural data provides insight on mobilizing of volcanic intrusions. Though emplacement of volcanic centers are believed to be placed along the axis of the Cedar-Hils area (Seager, 1975), new structural data reflects my new interpretation. Here, I suggest the development of these volcanic centers along an axis parallel the Cedar-Hills area, and derived new volcanic centers and cones from cross cutting tensional forces.

Conclusions

The Uvas Volcanic Field shows the structural complexity of monogenic volcanic systems. However, these calculated representations hold extreme value in providing a generalized concept for magma migration towards Uvas volcanic centers and their relationship to shallow underlying fractures. Based on the structure and quantitative analysis of the UVF, the following conclusions can be made.

1) Volcanic centers in the southern region share similar geometric parameters and orientation suggesting their magmatic propagation through the substrate was based on a magma feed fracture from distanced eruptive points. The results from the ellipticity, shape, and size of these cones correlate with behaviors of this suggested system with relatively high confining stresses. Cones that are preferentially more circular shaped to more elongated suggest their magma feed conduits are spaced away from each other, whereas elongated cones suggest closer magma-feed fractures. This does not exclude them from sharing the same magmatic conduit.

2) Volcanic centers in the centralized region are not as easily recognizable, but breach out as typical dissected cinder cones. Due to volcanic centers erupting as more elongated and breached cones, their eruptive points suggest they are more clustered than those of the simple cones. Though these cones are poorly developed, their spatial distribution to the center of the UVF strongly supports the suggestion for more clustered magmatic feed fractures. This again does not relate these volcanic centers to sharing the same magmatic conduit but does insist a closer relationship of conduits.

3) Magmatic migrations follow a possible perpendicular path from fractures in a NE/SW alignment. Though difficult to determine and represent, in cases where strong tensional forces are distributed, volcanism typically follows weakened areas rather than obstacles through the substrate. In this analysis determining post-dated fault movements may answer this alignment of faults.

4) The applications within the methodology are consistent with the inferred phenomenon for the magma-feed intrusions. The results from the aerial photos and structural analysis correlate with the structural and stratigraphic information. This research does not directly support any geometry of deep magmatic feed structures and displacements. However, future research is needed to see the behavior of deep magmatic intrusions and how they relate to proposed migration patterns.

References

Adıyaman, O., Chorowicz J., and Köse, O., 1998, Relationships between volcanic patterns and neotectonics in Eastern Anatolia analysis of satellite images and DEM: Journal of Volcanology Geothermal Research. v. 85, p.17–32.

Becerril, L., Cappello, A., Galindo, I., Neri, M. and Del Negro, C., 2013, Spatial probability distribution of future volcanic eruptions at El Hierro Island (Canary Islands, Spain): Journal of Volcanology and Geothermal Research v. 257, p. 21–30, doi:10.1016/j.jvolgeores.2013.03.005.

Best, G. M, Christiansen, E.H., de Silva, S., and Lipman, P. L., 2016, Slab-rollback ignimbrite flareups in the southern Great Basin and other Cenozoic American arcs: A distinct style of arc volcanism: Geological Society of America, v. 12, p. 1097-1135, doi: 10.1130/GES01285.1.

Bolós, X., Barde-Cabusson, S., Pedrazzi, D., Martí, J., Casas, A., Lovera, R., and Nadal-Sala, D., 2014, Geophysical exploration on the subsurface geology of La Garrotxa monogenetic volcanic field (NE Iberian Peninsula): International Journal Earth, v. 103, p. 2255-2269, doi:10.1007/s005531-014-1044-3.

Bonali, F.L., Corazzato, C., and Tibaldi, A., 2011, Identifying rift zones on volcanoes: An example from La Réunion Island, Indian Ocean: Bulletin of Volcanology, v. 73, p. 347–366.

Cather, S.M., 1990. Stress and volcanism in the northern Mogollon-Datil volcanic field, New Mexico: Effects of post-Laramide tectonic transition: Geological Society of America Bulletin, v. 102, p. 1447–1458.

Chapin, C. E., McIntosh, W. C., and Chamberlin, R. M., 2004, The late Eocene-Oligocene peak of Cenozoic volcanism in southwestern New Mexico, in Mack, G. H., and Giles, K. A., eds., The geology of New Mexico: A geologic history: New Mexico Geological Society Special Publication, v. 11, p. 271-293.

Clemons, R. E., and Seager, W. R., 1973, Geology of Souse Springs Quadrangle, New Mexico: New Mexico Bureau of Mines & Mineral Resources Bulletin 100.

Corazzato, C., and Tibaldi, A., 2006, Fracture control on type, morphology and distribution of parasitic volcanic cones: An example from Mt. Etna, Italy. Journal of Volcanology and Geothermal Research, v. 158, p. 177-194. doi: 10.1016/j.volgeores.2006.04.018.

Davis, J.M., Elston, W.E., and Hawkesworth, C.J., 1993, Basic and intermediate volcanism of the Mogollon-Datil volcanic field: Implications for mid-Tertiary tectonic transitions in southwestern New Mexico, USA: , in Prichard, H.M., Alabaster, T., Harris, N.B.W., and Neary C. R., eds., Magmatic processes and plate tectonics: Geological Society [London] Special Publication, v. 76, p. 469-488.

Davis, J.M., and C.J., Hawkesworth, 1994, Early calc-alkaline magmatism in the Mogollon-Datil Volcanic Field, New Mexico, USA: Journal of the Geological Society, v. 151 p. 825-843.

Davis, J.M., and C.J., Hawkesworth, 1995, Geochemical and tectonic transitions in the evolution of the Mogollon-Datil Volcanic Field, New-Mexico, USA: Chemical Geology, v. 119, p. 31-53.

Dohrenwend, J. C., Abrahams, A. D., Turrin, B. D., 1987, Drainage development on basaltic lava flows, Cima volcanic field southeast California, and Lunar Crater volcanic field, south-central Nevada. Geological Society of America Bulletin v. 99, no 11, p. 405-413.

Grosse, P. B., Van Wyk de Vries, Euillades, P. A., Kervyn, M., and Petrinovic, I. A., 2012, Systematic morphometric characterization of volcanic edifices using digital elevation models, Geomorphology, v. 136, p.114–131, doi:10.1016/j.geomorph.2011.06.001.

Gürer, D., Galland, O., Corfu, F., Leanza, H. A. & Sassier, C., 2015, Structure and evolution of volcanic plumbing systems in fold-and-thrust belts: A case study of the Cerro Negro de Tricao Malal, Neuquén Province, Argentina. Geological Society of America Bulletin v. 128, p. 315–31.

Keller, G.R. and Cather, S.M., 1994a, Basin of the Rio Grande Rift: Structure, Stratigraphy, and Tectonic Setting: Geological Society of America Special Paper, v. 291, p. 1-4.

Kempton, P.D., Fitton, J.D., Hawkesworth, C.J., and Ormerod, D.S., 1991, Isotopic and trace element constraints on the composition and evolution of the lithosphere beneath the southwestern United States: Journal of Geophysical Research, v. 96, p. 13713–13735.

Kereszturi, G. and Németh, K., 2012, Structural and morphometric irregularities of eroded Pliocene scoria cones at the Bakony–Balaton Highland Volcanic Field, Hungary: Journal of Geomorphology, v. 136, p. 45-58.

Kottlowski, F.E., 1953b, Tertiary-Quaternary sediments of the Rio Grande valley in southern New Mexico, New Mexico Geological Society Guidebook, Fourth annual field conference, Southwestern New Mexico, p. 144.

Le Corvec, N., Spörli, K.B., Rowland, J., and Lindsay, J., 2013a, Spatial distribution and alignments of volcanic centers: Clues to the formation of monogenetic volcanic fields: Earth Science Reviews, v. 124, p. 96-114.

Mack, G.H., 2004, Middle and late Cenozoic crustal extension, sedimentation, and volcanism in the southern Rio Grande rift, Basin and Range, and southern Transition Zone of southwestern New Mexico, in Mack G.H and Giles, K.A., eds, The Geology of New Mexico: A Geologic History: New Mexico Geological Society, Special Publication 11, p. 389-406.

McMillan, N., 1998, Temporal and spatial magmatic evolution of the Rio Grande rift: New Mexico Geological Society Guidebook, v. 49, p. 107-116.

McMillan, N.J., Dickin, A.P., and Haag, D., 2000, Evolution of magma source regions in the Rio Grande rift, southern New Mexico: Geological Society of America Bulletin, v. 112, p. 1582-1593.

Muirhead J.D., Van Eaton A.R., Re G., White, J.D.L., Ort M.H., 2016, Monogenetic volcanoes fed by interconnected dikes and sills in the Hopi Buttes volcanic field, Navajo Nation, USA. Bulletin of Volcanology.

Naranjo, M.F., Ebmeier, S.K., Vallejo, S., Ramón, P., Mothes, P., Biggs J., and Herrera F., 2016, Mapping and measuring lava volumes from 2002 to 2009 at El Reventador Volcano, Ecuador, from field measurements and satellite remote sensing: Journal of Applied Volcanology Society and Volcanoes, v. 5, doi:10.1186/s13617-016-0048-z.

Seager, W.R., 1973, Resurgent volcano-tectonic depression of Oligocene age, south-central New Mexico: Geological Society of America Bulletin, v. 84 no. 11 p. 3611-3626, doi: 10.1130/0016-7606(1973)84<3611:RVDOOA>2.0.CO;2

Seager, W.R., Clemons, R.E., and Hawley, J.W, 1975, Geology of Sierra Alta Quadrangle Doña Ana County, New Mexico, New Mexico Bureau of Mines & Mineral Resources Bulletin 102.

Seager, W.R., 1975, Cenozoic tectonic evolution of the Las Cruces area, New Mexico: New Mexico Geological Society 26th Annual Fall Field Conference Guidebook, p. 241-250.

Tadini, A., Bonali, F.L., Corazzato, C., Cortés, J.A., Tibaldi, A., Valentine, G.A., 2014, Spatial distribution and structural analysis of vents in the Lunar Crater Volcanic Field (Nevada, USA): Bulletin of Volcanology, v. 76 p. 1-15.

Yonkee, A., and Weil, A.B., 2015. Tectonic evolution of the Sevier and Laramide belts within the North American Cordillera orogenic system: Earth Science Reviews, v. 150, p. 531–93.

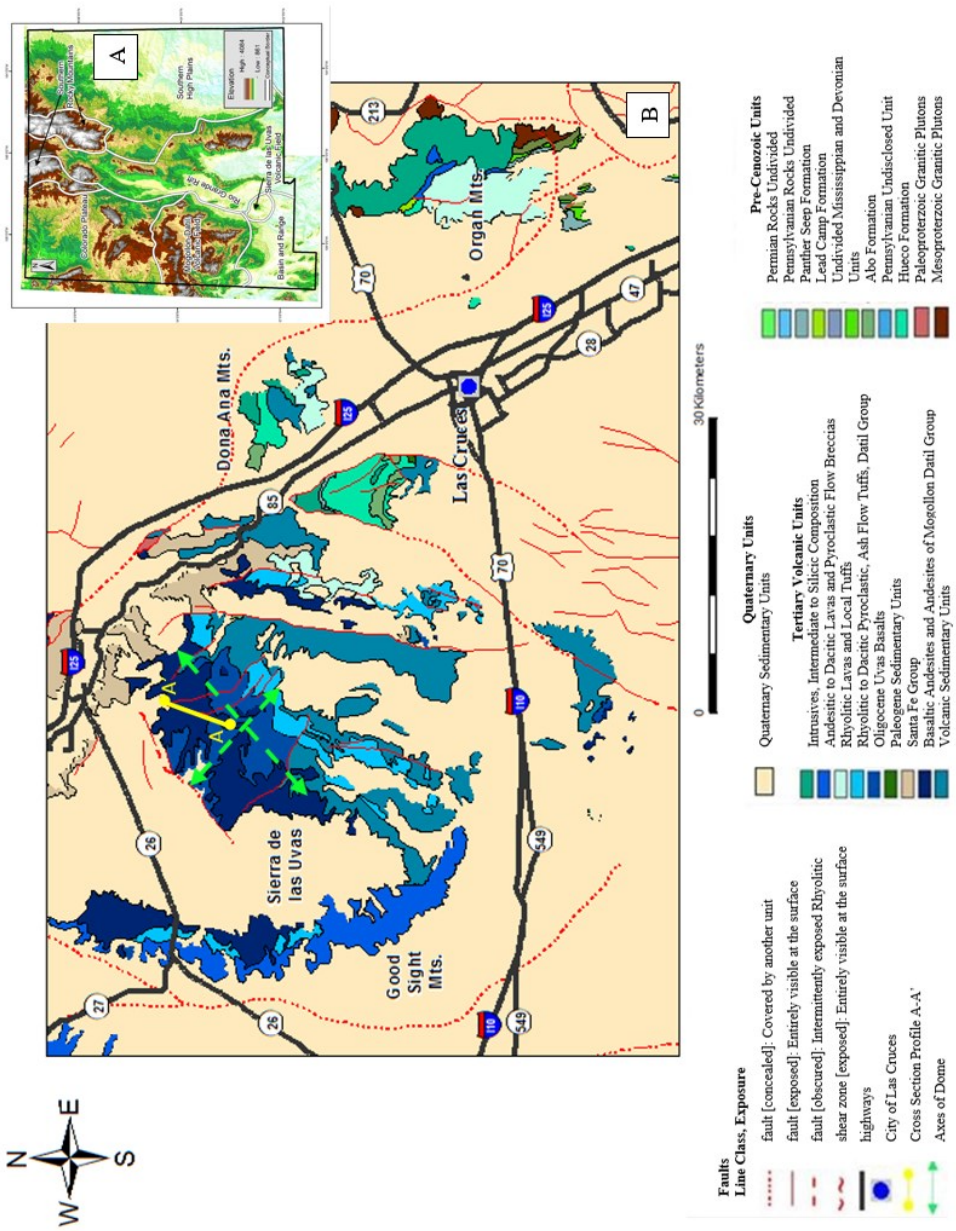

of Sierra de las Uvas Volcani
implified geology map of stu
s are presented (as green doul
s yellow segment).

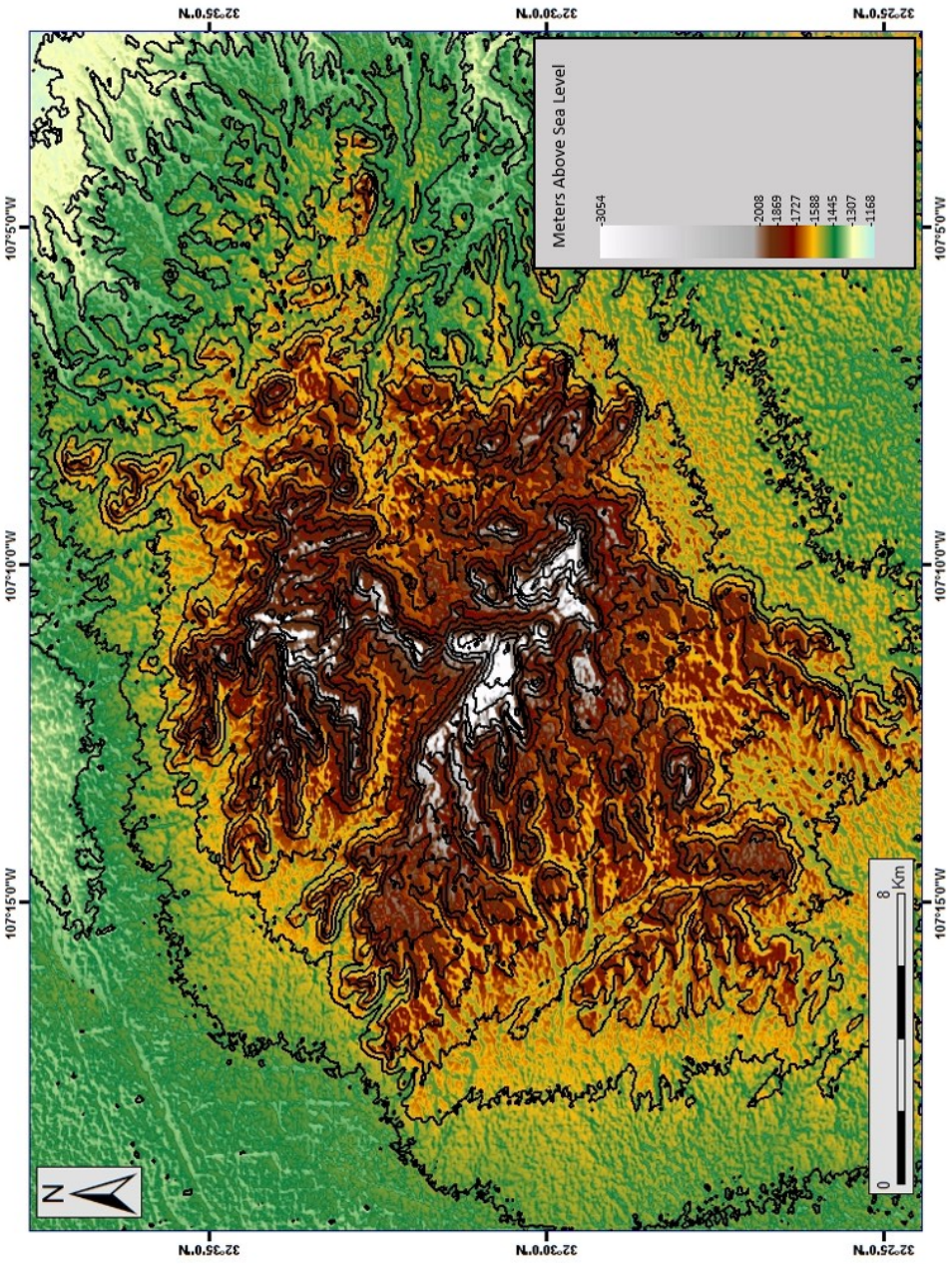

de las Uvas Volcanic Field (U
ıantly in the center location o
by the outward decreasing el

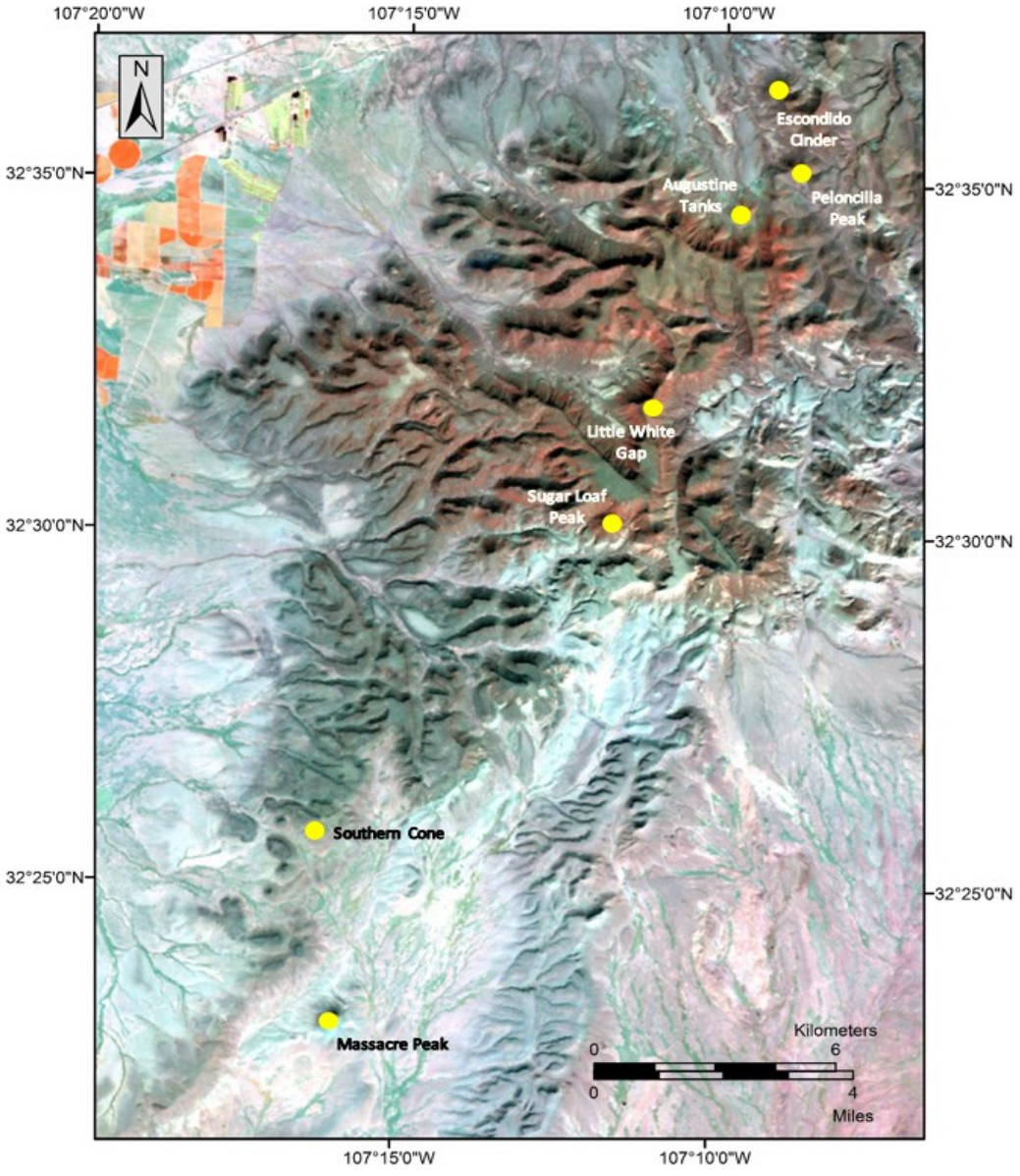

Figure 4.3: Remote-sensed Landsat image (false color RGB) of Sierra de las Uvas Volcanic Field. Volcanic centers and cones shown as yellow dots. Known volcanic centers include the Escondido Ranch, Augustine Tanks, and Little White Gap. Uvas lavas are distinguished from sedimentary and ash units by combination of difference in reflectance bands and geologic mapping. See Figure 4.4.

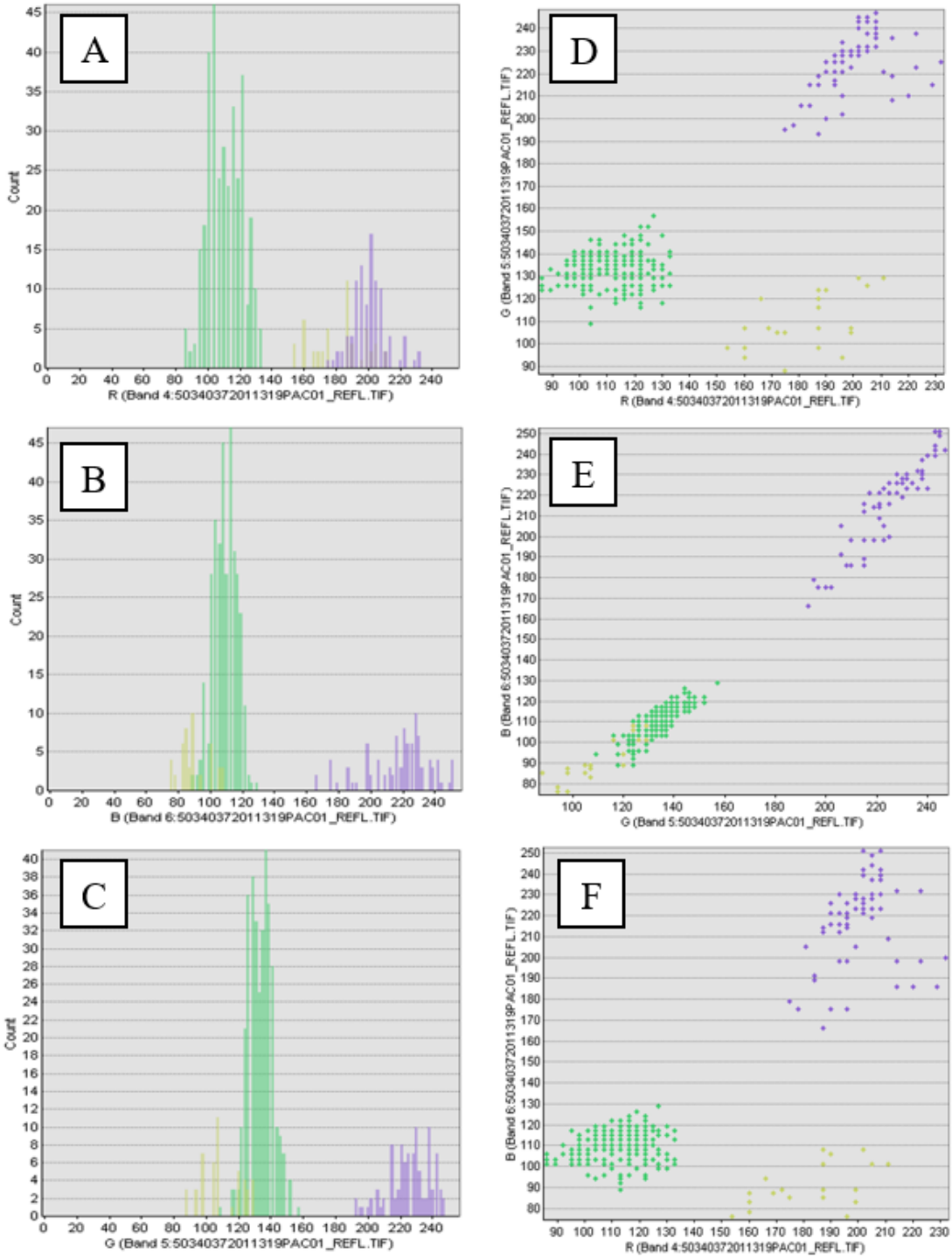

Figure 4.4: Histograms (A,B,C) and scatter plots (D,E,F) of bandwidths of the Uvas lavas, sedimentary and ash units of the Uvas Volcanic Field (UVF) from the remote-sensed Landsat image (false color RGB) in Figure 4.3. Uvas lavas are in green, sedimentary in yellow, and ash units in purple. Bandwidths between RGB values are compared to distinguish different reflectance patterns to help identify units of interest (Uvas volcanic centers).

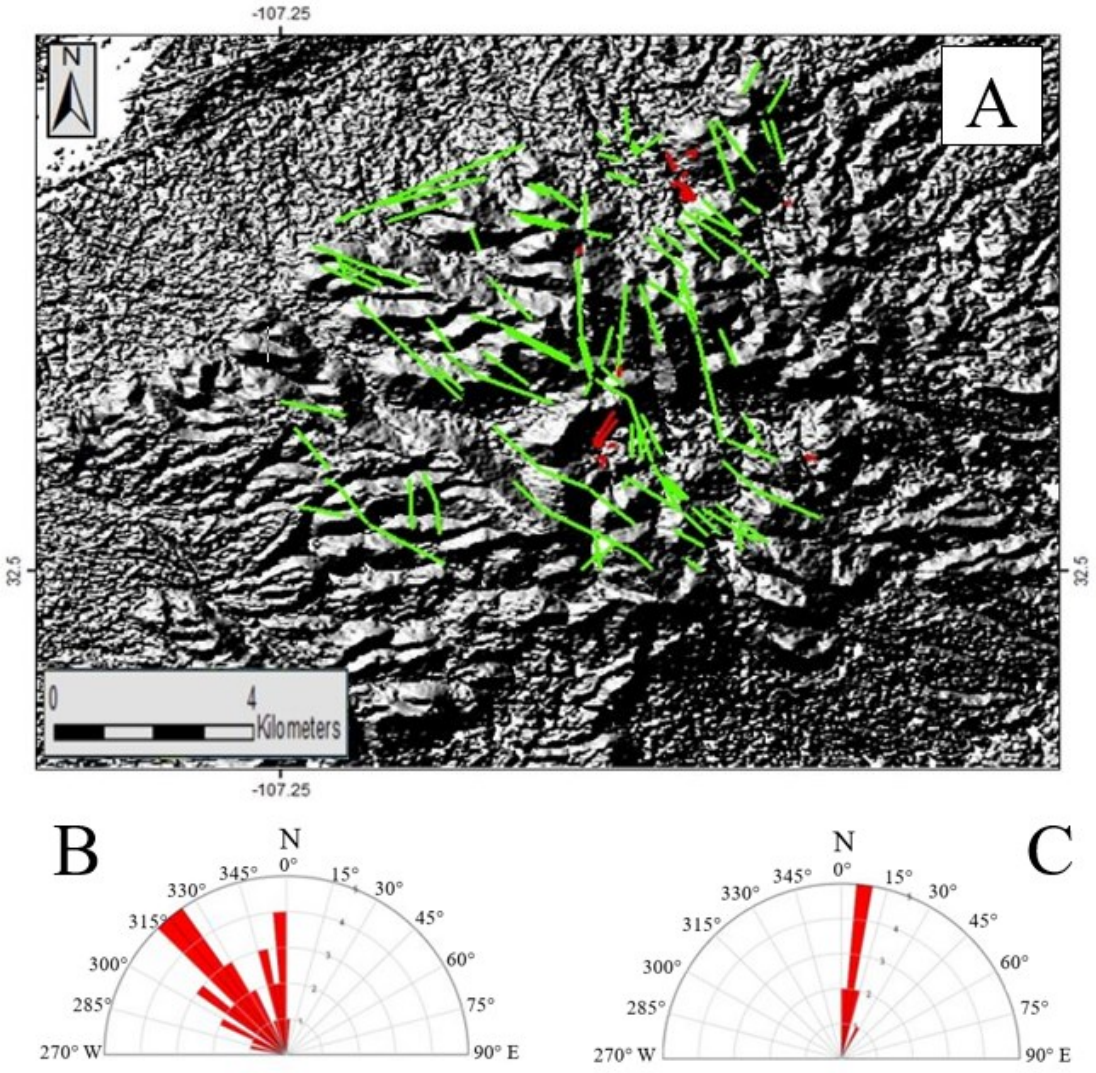

Figure 4.5: A) Volcanic-structural map of Sierra de las Uvas Volcanic Field (UVF). Faults are indicated as green lines and dikes as red lines. B) Rose diagram of fault orientations. Mapped faults on the volcanic structural map indicate that fault orientations follow a strong NW/SE trend. This trend suggests a bimodal distribution of NW/SE and N/S pathways. C) Rose diagram of the orientation for volcanic dikes and diatremes. Dike orientations follow a strong N/S trend and align with major N/S faults in the UVF. Fault and dike trends suggest possible relationships between one another. These relationships correspond to fractures providing vertical magma feed pathways (Ferril et al., 1997).

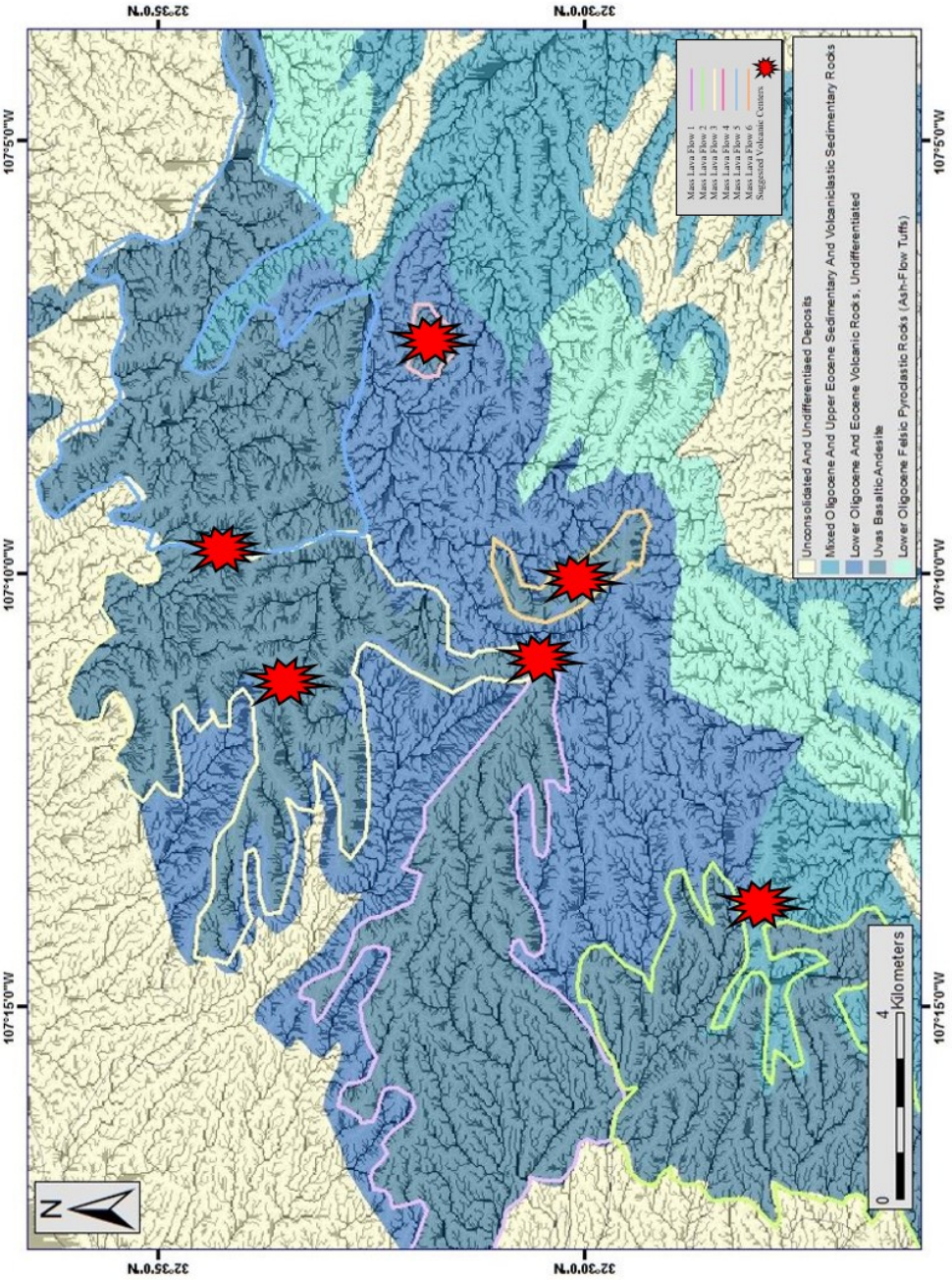

Sierra de las Uvas Volcanic
gested location of volcanic c
ss lava flow interpretations th

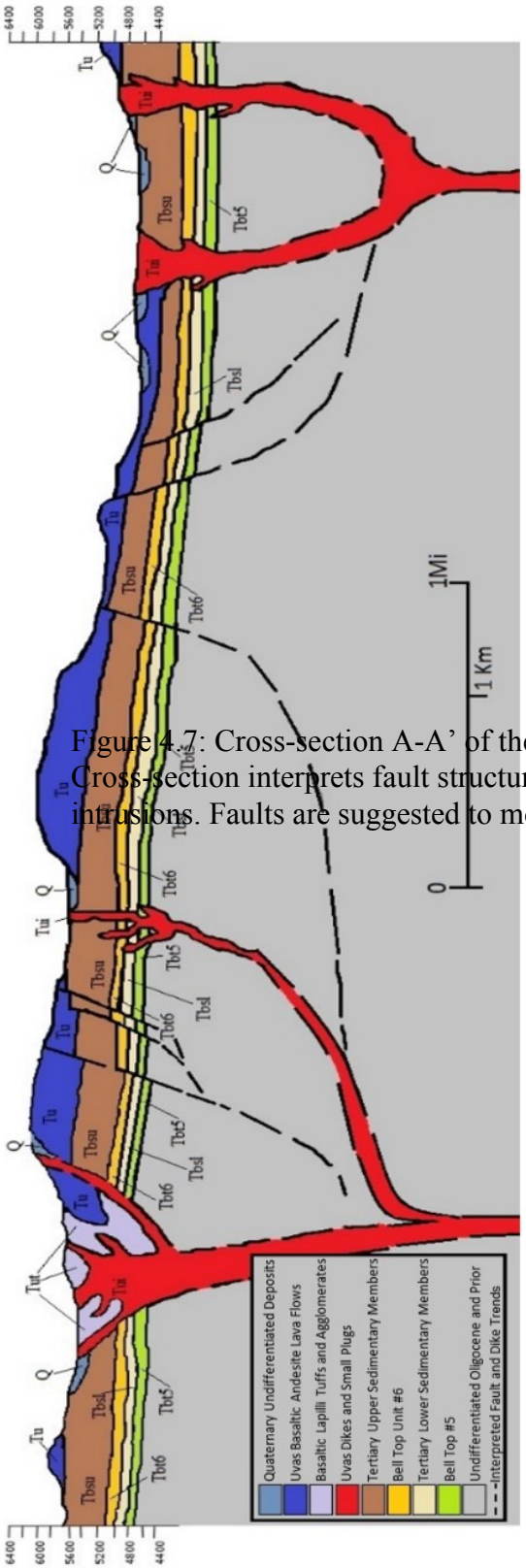

Figure 4.7: Cross-section A-A' of the Sierra de las Uvas Volcanic Field (UV
Cross-section interprets fault structures to share similar orientations as dike
intrusions. Faults are suggested to mobilize listric with increasing depth.

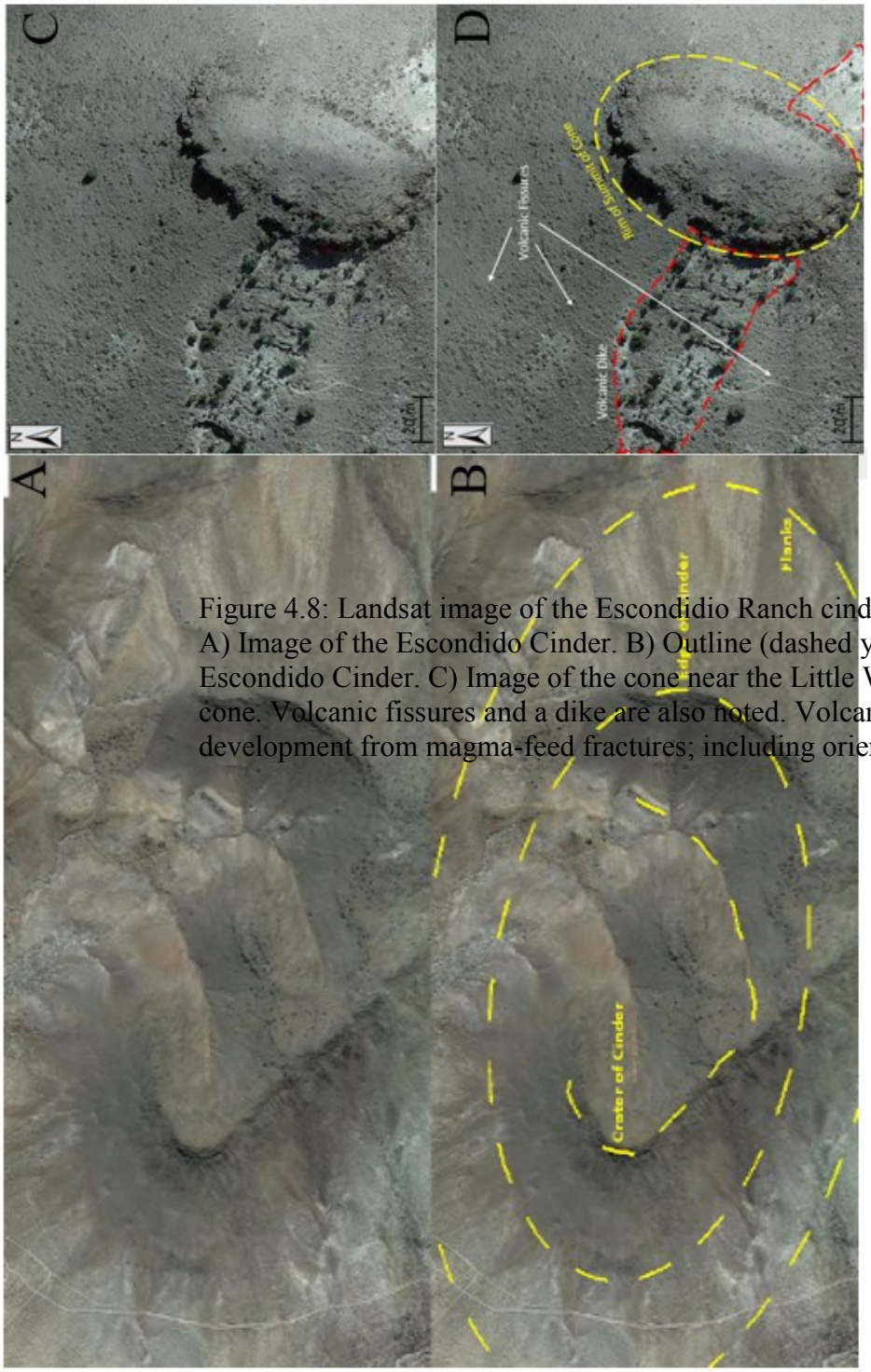

Figure 4.8: Landsat image of the Escondidio Ranch cinder cone (A and B) and cone near
A) Image of the Escondido Cinder. B) Outline (dashed yellow) the edge of the cinder fla
Escondido Cinder. C) Image of the cone near the Little White Gap. D) Outlines (dashed
cone. Volcanic fissures and a dike are also noted. Volcanic-structural analysis of these fe
development from magma-feed fractures; including orientations, volume, ellipticity, size

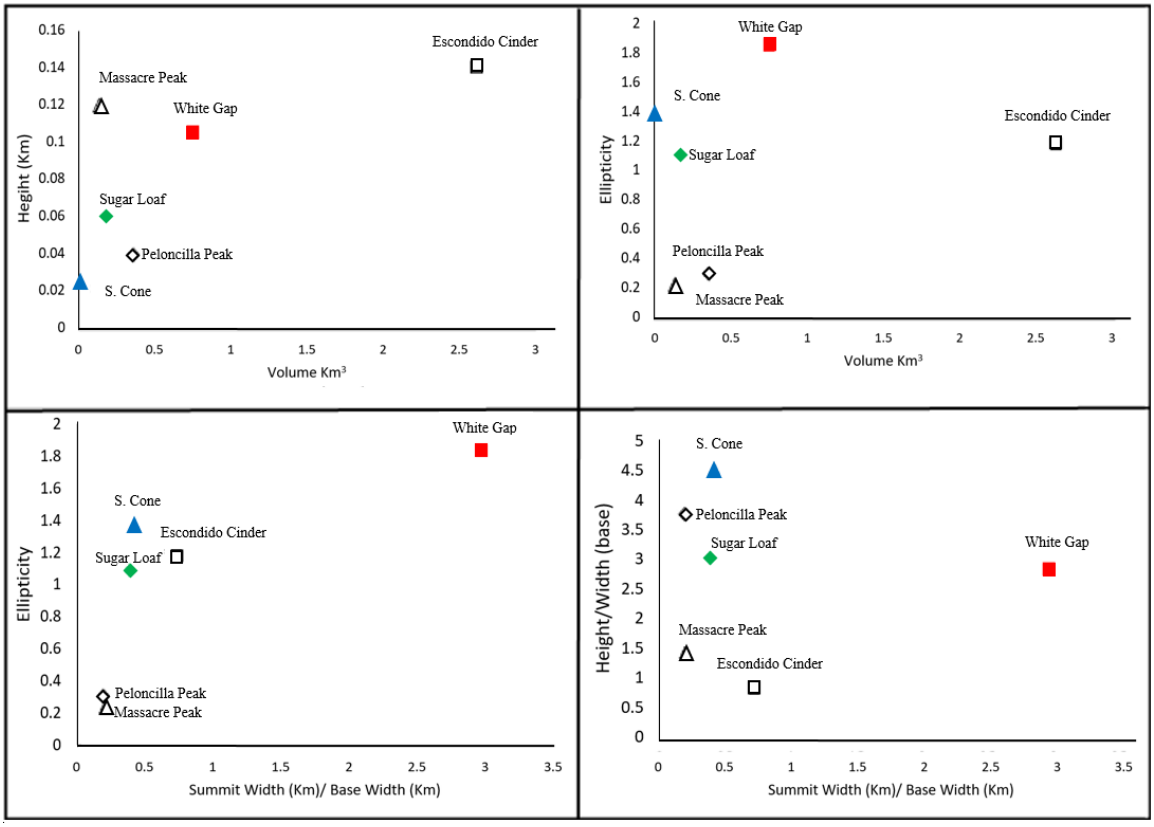
Height (Km)
Volume Km³
Escondido Cinder
Massacre Peak
White Gap
Sugar Loaf
Peloncilla Peak
S. Cone
Ellipticity
Volume Km³
White Gap
S. Cone
Escondido Cinder
Sugar Loaf
Peloncilla Peak
Massacre Peak
Ellipticity
Summit Width (Km)/ Base Width (Km)
White Gap
S. Cone
Escondido Cinder
Sugar Loaf
Peloncilla Peak
Massacre Peak
Height/Width (base)
Summit Width (Km)/ Base Width (Km)
S. Cone
Peloncilla Peak
Sugar Loaf
White Gap
Massacre Peak
Escondido Cinder

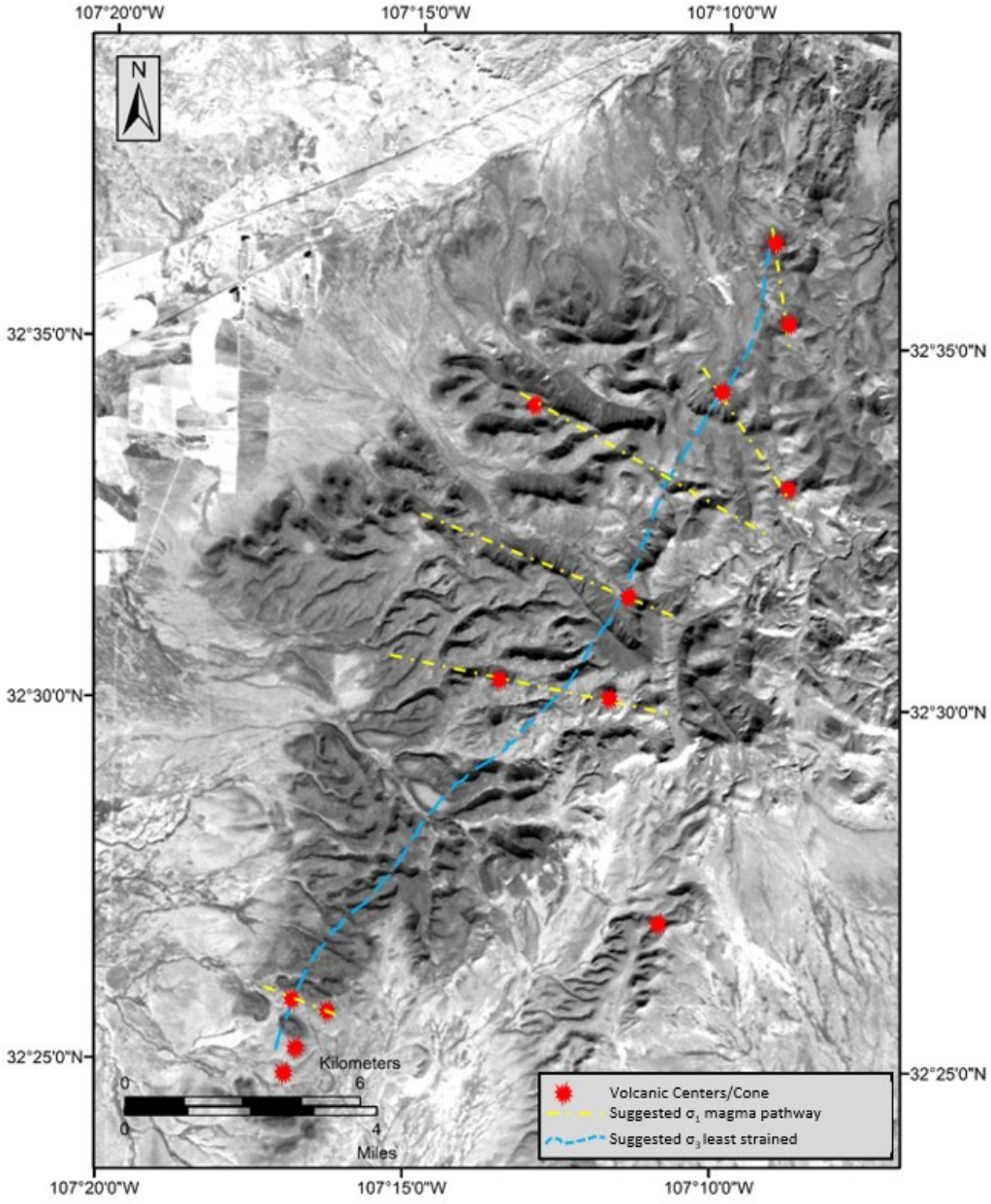

Figure 4.9: Scatter plots of structural parameters (height, weight, volume, and ellipticity) are compared to find distribution relationships between volcanic cones and centers in the UVF.

CHAPTER 5 – OXYGEN ISOTOPE VARIATIONS IN VOLCANIC ROCKS FROM SOUTH-CENTRAL NEW MEXICO: INSIGHT ON CRUSTAL CONTAMINATION AND MAGMATIC SOURCES

Abstract

Southern New Mexico's geological history is a record of complex tectonic and magmatic events between 45-27 Ma. Cenozoic tectonic events have left many questions about the magmatic sources and petrogenesis responsible for the volcanic activity distributed throughout New Mexico. Previous studies of the area propose continental arc magmatism (45-36 Ma) was triggered by slab "break-off" of the Farallon Plate, allowing inflow from the asthenosphere at around 28 Ma. Geochemical and isotopic signatures of volcanic rocks suggest crustal modification and hybridization by mafic magmas from the subducting Farallon Plate shifted source from a subduction-modified lithospheric mantle signature between 45-28 Ma to a more enriched or OIB-like mantle signature around 28 Ma. Continental basalts and andesites derived with lithospheric mantle signatures are interpreted to have low concentrations of Nb and Ta and high concentrations in Ba, Sr, Rb and low and variable ε_{Nd} (+2 to -8) compared to ocean island basalts (OIB). However, asthenospheric signatures from some upper Cenozoic basalts in the area suggest they are products from partial melting within the upwelling and decompressing asthenosphere.

These magmas have high Nb and Ta concentrations and ε_{Nd} values between +7 and +4, which are similar to concentrations and values of North American OIBs. Here I present isotopic data to evaluate the magmatic evolution of south-central New Mexico volcanic rocks through valuable, and formerly nonexistent, oxygen isotope data from the Uvas Basalts (28-27 Ma) and Rubio Peak Formation (45-36 Ma). These Oligocene and Eocene mafic to intermediate suites were selected based on their connection to the timing

Figure 4.10: Landsat image (false color) of the Sierra de las Uva Volcanic Field (UVF). Volcanic centers and cones are shown as red points, tensional fractures (σ_3) are shown as dashed yellow lines and the orientation of least stress(σ_1) is shown as a dashed blue line. Suggested volcanic centers, cones, tensional fractures and interpreted shallow fractures are overlaid on image to show spatial distribution and patterns. The combination of distribution and orientation patterns of volcanic centers, cones, faults, and dikes help provide interpreted shallow fractures in the crust. These fractures are reasonable pathways for magmatic migration to follow and allow propagating volcanism to occur.

of shifts in magmatic composition in the area. New oxygen isotope data from silicate mineral separates and mass balanced models in combination with Sr and Nd isotopic data

allows us to define the hybridization and modification of the crust during the transition from arc magmatism to Rio Grande rifting in southern New Mexico. I suggest that the Rubio Peak formation volcanic rocks represent a period of crustal contamination of large volumes of mantle basalts creating a mid-crustal hot zone. The Uvas basalts and andesites represent the first true mantle derived magmatism in the region and become progressively more hybridized over time.

KEYWORDS: andesites, crustal contamination, isotope ratios, magma genesis

Introduction

Over the past several decades, substantial contributions have been made looking at the immense Cenozoic volcanism throughout southern New Mexico (Davis et al., 1993; Davis and Hawkesworth, 1994; 1995; Seager, 1975; McMillan et al., 2000; Copeland et al., 2011; and Michelfelder and McMillan, 2012). In this region, three main stages of magmatic-tectonic evolution have been identified: Laramide continental arc (Late Cretaceous to Eocene), Mogollon-Datil volcanic field (55.8-23Ma) volcanism from slab relaxation, and late Rio Grande volcanism (10-0 Ma; Seager, 1975; Davis and Hawkesworth, 1993, 1994, 1995; McMillan 1998, 2004). These events are the result of the mantle sources in the region shifting from subduction-modified lithospheric mantle from arc magmatism to an upwelling asthenospheric mantle source during the transition to extension (McMillan et al., 2000). The volcanic rocks in this region have been divided into mantle sources based on geochemistry including radiogenic isotope ratios and major and trace element data (McMillan et al., 2000; McMillan 2004). While there is compelling evidence for the suggested mantle sources and melting mechanisms for the

volcanic rocks of southern New Mexico, the effect of crustal contamination on these magmatic systems is poorly understood.

Recently, new models have helped to identify and characterize the physical and chemical processes that are affect magma composition within open crustal magmatic systems in ways that more quantitatively describe the contaminants and sources (Bohrson and Spera, 2001; Dufek & Bergantz, 2005; Annen et al., 2006; Feeley et al., 2008; France et al., 2016). These processes in continental arc systems and transitioning magmatic systems require careful analysis and interpretation, and the use of high precision oxygen isotope values and trace element ratios more quantitatively describe the geochemical data to explain the evolution of these magmas (Feeley and Sharp, 1995; Bindeman, 2008; Freund et al., 2013; Loewen and Bindeman, 2016; Underwood and Clynne, 2017). Because wall rocks can be compositionally identical to plutonic and volcanic rocks from previous eruptive episodes through crustal hybridization, radiogenic isotope ratios and trace element concentrations alone may provide little information on the degree of crustal contamination. These methods alone are not significant enough to deduce the effects of crustal contamination through time (Feeley and Sharp, 1995; Bindeman, 2008, Feeley et al., 2008; Michelfelder et al., 2013). Previous studies from McMillan et al. (2000) suggests that Eocene magmas assimilated both upper and lower crustal components while Oligocene and late Cenozoic lavas with have lower crustal input. This idea suggest that the crust was heated from early Eocene magmatism during Laramide magmatism in southern New Mexico (Davis and Hawkesworth, 1994, 1995; McMillan et al., 2000).

In this paper, I explore the combination of oxygen isotope values, major and trace element concentrations, radiogenic isotope ratios to further the understand the mantle and

crustal assimilation record linked to the magmatic evolution in southern New Mexico. This project is to better understand the major shift from continental arc magmatism to Rio Grande rifting by determining the relationship between the radiogenic isotope ratios and oxygen isotope values that may reflect the transition in igneous rock compositions.

To better analyze and differentiate between parental magmas and contaminated magmas this paper presents oxygen isotope values from two units in southern New Mexico to help differentiate the crustal and magmatic sources. These oxygen isotope values are used to help identify and quantify hybridization between the magma with the crustal contaminants, as well as add key variables in their connection to timing of these events.

Geologic Setting

South-central New Mexico is characterized by several volcanic fields, structural uplifts and widespread ash-flows produced by Laramide and post-Laramide magmatism (Cather, 1990; Mack et al., 1994; McMillan et al., 2000; Chapin et al., 2004; Zimmer and McIntosch, 2013; Lipman and Bachmann, 2015). Subduction of the Farallon Plate (Late Cretaceous- Eocene) along the western margin of North American is responsible for the immense span of the magmatic and volcanological record (Seager, 1975; Chapin et al., 2004; Michelfelder and McMillan, 2012). In this changing tectonic regime, not only are evident changing styles of volcanism present, but implications for subducting lithosphere, upwelling asthenosphere, upper and lower crust are recognized in the compositions of igneous rocks across southern New Mexico (McMillan et al., 2000). The Sierra de las Uvas volcanic field (UVF) and Mogollon-Datil volcanic field (MDVF) are the expression

of Laramide through Rio Grande volcanic rocks (Fig 5.1 and 5.2). These areas are particularly important because their volcanic events correspond to the evolving lithospheric mantle during Laramide subduction (Foder, 1975; Seager, 1975; Cather, 1990).

Laramide Subduction. During the Late Cretaceous approximately 80 Ma, Laramide tectonic activity began along the western margin of North America causing mountain building, widespread magmatism, and structural deformation throughout the western region, ending around early-mid (Eocene 55-35 Ma; Cather, 1990; Mack et al., 1994; Mack, 2004). Laramide subduction in southern New Mexico is expressed as shallow-angle subduction beneath the North American plate (de Silva, 2008). Models suggest that as the Farallon plate subducted beneath the North American plate, the slab rolled back and potentially broke off into the mantle (also known as "slab breakoff"), resulting in the upper crust being exposed to the hot asthenospheric mantle around 36 Ma (Davis et al., 1993; Davis and Hawkesworth, 1994; Ferrari et al., 2007; Copeland et al., 2011).

Major changes in mantle magma productivity after slab rollback produced a nearly continuous supply of magmatism resulting in the initiation of an ignimbrite flare-up (Farmer et al., 2008). The ignimbrite flare-up is marked by Tertiary pyroclastic material including bimodal basalt and rhyolite composition rocks related to steepening subduction of the Farallon plate (McMillan, 2004). Magmas are expressed as two phases in New Mexico, early (80-64 Ma) and late (64-48 Ma) Laramide (McMillan, 2004). Early phase magma are orogenic andesites, granites, and intrusive stocks (Davis et al., 1993; Zimmer and McIntosh, 2013; Best et al., 2016). Later stage magmas are expressed as the

Rubio Peak Formation, which consist of basalt and andesite lava flows, and intrusive rocks (Davis et al., 1993). The distinction in these changes are based on differences in magmatic deformation represented by eruption ages and folded structures. The expression of Laramide activity is located as far east as the Black Hills, South Dakota and between southern Canada and northern Mexico (English and Johnston, 2004). Four major magmatic regions in New Mexico are included: Colorado Plateau (Precambrian-Tertiary), Basin and Range Province (early Miocene, 17 Ma), Southern Rocky Mountain extent (Laramide), Rio Grande rift (Miocene-Present, 24-0 Ma) and the Mogollon-Datil volcanic field (Eocene-Oligocene, 55-30Ma); (McMillan et al., 2000; Gans and Bohrson, 1998).

Rio Grande Rifting. Between 35-29 Ma, continental rifting of the Rio Grande rift began thinning and spreading apart the Earth's surface from the Colorado Plateau in central Colorado, USA down to Chihuahua, Mexico. This tectonic movement was a "zipper-like" opening with earliest thinning in Big Bend, TX around 45 Ma and progressively getting younger to the north (Kluth and Schaftenaar, 1994; McMillan et al., 2000; Michelfelder and McMillan, 2012). Relation of Laramide subduction compression to Rio Grande rift extension triggered volcanism throughout the region while leaving a clear record of changes in mantle and crustal interactions (Kluth and Schaftenaar, 1994). These changes are indicated by the variations in radiogenic isotope ratios and major and trace element concentrations within the volcanic and sedimentary units of the Rio Grande rift (McMillan, 1998; McMillan et al., 2000). Tectonic models of south-central New Mexico (Fig. 5.3) represent a shift suggesting contamination from distinct upper- and

lower-crustal sources within the magmatic source regions of the lithosphere (McMillan et al., 2000; Michelfelder and McMillan, 2012).

Lithospheric Mantle Source. The magmatism suggested to be associated with lithospheric mantle sources is represented by the Uvas volcanic field (28-26 Ma), Bell Top Formation (36-28.5 Ma), and the Rubio Peak Formation (45-36.7 Ma; Gibson et al., 1995; Davis and Hawkesworth 1994; McMillan, 1998). The Uvas lavas are the most mafic volcanic rocks from this source, and are geochemically characterized by ε_{Nd} (± 0.8), $^{87}Sr/^{86}Sr$ ratios (0.704738), variable Pb isotope ratios ($^{206}Pb/^{204}Pb$= 17.332, $^{207}Pb/^{204}Pb$= 15.434, and $^{208}Pb/^{204}Pb$= 37.639; McMillan, 1998). Though these isotopic signatures could be in part from inherited lower crustal contamination, enriched arc-like trace elements (low Nb and Ta and high Ba, and Rb) suggest that the Uvas source to be from a slightly contaminated lithospheric mantle.

Geologic Units. The stratigraphy of south-central New Mexico between 60 Ma to present is predominantly represented by Cenozoic volcanic and sedimentary formations with only short gaps of missing strata from early Paleocene and late Miocene (Seager, 1975; Mack, 2004). As magma sources shifted in the region, volcanic rock compositions did as well from calc-alkalic andesites (45-24 Ma) to alkalic basalt-basaltic andesites (10-0 Ma; McMillan et al., 2000). Changes in composition and eruptive styles separate these distinctive volcanic units (McMillan et al., 2000). Mid-Tertiary (late Eocene-Oligocene) volcanism is described by two volcanic sequences, a late Eocene and an Oligocene sequence, both of which are associated with plutons (Seager, 1975). The late Eocene (Rubio Peak Formation) consists primarily of andesitic lava flows and widespread laharic deposits around the volcanic centers while the Oligocene sequence is represented as

mostly ash-flow tuffs (Bell Top Formation) and local basalts (Uvas volcanic field; Seager, 1975; McMillan et al., 2000).

Rubio Peak Formation of the Mogollon-Datil Volcanic Field. The Rubio Peak Formation (46.3 ± 0.3 to 37.6 ± 2 Ma; McMillan, et al., 2000) is found throughout southern New Mexico (Fig. 5.2). Volcanic rocks range in composition from basalt to dacite but predominantly consist of plagioclase and hornblende bearing andesites (58-62% SiO_2; Clemons, 1979; 1982; Davis et al., 1993; Davis and Hawkesworth, 1994; 1995; McMillan, 1998; McMillan et al., 2000). This calc-alkaline volcanic suite includes a variety of lava flows, volcaniclastic and small-volume ash flows with some regions, such as the Lake Valley Area, Sierra County, New Mexico, being describe as a trachydacite to trachyandesite (McMillan et al., 2000; O'Neill, 2002). Thickness of the unit varies from less than a 100 m to around 900 m but is suggested by Seager (1975) to be around 1980 m at the type section near the town of Deming, New Mexico. Variation in thickness is related to the pre-existing topography and volcanic structures, allowing some basins to consume more eruption fill than other areas (McIntosh, 1989; McMillan, 1998). The Rubio Peak Formation along with the Palm Park Formation, and the Orejon andesites are correlated with the construction of Eocene composite cones in the region (McMillan et al., 2000). Evidence of "arc-like" geochemical signatures in Rubio Peak rocks suggest this unit represents the Laramide continental arc in New Mexico. Incompatible element diagrams presented in McMillan et al. (2000) show arc-like trace element patterns from high Ba/Nb, Ba/Ta, Ba/La, and La/Ta ratios and low ε_{Nd} (+2 to -8) values. Based on geochemistry of enriched isotopic compositions (low and variable ε_{Nd} (+2 to -8), intermediate $^{87}Sr/^{86}Sr$ ratios (0.704 to 0.712), arc-like trace elements (low concentrations

of Nb and Ta and high concentrations in Ba, Sr, Rb), and alkalinity (poor), it is recognized that the Rubio Peak signatures represent the subduction-modified lithospheric mantle source (McMillan, 1998). These signatures further suggest that these volcanic rocks assembled from this source are partial melts from the subcontinental lithosphere These "arc-like" values provide a key to reason that the Rubio Peak may have consequently derived in response to Laramide low-angle subduction from the Farallon Plate, ultimately responsible for the widespread late Eocene volcanism.

Major element trends (see McMillan et al., 2000; Fig. 5.3) of the Rubio Peak correlate linearly and coincide with stratigraphically with successive units, Bell Top Formation (36.2-28.6 Ma) and the Uvas volcanic field (28-24 Ma; McMillan et al., 2000). It is suggested this significance represents a gradual shift in magmatic sources between the units. Davis and Hawkesworth (1994) claim the Mogollon-Datil Rubio Peak basaltic andesites have trace element and $^{87}Sr/^{86}Sr$ ratios that are representative of a closed system fractional crystallization process, while Rubio peak andesites reveal evidence of an open system differentiation. This idea suggests that the basaltic andesites were compositionally primitive magmas that progressively became contaminated through assimilation of crustal input. These proposed ideas of open and closed systems for the Rubio Peak source both indicate a period of crustal contamination with upper and lower crustal components. Because the Rubio Peak volcanism consist of a complex and evolved magmatic system, it is unclear to deduce how these magma compositions derived based upon existing geochemical data.

Uvas Basaltic Andesites. The Uvas Basalts of the UVF, located northwest of Las Cruces near the town of Hatch. The lavas from the Uvas volcanic field are calc-alkalic

(moderate to high K_2O) basaltic andesites, andesites, and tholeiitic basalts (McMillan et al., 2000). These lavas flows erupted immediately after the ash flow tuffs and contribute to the Southern Cordilleran Basaltic Andesite (SCORBA) suite (Cameron et al., 1989). These basalts are correlative with the Bear Spring Basalts in the Cookes Range and the Black Range northwest of Hillsboro (McMillan et al., 2000). To the southeast, basaltic andesite flows reach up to approximately 800 ft (~243 m) in the Goodsight-Cedar Hills Depression (Seager, 1975).

The Goodsight-Cedar Hills depression is classified by Seager (1975) as a volcano-tectonic structure associated with the early Oligocene rifting. Evidence from local depressions, subsidence fractures, intrusive masses and associated domes suggest that this volcanic feature was a precursor and/or played a role in the late Tertiary Basin and Range structures (Seager, 1973). Along the eastern side of this depression rhyolitic intrusives, vents, and flow banded-domes are represented within the north trending Cedar Hills vent/fault zone which extends for approximately 32 Km and 6.5 Km wide (Seager, 1975). This illustrates that while rift faulting was occurring (~26 Ma) overlapping basaltic andesite volcanism was also in progress (Seager, 1975). It is within the Cedar Hills vent zone that the sources, at least 6 mapped vents, for the Uvas basaltic andesites exist at the center of its basin (Seager, 1975). These sources are characterized as buried cinder cones with some taking form as volcanic plugs and dikes (Seager, 1975). Spatial location of several vents and accumulated thick flows suggest the volcanic field initially appeared as a broad shield-like feature, known as the Sierra de las Uvas Dome. (Seager, 1975). The dome, at about 16 km. in diameter and 600 m in relief, is suggested to have formed from resurgent magma and uplifting (Seager, 1975). Although timing for the

formation of the dome is still uncertain, evidence points to the Sierra de las Uvas Dome, Uvas lavas, and the initial faulting of the Rio Grande Rift to have occurred together or shortly after one another (Seager, 1975).

The Uvas lava flows share major element, ε_{Nd} (-4.5 to 0.8) value trends and $^{87}Sr/^{86}Sr$ (0.704404 to 0.707085) ratios with the former Bell Top and Rubio Peak units. These units are relatively depleted in Nb and Ti concentrations compared to other incompatible elements (McMillan et al., 2000). In addition, this suite exhibits the least-radiogenic Pb isotope ratios of Cenozoic magmas in the region: $^{206}Pb/^{204}Pb$ (17.039 to 18.084), $^{207}Pb/^{204}Pb$ (15.404 to 15.498), and $^{208}Pb/^{204}Pb$ (37.094 to 38.130; McMillan et al., 2000). McMillan et al. (2000) suggested that the Uvas lavas are derived from the heating of the lithosphere from the convecting asthenosphere displacing areas of the ruptured and subducting Farallon Plate. This claim with geochemical data suggest that the Uvas parental source was derived through an evolving fractional crystallization process with the assimilation of granulite facies lower crust.

Analytical Procedures

Sample Preparation. Thin sections (30μm thick) from both Uvas basaltic-andesite and Rubio Peak Formation lava flows samples were made at Missouri State University's (MSU) geology rock lab to determine phenocryst phases and describe textures (Fig. 5.4). Reported unweathered quartz, plagioclase, biotite, magnetite, and pyroxene mineral separates were picked from crushed and sieved fraction (100 μm) of the whole rock. Samples picked were chosen based on their freshness and pureness to obtain the most representative results of their fractional crystallization. Alterations of grains ran

in analyses may not attest to the trueness of the samples and were therefore avoided. Approximately 10mg or more of grains for each mineral phase were collected and then cleaned in a diluted nitric acid bath solution (10:2).

Mineralogy and Petrology. Mineralogical and petrographic analysis of thin sections for Uvas and Rubio Peak samples were performed using equipment at MSU). Petrographic analysis of the samples was investigated to determine mineral constituents and provide stratigraphic comparisons between different mineral assemblages. Observed petrographic textures (Fig. 5.4) were then compared with previous research from Seager and Clemons (1975).

Whole Rock Geochemistry. Whole rock major and trace element geochemistry were ran at Washington State University in Pullman, Washington. Calibration of $^{87}Sr/^{86}Sr$ isotopic ratios were calculated using the $^{86}Sr/^{88}Sr$ ratio analyzed at 3.0 V aiming intensity and normalized to 0.1194 using NBS 987 Standard (0.710298 + 0.000010) to monitor the precision of the analyses. Sr was isolated using Sr-Spec resin column chromatography by the method described in Ramos and Reid (2005). Nd was separated using REE (rare-earth elements) resin column chromatography using the digested split of prepared sample for Sr chromatography. Nd isotopes were normalized to $^{143}Nd/^{144}Nd = 0.7219$ and results for JNDi-1 were $^{143}Nd/^{144}Nd = 0.512103 \pm 0.000011$ for five analyses. Pb isotopes were separated from the same digested samples used for Sr and Nd isotope ratios. Pb separations used ~2 mL of anion exchange resin in a high-aspect ratio glass column with an eluent of 1N HBr and 7N HNO_3. Purified samples were then dried and re-dissolved in 1 mL of 2% HNO_3 containing 0.01 ppm Tl. Samples were analyzed on a ThermoFinnigan Neptune multi-collector ICP-MS equipped with nine Faraday collectors and an ion

counter. The standard NBS 981 ($^{208}Pb/^{204}Pb \approx 36.662 \pm 0.002$, $^{207}Pb/^{204}Pb \approx 15.462 \pm 0.001$, $^{206}Pb/^{204}Pb \approx 16.928 \pm 0.001$) was used for accuracy corrections and to monitor precision of the analyses. The values measured for NBS 981 were within the error of published ratios for NBS 981 (Tod et al., 1998) and therefore corrections were not applied to unknown sample ratios.

Oxygen Isotope Analysis. Oxygen isotope measurements were then obtained and analyzed in the GeoAnalytical Laboratory at Washington State University by the method of Takeuchi and Larson, (2005). One standard of UWG-2 garnet of Valley et al. (1995) was measured with a difference of 0.2‰ from the published value of 5.89‰, relative to standard mean ocean water (SMOW) was used to acquire measurements. Data is illustrated in figures and presented in T 1 in permil using standard delta notation relative to SMOW.

Results

Uvas Basaltic Andesites. Majority of the basalts and basaltic-andesite lava flows from the Sierra de las Uvas volcanic field (UVF) are fine-grained with variable vescularity (0-35%; Fig. 5.4). These fine-grained textures are mostly hypocrystalline with a predominantly rich plagioclase groundmass. Percentage of minerals by volume include plagioclase (73.2-46.8%), clinopyroxene (38.1-9.2%) and hornblende (20.0-1.8%) with trace amounts of olivine (24.8-1.0%) and Fe-Ti oxides (14.1-1.0%). Plagioclase compositions are mostly andesine (An 30-50%) and are subhedral to euhedral. Plagioclase phenocryst range from 500μm to 1mm. Hornblendes are prevalent in some lavas and minor in others, with subhedral to anhedral grains ranging from approximately

10μm to 1mm. Olivine is primarily anhedral approximately 10μm to 150μm. Clinopyroxene is anhedral to subhedral approximately 10μm to 0.75mm. Fe-Ti oxides are mostly anhedral and approximately 10μm to 0.5mm Most of the of the lava flows are typically microvesicular to vesicular. High vesicular flows contain large calcite amygdules. Some of these amygdules include olivine and pyroxene grains that have been secondary replaced by calcite and quartz. (Fig. 5.4). Samples do not contain mantle xenoliths as seen in similar composition rocks from the younger Portillo volcanic field to the south (Thompson et al., 2005).

Rubio Peak Formation. Rubio Peak andesite lavas from the Mogollon-Datil volcanic field (MDVF) are very fine grained to fine grained with little vascularity (Fig. 5.4). Majority of these andesites contain a groundmass volume consisting of hornblende (14.8-2.2%), clinopyroxene (7.0-0.5%) and plagioclase (90.5-4.4 %). Fig. 5.4 displays this aphanitic texture. Hornblendes of these samples show clear euhedral boundaries and are found up to approximately 500μm, while plagioclase phenocryst (9.5-1.0%) are mostly subhedral. Rubio Peak Fe-Ti oxide phases are less common than Uvas lavas. Rubio Peak samples collected did not contain mantle xenoliths or glomerocryst.

Whole Rock Geochemistry. Whole rock geochemistry was determined for samples that include new data for radiogenic isotope ratios of the Uvas, Bell Top, Cooney Canyon, and Rubio Peak rocks. Major and trace element data were combined with data from McMillan et al. (2000). New radiogenic isotope ratios collected for UVF and RP samples coincide with previous published data from Davis and Hawkesworth, 1994; 1995) and McMillan et al. (2000). The whole rock geochemistry includes Rb, Sr, $^{87}Sr/^{86}Sr$, $^{143}Nd/^{144}Nd$ and ε_{Nd} values (Table 5.1). Fig. 5.6 displays the results for $^{87}Sr/^{86}Sr$

ratios vs ε_{Nd} values, with the tectonic and magmatic events associated with the Rubio Peak, Bell Top, and Uvas volcanic field to compare signatures to shifting tectonic regimes. Though $^{87}Sr/^{86}Sr$ ratio ranges are nearly similar for Rubio Peak and Uvas, ε_{Nd} values discriminate these magmatic events by the Rubio Peak having a relatively narrow range from approximately -5.6 to -3.5 (Fig. 5.6). As tectonics progressed and magmatism evolved ε_{Nd} ranges expand respectively in the volcanic rocks.

Oxygen Isotope Values. The oxygen isotope values for the Rubio Peak and Uvas lavas were sampled in several locations in the study area (Fig. 5.2). The Rubio Peak samples were obtained near the Winston area of the MDVF in a spatially distributed fashion. The Uvas volcanic rock samples were obtained from basalt and basaltic-andesite lava flows erupted from several scoracious cinder cones and low-local volcanic vents in the Big-White Gap area in a stratigraphic fashion (Fig. 5.2). The $\delta^{18}O$ values of basalt to andesite rocks were measured for comparison to one another and used to constrain their roles in magma genesis and potential crustal contamination. These values were used to measure the potential amount of crustal contamination and hybridization over the lifespan of the Rubio Peak and Uvas suite. Oxygen isotope data was collected from Uvas and Rubio Peak mineral separates including: pyroxene, plagioclase, quartz, and magnetite. Additional oxygen isotope data was collected from mineral separates, quartz, bitotite, and plagioclase in the Kneeling Nun and the Cooney Canyon tuff (Bell Top age) samples. Oxygen isotope values from the collected volcanic units showed a wide range in calculated values upon different mineral constituents (Fig. 5.7). Oxygen isotope values for the Rubio Peak range from (4.88-5.40), Uvas suite ranges from (2.10-18.90), Kneeling Nun (4.82-8.01), and the Cooney Canyon tuff (5.21-8.23) Two unidentical

trends were observed from these ranges. The $\delta^{18}O$ values from the Rubio Peaks mineral separates show a nearly linear trend along the "normal differential array". Given that the compositions in the Rubio Peak lavas are quite different to each other, the $\delta^{18}O$ values between samples of varying composition reflect a restricted and small range. These $\delta^{18}O$ values suggest that the Rubio Peak lavas were from a compositionally homogenous magma at equilibrium. The values from the Kneeling Nun and Cooney Canyon tuff share a similar range in values. These values are modeled just slightly below the normal differential array and above which reflect a nearly homogenous magma reservoir. The mineral separates from the Kneeling Nun and the Cooney Canyon tuff show similar $\delta^{18}O$ values that coincide with each other and the Rubio Peak Formation. The $\delta^{18}O$ values from the Uvas mineral separates show a relatively wider range than the Rubio Peak lavas, Kneeling Nun tuff and Cooney Canyon tuff. These values are above and below the normal differential array, indicating that these are were high and low $\delta^{18}O$ magmas. This systematic variation suggest that the Uvas lavas were associated to a heterogenous melt at disequilibrium and significant crustal contamination.

Discussion

Determining the degree of crustal contamination in magmatic sources for the Sierra de las Uvas volcanic field (UVF) is problematic due to the complexity of radiogenic isotope ratios and trace element concentrations in the basement of southern New Mexico. Thus suggested models have only qualitatively determined the effects of crustal contamination on magma differentiation in the UVF and Rubio Peak Formation. Oxygen isotope values combined with these data better differentiate the suggested

boundary between crustal and magmatic sources and allow for the quantitative volume of each source. These oxygen isotope values help identify and quantify the hybridized magma and crustal contaminants (Michelfelder et al., 2013).

Oxygen isotope variation of Uvas basaltic-andesitic melts and derived sources in crustal contaminated environments. Geochemical data of the Uvas basaltic-andesite lavas provide important insights on Uvas magma source migration from lithospheric melting to extensive volcanism. From the model in Figure 5.7 the stratigraphic and $\delta^{18}O$ value relationships of Uvas lava units can be considered. Figure 5.7 depicts the $\delta^{18}O$ value Uvas lavas to be above and below the normal differential array, resulting from an open-system between crustal assimilation and melt. Lower stratigraphic lava flows show respectively higher $\delta^{18}O$ values (7.52-18.90) than upper flows (2.10-5.64). The most plausible and simplest explanation for the UVF magmatic source to consist of high $\delta^{18}O$ values is that the lithospheric parental melts incorporated lower and upper crustal components upon migration to the surface. This interpretation is consistent with new radiogenic data and isotopic data from McMillan et al. (2000), which show wide scattering of Sr, Nd, and Pb isotopic data from UVF rocks and compared to $\delta^{18}O$ values (Fig. 5.5 and 5.8). Plagioclase and one quartz mineral separate coincide with the crustal contamination suggested from $^{87}Sr/^{86}Sr$ ratios. Plagioclase $\delta^{18}O$ values range from 12.87-18.90 and one high quartz value of 7.52. These high $\delta^{18}O$ values for some Uvas plagioclase suggest that they are contaminants consumed during assimilation and not from the magma reservoir during fractional crystallization (France et al., 2016). This variability in $\delta^{18}O$ values reflects that the composition of the Uvas magma chamber did not homogenized prior to eruption (Eiler 2001; Binderman, 2008).

Magmatic migration is suggested by radioactive signatures ($^{87}Sr/^{86}Sr$ and ε_{Nd}) that indicate the Uvas magmas assimilated upper- lower crustal components and low $^{18}\delta O$ values (5.64-2.1). The large array of $^{87}Sr/^{86}Sr$ (0.704404 to 0.707085) isotope values reflect the increasing infiltration of wall rocks from both upper and lower crust, which reflects a magmatic system in disequilibrium. Interpreting $^{87}Sr/^{86}Sr$ ratios provide the ability to suggest the involvement of upper and lower crustal components that were incorporated in the mobilizing magma, but more importantly whether they were fractionally crystallized at shallower or deeper depths. Similar studies show that crustal input in continental arc settings has been estimated by at other arc settings, such as the Central Andes and the Cascades (Feeley and Sharp 1995; Feeley et al., 2008). The disequilibrium of the Uvas lavas accounts for variations in the degree of melting, parental source composition, and fractional crystallization processes (Eiler, 2001).

The low $\delta^{18}O$ values, found below the "normal-differential array", signify an involvement with hydrothermal altered component (Bindeman, 2008). These values were determined in quartz and pyroxene phenocryst to contain values between 2.1-4.29‰. This is observed only in the stratigraphic lowest lavas. Additionally, the mineral-melt isotopic fractionation factor is relatively high (+7.0‰) in measured $\delta^{18}O_{\text{plagioclase}} - \delta^{18}O_{\text{pyroxene}}$ values. This suggest that secondary alteration is present rather than an inheritance from an unaltered primary magmatic source.

Rubio Peak lavas oxygen isotope variations and their basaltic-andesitic melts derived sources in crustal contaminated environments. The $\delta^{18}O$ values of the andesite lavas from the MDVF are relatively linear and similar for a particular composition within the normal differential array (Fig. 5.8). Rubio Peak samples are

suggested to have differentiated from a complex magmatic system, which raises the questions of what implications could prior be involved with this andesitic system. Interpretations in this regard promote the ideas of remobilization of magmatic storage, and filtration and recharge for propagating parental magmas to erupt homogenously (Kent et al., 2010; Cooper and Kent, 2014). In these remobilizing systems, it is theorized that eruption filters effectively intermingle between magmas but their densities and thermal constraints refrain them from mixing (Kent et al., 2010). Remobilization of the constrained magma from the bulk reservoir then migrates through the crust and fractional crystallization produces a new homogenous composition (Kent et al., 2010). This explanation would account for why there is little detection of crustal contamination in the homogenous composition of Rubio Peak andesites with ample scattering of radiogenic values.

If crustal sources were to be as isotopically heavy, they would account for an increase in $\delta^{18}O$ values of the andesite samples. No signature of assimilations are detected in phenocryst from Rubio Peak rocks. These phenocrysts coincide along the normal differential array, indicating that these volcanic rocks fractionally crystallized from a homogenous magma. Furthermore, the crystal fractionation of the andesites have constrained $^{87}Sr/^{86}Sr$ ratios that are not isotopically higher than the lavas regarding crustal sources. This evidence suggest that the Rubio Peak volcanic rocks were not significantly displaced enough in the crust to introduce the idea of magma mixing ratios (Cooper and Kent, 2014).

In the Kneeling Nun tuff I see similar $\delta^{18}O$ values to the Rubio Peak, along the normal differential array (Fig. 5.8). These $\delta^{18}O$ values tend to be slightly higher, as

expected for a more felsic suite and analyzed quartz and biotite (Bindeman, 2008). The increase in these values may also be due to the eruptive episodes having a high flux heating, causing the assimilation of crustal constituents prior to eruption. Similarly, I see that the Cooney Canyon tuff shares the same oxygen isotope ratios for its phenocrysts (quartz, biotite, and plagioclase). These isotopic correlations between the Kneeling Nun and Cooney Canyon tuffs suggest they may have similar petrogenesis, which may shed light in understanding the magmatic processes associated with the Rubio Peak.

Model for AFC crustal contamination and $\delta^{18}O$ differentiation. To track and trace crustal contamination within a melt, close examination of the calculated oxygen isotopes values must first be utilized to consider the composition of the parental melt and crustal contaminants. The parental melt is particularly important to estimate the fractionation factor between the observed phenocryst and the parental melt. At equilibrium, such volcanic rocks should have a clear and consistent values of minerals, $\delta^{18}O_{mineral\text{-}mineral}$ and $\delta^{18}O_{mineral\text{-}melt}$ isotopic fractionations (Bindeman, 2008). This amount of $\delta^{18}O$ heterogeneity is vital in that provides fractionation of

$$\Delta^{18}O_{mineral\text{-}melt} = \delta^{18}O_{mineral} - \delta^{18}O_{melt}$$

However, some petrogenetic processes distort a system into having and a larger array of $\delta^{18}O$ values and $\delta^{18}O_{mineral\text{-}melt}$ disequilibrium (Bindeman, 2008). These processes include: (1) Interactions with waters or brines derived from country rocks or stopped blocks, (2) rapid assimilation of rocks significantly different in $\delta^{18}O$ that it affects magma and not protocryst, (3) partial melting of rocks with groundmass that has suffered hydrothermal alteration followed by mixing with more normal magma, and (4) complete

or bulk melting of shallow hydrothermally-altered rocks followed by an eruption of magma at the surface (Bindeman, 2008).

The difference between the calculated $\delta^{18}O$ values for Rubio Peak magmatism versus Oligocene Uvas volcanism is best explained as two separate processes. Rubio Peak lavas derived from parental compositions that were differentiated from fractional crystallization and residual magmas that further underwent magma recharge filtering. The Uvas lavas reflects a systems that derived from parental magmas assimilating both upper and lower crustal components (Fig. 5.9). Though both of these units are classified as andesitic compositions, their magma processes are suggested by their bulk chemical changes.

In Figure 5.9 the rock types of the Rubio Peak, Uvas, Kneeling Nun, and Cooney Canyon are modeled from Feeley and Sharp (1995), in respect to their weight percentage of SiO_2 and $\delta^{18}O$ values. The normal $\delta^{18}O$ array shown, indicates rocks of parental composition and an interpreted assimilation fractional crystallization (AFC) curve is provided to illustrate the effects of fractional crystallization and assimilation processes. Additionally, arrows provided to show mixing and mingling of open-system processes with heterogeneous melts. Because of little scattering and nearly segregated values based on weight percentage SiO_2, the likelihood of mixed or mingled reservoirs between these units is not emphasized. The AFC curve represents the potential differences in assimilation and fractional crystallization processes. Because plagioclase phenocrysts of the Uvas are indicated at such high $\delta^{18}O$ values, I suggest these phenocrysts are potential contaminants that not are not from the Uvas host lavas. To evaluate the differences of the Rubio Peak and Uvas rocks I determined the $\delta^{18}O$ value ranges for mineral separates

from these units. Pyroxene and plagioclase $\delta^{18}O$ values from these units suggest two different magmatic systems. As discussed, Uvas rocks have a large scattering of high and low $\delta^{18}O$ values indicating input of crustal contamination, while Rubio Peak rocks have similar $\delta^{18}O$ values indicating a homogenous source. Figure 5.9 illustrates these two different systems do not converge at low SiO_2 content or similar $\delta^{18}O$ values. This suggests that the parental magma compositions from both of these calc-alkaline units did not result from common magmatic processes (Feeley et al., 2008).

Conclusions

Oxygen isotope data from volcanic rocks of the Sierra de las Uvas volcanic field (UVF) and the Mogollon-Datil volcanic field (MDVF) record the importance of crustal contamination and evolving temporal magmatic systems. The oxygen isotope analyses of the Uvas lavas reveal crustal components were assimilated based on high $\delta^{18}O$ values present in lower stratigraphic flows. Evidence is supported by $\delta^{18}O$ variations of UVF lavas vs nearly consistent $\delta^{18}O$ values in the Rubio Peak. New oxygen isotope data proposes and correlates with data from McMillan et al., (2000) that upper-crustal components were involved in assimilating Eocene arc-magmatism (F 5.7) and the Uvas basaltic-andesites consist of upper and lower crustal contaminants.

Upper crustal components of early Oligocene volcanic rocks are suggested to be detected in the earliest of Uvas lavas. Furthermore, isotopic trends of lower crustal signify that interactions between the lithospheric melts from the Uvas are also consistent with the proposed idea of assimilating local-lower crust in the Uvas magmatic system. The contributions of both upper and lower crust in the differentiated lavas from the UVF

further agree with previous research that lithospheric melts incorporated lower crust with the lithospheric mantle becoming highly ductile during the Oligocene extension (Morgan et al., 1986; McMillan et al., 2000). In conclusion, I have made five observations based on the $\delta^{18}O$ values for the studied rock samples:

1) I observed an increase in $\delta^{18}O$ values in mid-stratigraphic lava flows of the UVF followed by a decreasing trend for overlying lava flows.

2) I observed that pyroxene mineral separates predominately followed a trend slightly below the "normal differential array".

3) I observed that $\delta^{18}O$ values for Rubio Peak samples were linear with the "normal differential array" (4.88-5.4). Rubio peak samples show little crustal contamination, this data suggest that the Rubio Peak andesites were composed of melts that differentiated through fractional crystallization versus the previous idea that the andesites were composed to mixing melts.

4) I observed that Kneeling Nun tuff and Cooney Canyon tuff samples represented nearly identical high $\delta^{18}O$ values from their quartz and plagioclase phase. Both of these units are relatively close in age, and I find it that these results are a representative value for these rocks. In addition, I interpolate that their parental melts correspond with elevating $\delta^{18}O$ values from the exchanging and assimilation of crustal rocks. I believe at this significant eruption, the temporal trend from progressive arc-magmatism begins to shift and the Farallon Plate in being recycled back into the mantle.

5) Despite increasing $\delta^{18}O$ values of plagioclase from Rubio Peak to the UVF there is question if all values correspond effectively to the trend. Alteration by meteoric waters may be the link for the diversity in these values.

References

Annen, C., Blundy, J and Sparks, R., 2006, The genesis of intermediate and silicic magmas in deep crustal hot zones: Journal of Petrology, v. 47, p. 505-539.

Best, G.M., Christiansen, E.H., de Silva, S., and Lipman, P. L., 2016, Slab-rollback ignimbrite flareups in the southern Great Basin and other Cenozoic American arcs: A distinct style of arc volcanism: Geological Society of America, v. 12, p. 1097-1135, doi: 10.1130/GES01285.1.

Bindeman, I., 2008, Oxygen isotope in mantle and crustal magmas as revealed by single crystal analysis: Mineralogical Society of America, v. 69, p. 445-478, doi:10.2138/rmg.2008.69.12.

Bohrson, W.A. and Spera, F.J., 2001, Energy-constrained open-system magmatic processes II: application of energy-constrained assimilation–fractional crystallization (EC-AFC) model to magmatic systems: Journal of Petrology, v. 42, p. 1019–1041.

McIntosh, W.C., 1989, Timing and distribution of ignimbrite volcanism in the Eocene–Miocene Mogollon-Datil volcanic field, in Chapin, C.E., and Zidek, J., eds., Eocene–Miocene Mogollon-Datil volcanic field, New Mexico, Excursion 6A: IAVCEI Field Excursions, New Mexico Bureau of Mines and Mineral Resources, Memoir 46. p. 58-59.

Cameron, K.L., Nimz, G.J., and Kuentz, D., 1989, Southern cordilleran basaltic andesite suite, southern Chihuahua, Mexico: A link between Tertiary continental arc and flood basalt magmatism in North America: Journal of Geophysical Research, v. 94, p.7817-7840.

Cather, S. M. 1990. Stress and volcanism in the northern Mogollon-Datil volcanic field, New Mexico: Effects of post-Laramide tectonic transition: Geological Society of America Bulletin, v. 102, p. 1447–1458.

Chapin, C.E., McIntosh, W. C., and Chamberlin, R. M., 2004, The late Eocene-Oligocene peak of Cenozoic volcanism in southwestern New Mexico, in Mack, G. H., and Giles, K. A., eds., The geology of New Mexico: A geologic history: New Mexico Geological Society Special Publication, v. 11, p. 271-293.

Clemons, R. E., 1979, Geology of Good Sight Mountains, Luna County, New Mexico: New Mexico Bureau of Mines and Mineral Resources Circular, v. 169, p. 32.

Clemons, R.E., 1982, Geology of Massacre Peak quadrangle, Luna County, New Mexico: New Mexico Bureau of Mines and Mineral Resources, Geologic Map 51, scale 1:24,000.

Cooper, K.M., and Kent, A.J.R., 2014, Rapid remobilization of magmatic crystals kept in cold storage: Nature, v. 506, p. 480-483.

Copeland, P., Murphy, M.A., Dupré, W.R., and Lapen T.J., 2011, Oligocene Laramide deformation in southern New Mexico and its implications for Farallon plate geodynamics: Geosphere, v.7, p. 1209-1219.

Davis, J.M., Elston, W.E., and Hawkesworth, C.J., 1993, Basic and intermediate volcanism of the Mogollon-Datil volcanic field: Implications for mid-Tertiary tectonic transitions in southwestern New Mexico, USA, in Prichard, H.M., Alabaster, T., Harris, N.B.W., and Neary C. R., eds., Magmatic processes and plate tectonics: Geological Society [London] Special Publication, v. 76, p. 469-488.

Davis, J.M., and C.J., Hawkesworth, 1994, Early calc-alkaline magmatism in the Mogollon-Datil Volcanic Field, New Mexico, USA: Journal of the Geological Society, v. 151 p. 825-843.

Davis, J.M., and C.J., Hawkesworth, 1995, Geochemical and tectonic transitions in the evolution of the Mogollon-Datil Volcanic Field, New-Mexico, USA: Chemical Geology, v. 119, p. 31-53.

de Silva, S.L., 2008, Arc magmatism, calderas, and supervolcanoes: Geology, v. 36, p. 671–672, doi:10.1130/focus082008.1.

Dufek, J. and Bergantz, G.W., 2005, Lower crustal magma genesis and preservation: A stochastic framework for the evaluation of basalt–crust interaction: Journal of Petrology, v. 46, p. 2167-2195, doi: https://doi.org/10.1093/petrology/egi049.

Eiler, J.M., 2001, Oxygen Isotope Variations of Basaltic Lavas and Upper Mantle Rocks: Reviews in Mineralogy and Geochemistry, v. 43, p. 319-364, doi: 10.2138/gsrmg.43.1.319.

English, J.M., and S. T. Johnston, 2004, The Laramide Orogeny: What were the driving forces?: International Geologic Review, v. 46, p. 833–883.

Farmer, G.L., Bailey, T., Elkins-Tanton, L.T., 2008, Mantle source volumes and the origin of the mid-Tertiary Ignimbrite flare-up in the Southern Rocky Mountains, western U.S: Lithos, v. 102, p. 279-294.

Feeley, T.C., and Sharp, Z.D., 1995, 18O/16O isotope geochemistry of silicic lava flows erupted from Volcan Ollagüe, Andean Central Volcanic Zone: Earth and Planetary Science Letters, v. 133, p. 239-254.

Feeley, T.C., Clynne, M.A., Winer, G.S., and Grice W.C., 2008, Oxygen isotope geochemistry of the Lassen Volcanic Center, California: Resolving crustal and mantle contributions to continental arc magmatism: Journal of Petrology, v. 49, p.971-997.

Ferrari, L., Valencia-Moreno, M., and Bryan, S., 2007, Magmatism and tectonics of the Sierra Madre Occidental and its relation with the evolution of the western margin of North America, in Alaniz-Alvarez, S.A., and Nieto-Samaniego, A.F., eds., Geology of Mexico: Celebrating the Centenary of the Geological Society of Mexico: Geological Society of America Special Paper, v. 422, p. 1–39, doi:10.1130/2007.2422(01).

Fodor, R.V., 1975, Petrology of basalt and andesite of the Black Range, New Mexico: Geological Society of America Bulletin, v. 85, p. 295-304.

France, L., Demacon, M., Gurenko, A.A., and Briot, D., 2016, Oxygen isotopes reveal crustal contamination and a large, still partially molten magma chamber in Chaîne des Puys (French Massif Central): Lithos, v. 260 p. 328-338.

Freund, S., Beier, C., Krumm, S., Haase, K.M., 2013, Oxygen isotope evidence for the formation of andesitic–dacitic magmas from the fast-spreading Pacific–Antarctic Rise by assimilation–fractional crystallization: Chemical Geology, v. 347, p. 271–283.

Gans, P.B., and Bohrson, W.A., 1998, Suppression of volcanism during rapid extension in the Basin and Range province, United States: Science, v. 279, p. 66-68.

Gibson, S.A., Thompson, R.N., Leonardos, O.H., Dickin, A.P., and Mitchell, J.G., 1995, The Late Cretaceous impact of the Trindade mantle plume: Evidence from large-

volume, mafic, potassic magmatism in SE Brazil: Journal of Petrology, v. 36, p. 189-229.

Johnson, C.M., Lipman, P.W., and Czamanske, G.K., 1990, H, O, Sr, Nd, and Pb isotope geochemistry of the Latir volcanic field and cogenetic intrusion, New Mexico, and relations between evolution of a continental magmatic center and modifications of the lithosphere: Contributions to Mineralogy and Petrology, v. 104, p. 99–124, doi:10.1007/BF00310649.

Kent, A.J.R., Darr, C., Koleszar, A.M., Salisbury, M.J., and Cooper, K.M., 2010, Preferential eruption of andesitic magmas through recharge filtering: Nature Geoscience, v.3, p. 631-636.

Kluth, C. F., and Schaaftenaar, C. H., 1994, Depth and geometry of the northern Rio Grande rift in the San Luis basin, south-central Colorado, in Keller, G. R., and Cather, S. M., eds., Basins of the Rio Grande rift: Structure, stratigraphy, and tectonic setting: Geological Society of America Special Paper, v. 291, p. 27–37.

Lipman, P.W., and Bachmann, O., 2015, Ignimbrites to batholiths: Integrating perspectives from geological, geophysical, and geochronological data: Geosphere, v. 11, p. 705–743.

Loewen, M.W., Bindeman, I.N., 2016. Oxygen isotope thermometry reveals high magmatic temperatures and short residence times in Yellowstone and other hot-dry rhyolites compared to cold-wet systems: American Mineralogist v. 101, p. 1222-1227, doi: 10.2138/am-2016-5591.

Mack, G.H., Nightengale, A.L., Seager, W.R., and Clemons, R.E., 1994, The Oligocene Goodsight-Cedar Hills half graben near Las Cruces and its implications to the evolution of the Mogollon-Datil volcanic field and to the southern Rio Grande rift: New Mexico Geological Society 45th Annual Fall Field Conference Guidebook, p. 135-142.

Mack, G.H., 2004, Middle and late Cenozoic crustal extension, sedimentation, and volcanism in the southern Rio Grande rift, Basin and Range, and southern Transition Zone of southwestern New Mexico, in Mack G.H and Giles, K.A., eds, The Geology of New Mexico: A Geologic History: New Mexico Geological Society, Special Publication 11, p. 389-406.

McMillan, N., 1998, Temporal and spatial magmatic evolution of the Rio Grande rift: New Mexico Geological Society Guidebook, v. 49, p. 107-116.

McMillan, N.J., Dickin, A.P., and Haag, D., 2000, Evolution of magma source regions in the Rio Grande rift, southern New Mexico: Geological Society of America Bulletin, v. 112, p. 1582-1593.

Michelfelder, G.S., and McMillan, N.J., 2012, Geochemistry, origin, and U-Pb zircon ages of the Sierra Cuchillo laccolith, Sierra County, New Mexico, New Mexico Geological Society Guidebook, 63rd Field Conference, p. 249-260.

Michelfelder, G.S., Feeley, T.C., Wilder, A.D., and Klemetti, E.W., 2013, Modification of the Continental Crust by Subduction Zone Magmatism and Vice-Versa: Across-Strike Geochemical Variations of Silicic Lavas from Individual Eruptive Centers in the Andean Central Volcanic Zone: Geosciences, v. 3, p. 633-667.

Morgan, P., Seager, W. R. & Golombek, M. P., 1986, Cenozoic thermal, mechanical and tectonic evolution of the Rio Grande rift: Journal of Geophysical Research, v. 91, p. 6263–627.

Norini, G., Groppelli, G., Sulppizio, R., Nunez, G.C., and De Franco, R., 2015, Structural analysis and thermal remote sensing of the Los Humeros Volcanic Complex: Implications for volcano structure and geothermal exploration: Journal of Volcanology and Geothermal Research, v. 301 p. 221-237.

O'Neill, J.M., 2002, Geologic investigations in the Lake Valley area, Sierra County, New Mexico: U.S. Geological Survey, Professional Paper 1644, 4 Chapters, 1 plate, 78 p. D-B&R (TZ).

Ramos, F.C., and Reid, M.R., 2005, Distinguishing melting of heterogeneous mantle sources from crustal contamination: Insights from Sr isotopes at the phenocryst scale, Pisgah Crater, California: Journal of Petrology v. 46, p. 999-1012, https://doi.org/10.1093/petrology/egi008.

Seager, W.R., 1975, Cenozoic tectonic evolution of the Las Cruces area, New Mexico: New Mexico Geological Society 26th Annual Fall Field Conference Guidebook, p. 241-250.

Seager, W.R., and Clemons, R.E., 1975, Middle to late Tertiary geology of the Cedar Hills–Selden Hills area, New Mexico: New Mexico Bureau of Mines and Mineral Resources Circular, v. 133, p. 1-24.

Takeuchi, A. and Larson, P.B., 2005, Oxygen isotope evidence for the late Cenozoic development of an orographic rain shadow in eastern Washington, USA: Geological Society of America, v. 33, p. 313-316.

Thompson, R. N., Ottley, C. J., Smith, P. M., Pearson, D. G., Dickin, A. P., Morrison, M. A., Leat, P. T. & Gibson, S. A., 2005, Source of the Quaternary alkalic basalts, picrites and basanites of the Potrillo Volcanic Field, New Mexico, USA-lithosphere or convecting mantle?: Journal of Petrology, v. 46, p. 1603-1643.

Underwood, S.J. and Clynne, M.A., 2017, Oxygen isotope geochemistry of mafic phenocrysts in primitive mafic lavas from the southernmost Cascade Range,

California: Mineralogical Society of America, v. 102, p.252-261, doi: https://doi.org/10.2138/am-2017-5588.

Valley, J.W., Kitchen, N., Kohn, M.J., Niendorf, C.R., and Spicuzza, M.J., 1995, UWG-2, a garnet standard for oxygen isotope ratios: Strategies for high precision and accuracy with laser heating, Geochimica et Cosmochimica Actav., v. 59, p. 5223-5231.

Zimmer M.J. and McIntosch W.C., 2013, crustal in Geochronologic evidence of upper-magmatism situ differentiation: Silicic Mexico: at the Organ caldera complex, New Geosphere, v. 9, p. 155-169.

Table 5.1: Radiogenic variations of Uvas lavas, Rubio Peak lavas and Cooney Canyon tuffs from whole rock samples.

Samples	Rb	Sr	$^{87}Sr/^{86}Sr$	$^{143}Nd/^{144}Nd_i$	$^{147}Sm/^{144}Nd$	$^{206}Pb/^{204}Pb$	$^{207}Pb/^{204}Pb$	$^{208}Pb/^{204}Pb$
CC-01	283	93	0.715022	0.512197	0.130395	18.430	15.561	38.474
UV-1	41	788	0.705075	0.512361	0.440969	17.209	15.424	37.210
UV-5	26	983	0.704767	0.512591	0.134127	17.587	15.466	37.733
TRP-6	43	646	0.706046	0.512339	0.124124	17.537	15.467	37.658

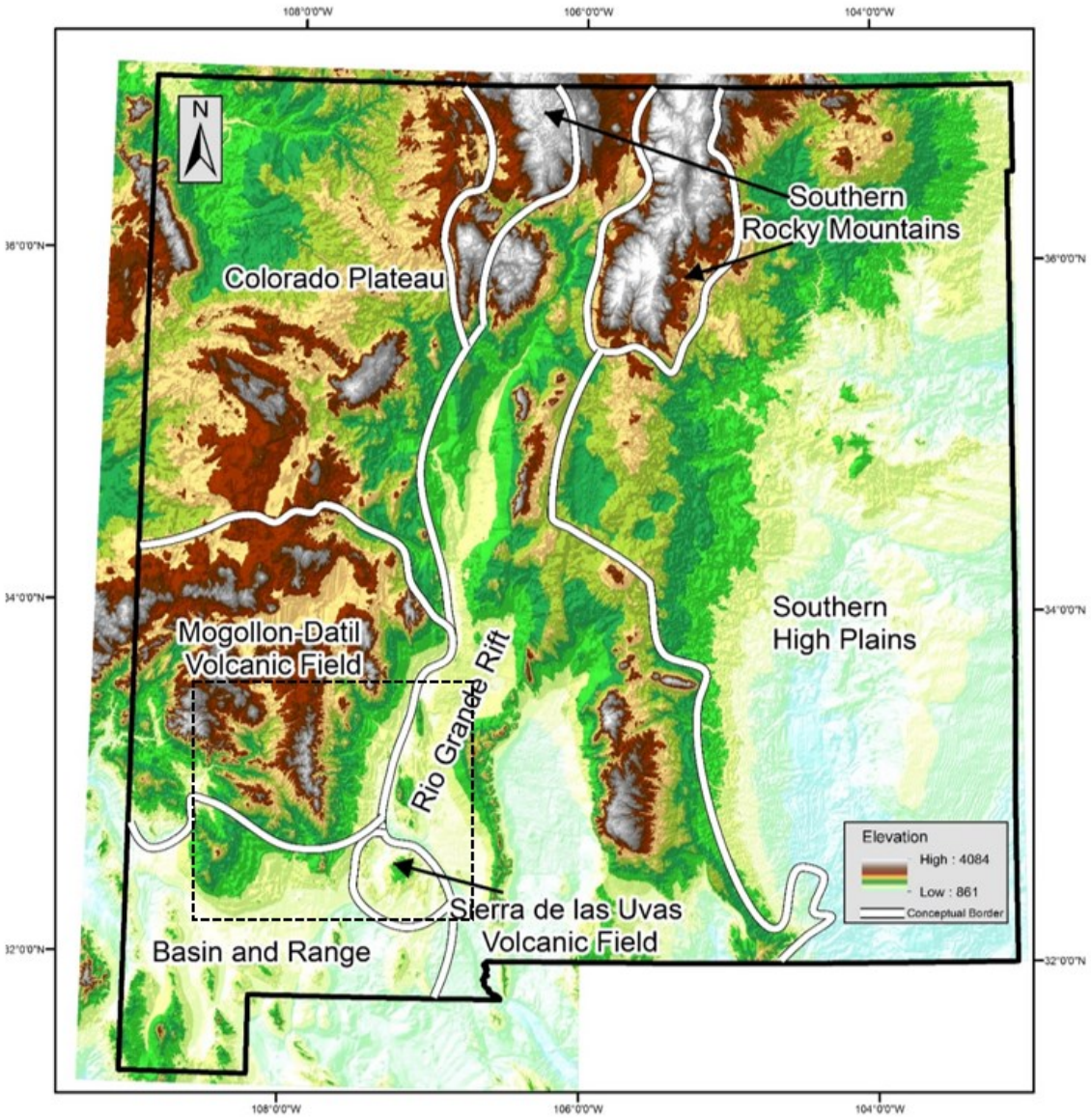

Figure 5.1: Digital Elevation Model (DEM) of New Mexico. Significant physiographic provinces are outlined to show boundaries of landforms and tectonic regimes. These provinces include: Southern Rocky Mountains (1.6-1.7 Ga), Colorado Plateau (1.6 Ga), Southern High Plains, Rio Grande Rift, Basin and Range (17 Ma), MDVF (40-24 Ma), and UVF (28-24 Ma). The study area consists of the UVF and the southern half of the MDVF.

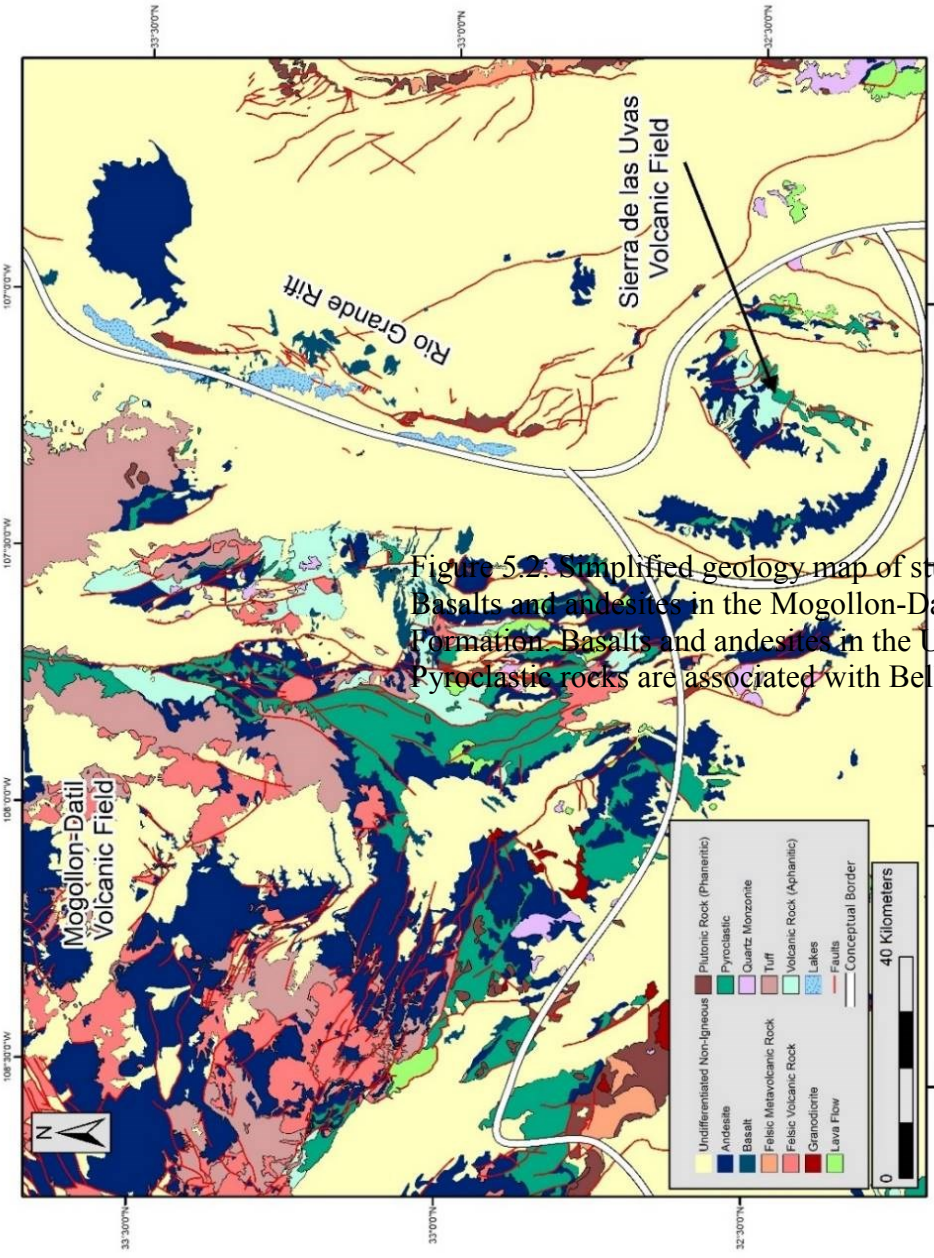

Figure 5.2. Simplified geology map of study area in southern New Me
Basalts and andesites in the Mogollon-Datil Field and associated with
Formation. Basalts and andesites in the UVF are associated with the U
Pyroclastic rocks are associated with Bell Top aged units.

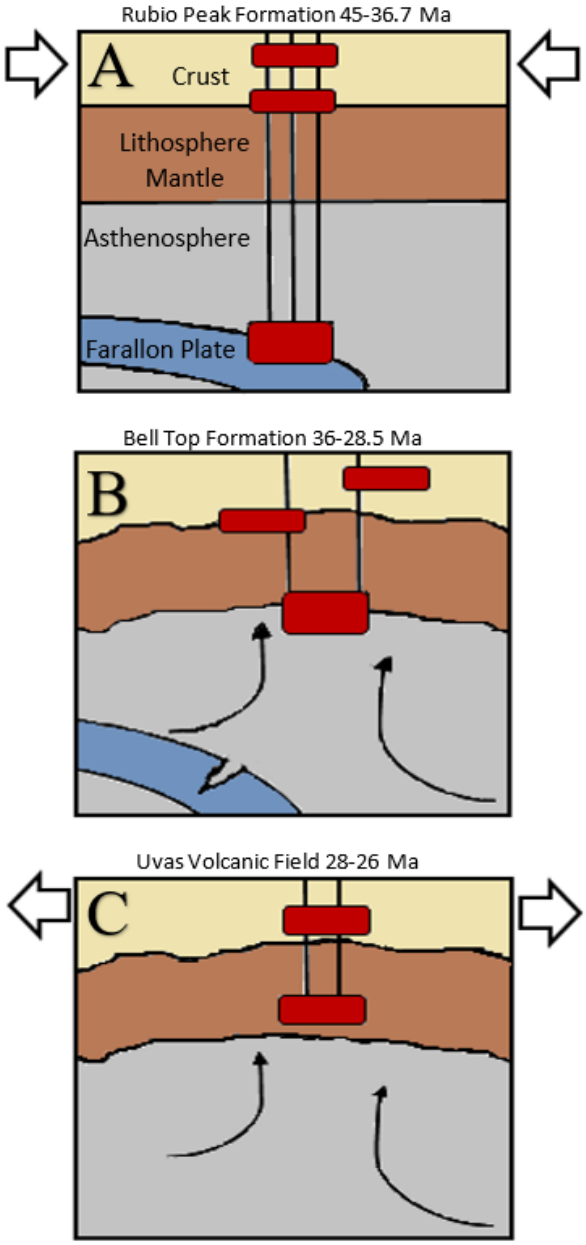

Figure 5.3. Schematic cross section illustrating a model of evolving magma sources during different tectonic regimes in southern New Mexico. A) Shows the continental arc magmatism associated with the subducting Farallon Plate. The Rubio Peak Formation is associated with this volcanism. B) Shows a model the Farallon Plate break-off. The volcanism associated with the slab break resulted in the ignimbrite flare-up, a switch from andesitic volcanism to bimodal volcanism, forming the Bell Top Formation. C) Showss the extensional tectonic stress regime where partial melts of lithospheric mantle were the sources of volcanism for the Uvas lavas. Modified from McMillan et al. (2000) and Michelfelder and McMillan (2012)

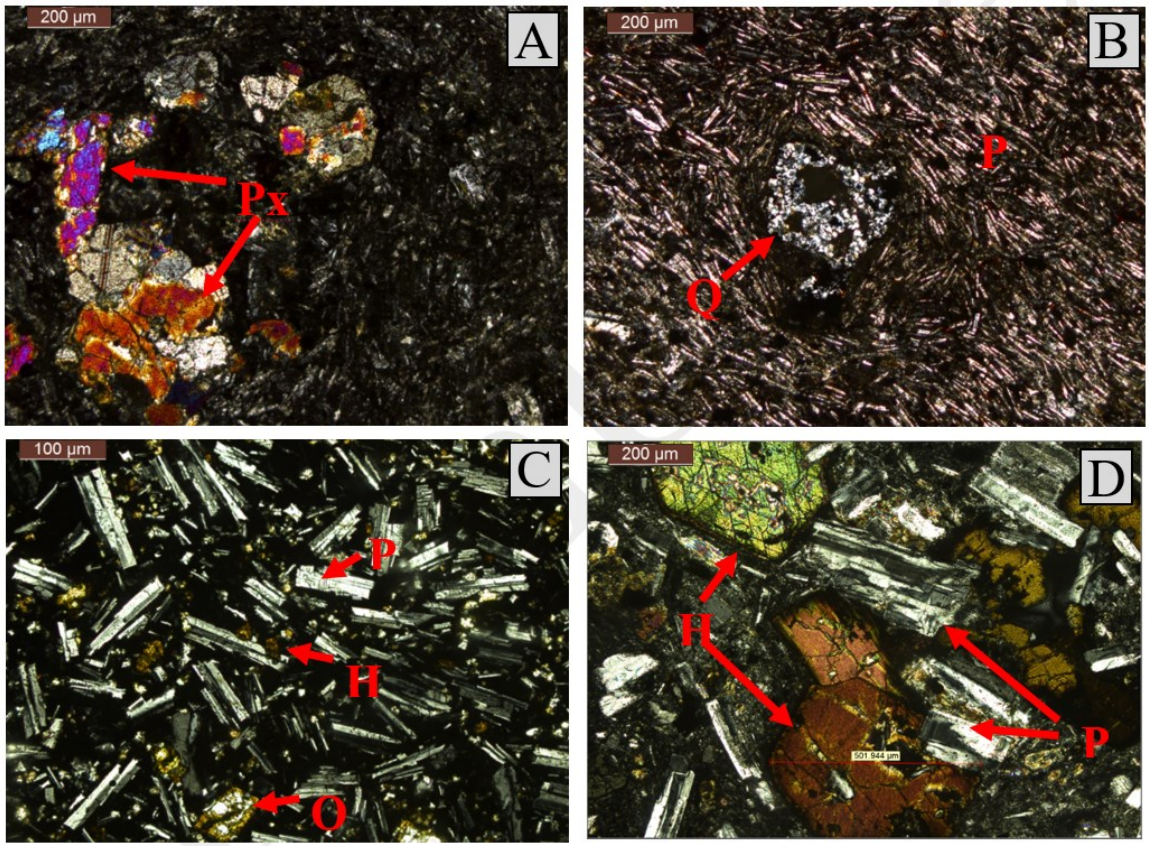

Figure 5.4: Illustrates the variations of phenocryst and textures in the Uvas basalt-basaltic andesites and the Rubio Peak andesites. A) Represents the lower Uvas lavas representing a very fine groundmass with pyroxene phases. B) Represents an upper Rubio Peak lava flow with nearly unidirectional flow banding around a quartz glomercryst. The quartz grain was most likely inherited from the lower sandstone substrate. C) Represents a very find grained Uvas with plagioclase grain not following a flow banding texture. D) Represents a Rubio Peak andesite showing relatively similar sizes of hornblende and plagioclase.

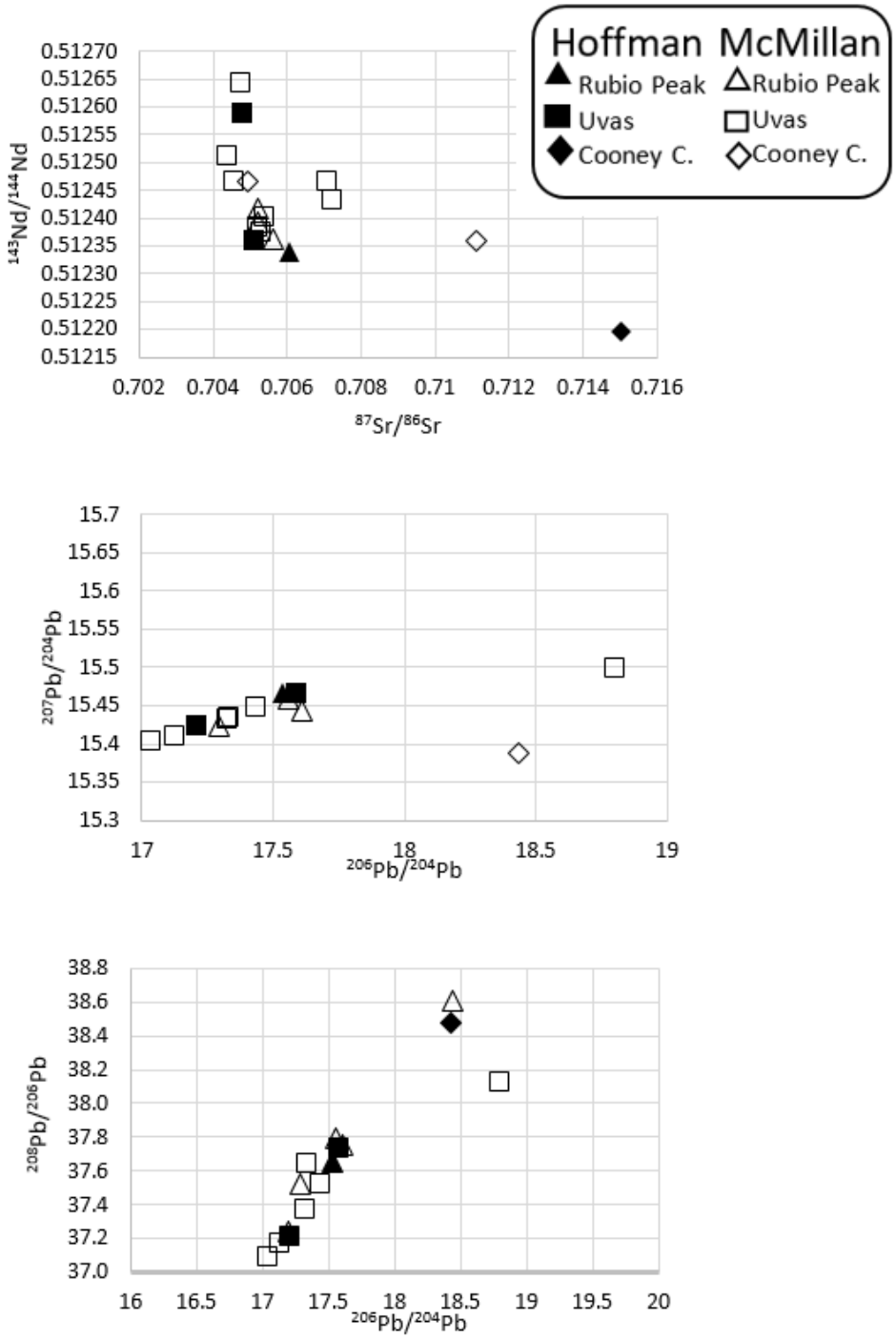

Figure 5.5: Radiogenic isotope compositions ($^{87}Sr/^{86}Sr$, $^{144}Nd/^{143}Nd$, $^{206}Pb/^{204}Pb$, $^{207}Pb/^{204}Pb$, $^{208}Pb/^{204}Pb$) compared of the Sierra de las Uvas basalts, Rubio Peak andesites and Coon Canyon tuff in south-central New Mexico. Data points are compared to prior research from McMillan et al. (2000).

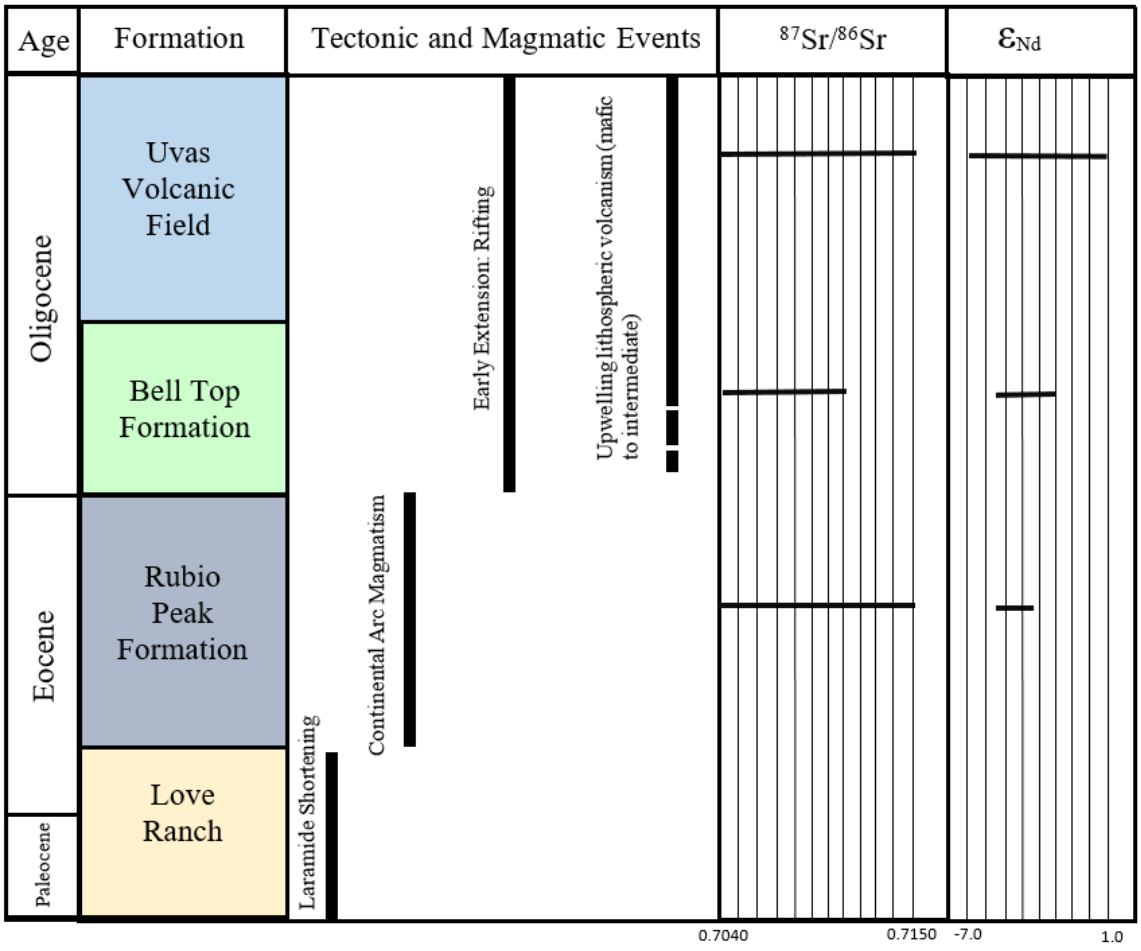

Figure 5.6: Tectono-stratigraphic column of south-central New Mexico. Modified from McMillan et al. (2000). Tectonic and magmatic events are compared to $^{87}Sr/^{86}Sr$ and ε_{Nd} to reflect changes in the shifting tectonic regime.

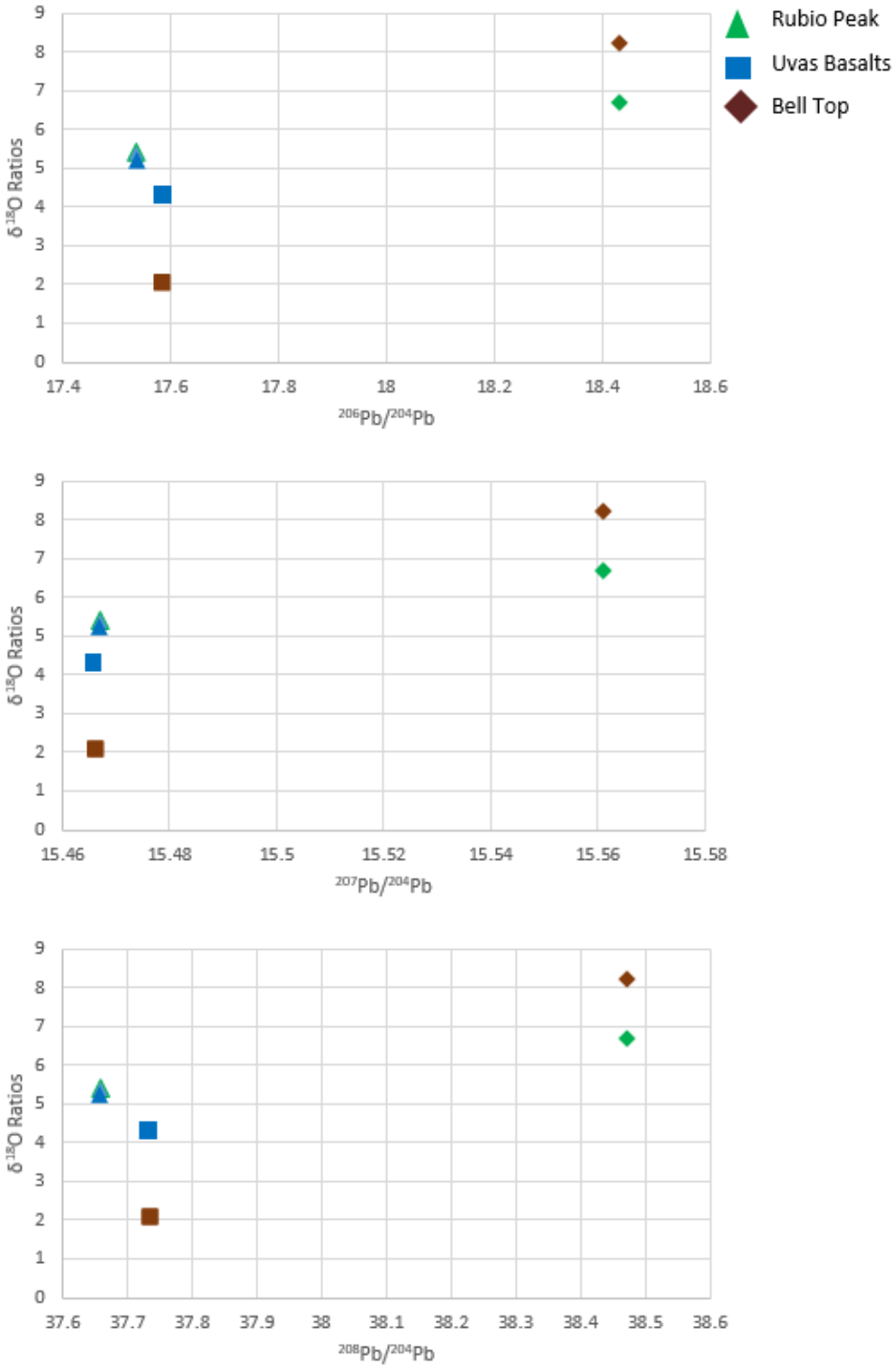

Figure 5.7: Radiogenic isotope compositions compared to oxygen isotope values of the Sierra de las Uvas basalts, Rubio Peak andesites and the Cooney Canyon tuffs in south-central New Mexico.

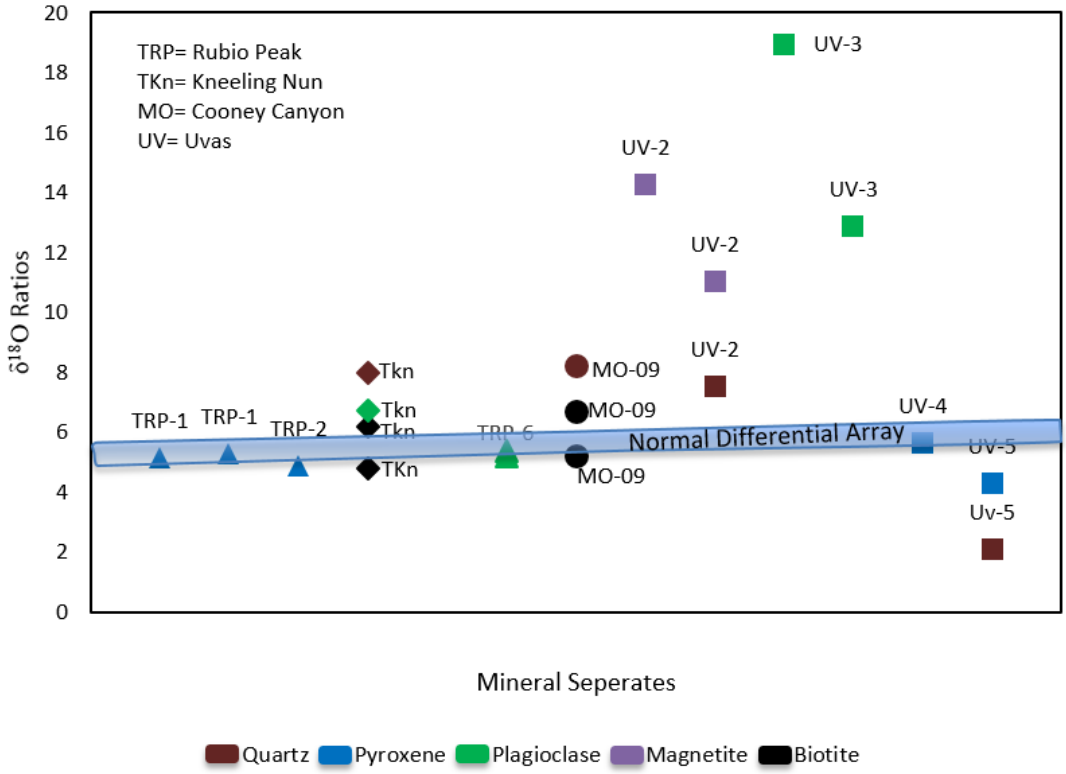
TRP= Rubio Peak
TKn= Kneeling Nun
MO= Cooney Canyon
UV= Uvas
δ18O Ratios
20
18
16
14
12
10
8
6
4
2
0
UV-3
UV-2
UV-3
UV-2
UV-2
Tkn
Tkn
Tkn
TKn
MO-09
MO-09
MO-09
UV-4
UV-5
Uv-5
TRP-1
TRP-1
TRP-2
TRP-6
Normal Differential Array
Mineral Seperates
Quartz
Pyroxene
Plagioclase
Magnetite
Biotite

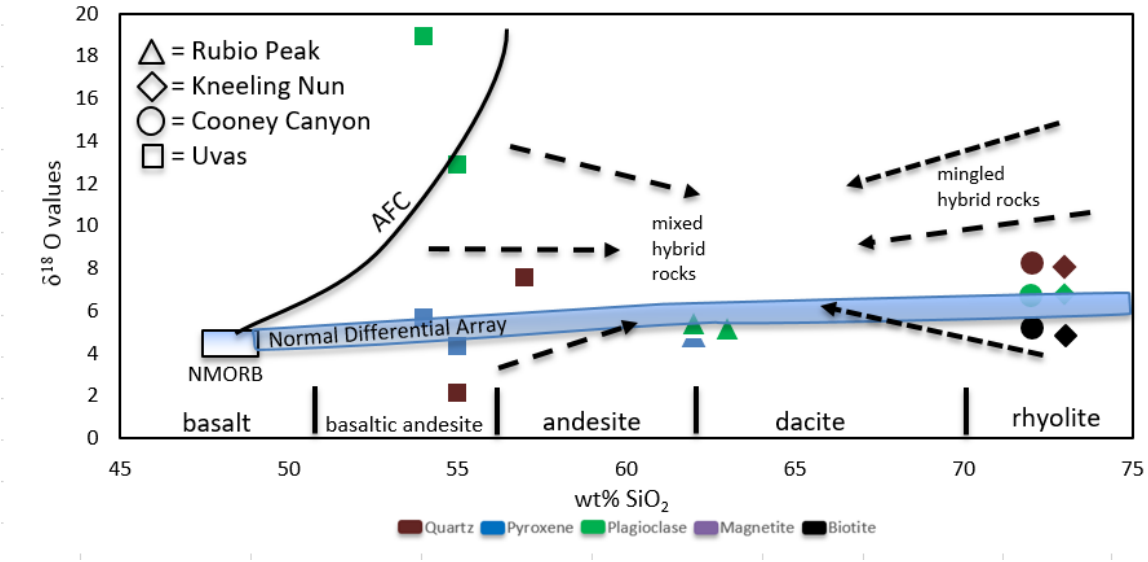

Figure 5.8: Oxygen isotope values from sampled volcanic rocks from the Sierra de las Uvas Volcanic Field (UVF) and Rubio Peak, Kneeling Nun tuff and Cooney Canyon tuffs from the Mogollon-Datil Volcanic Field (MDVF). Normal differential array from Bindeman, (2008).

CHAPTER 6 – CONCLUSIONS

In this chapter, the conclusions from both manuscripts presented above are summarized in addition to how the two studies relate to one another. The following provides a summary of the magmatic implications for the UVF and the Rubio Peak Formation of the MDVF; and to explain how their geologic record provides insight on crustal contamination and their evolving temporal magmatic systems. Shallow and deep magmatism are observed in this study to understand the role of crustal magmatism in south-central New Mexico. I use geochemical, remote-sensing, and statistical analysis in combination to determine if the probable sources associated with the UVF and the MDVF, help understand the shallow and deep magmatic migration, and the reflection of crustal contaminants involved.

Figure 5.9: Oxygen isotope values of mineral separates in the Sierra de las Uvas (UVF) and Mogollon-Datil (MDVF) volcanic rocks vs whole-rock SiO_2 wt %. The normal $\delta^{18}O$ differential array, roughly between 5.7±0.2‰, represents the most common parental basaltic magmas from mid-ocean ridges separating the low $\delta^{18}O$ and the high $\delta^{18}O$ fields (Bindeman, 2008). The normal $\delta^{18}O$ array illustrates a suggested closed-system while low $\delta^{18}O$ and high $\delta^{18}O$ magmas correlate to open-systems (Bindeman, 2008). The continuous curve labeled "AFC" corresponds to illustrate the effect of fractional crystallization with the addition of assimilating (high $\delta^{18}O$) heterogenous crust (Feeley et al., 2008). Dashed arrows illustrate the interpolated effect of mixed hybrid rocks (basaltic-andesites of UVF) and mingled hybrid rocks (rhyolitic tuffs and lavas of the MDVF).

The UVF shows many complex structural features, such as the Sierra de Las Uvas dome, large dissected cinder cones, buried volcanic centers, and fault patterns that account for its prior magmatic migration and volcanism. Structural and surface analysis using geospatial tools along with remote-sensed imagery provide calculated feedback to help better understand and explain the relationship between the Uvas lavas magmatic migration and the associated shallow-underlying fractures. From the combination of previous studies and mapping and new geospatial analysis, I have observed four magmatic implications associated with the development of the UVF:

1) The volcanic centers in the southern region share similar geometric parameters and orientation suggesting their magmatic propagation through the substrate was based on a magma feed fracture from distanced eruptive points. The results from the ellipticity, shape, and size of these cones correlate with behaviors of this suggested system with relatively high confining stresses. Due to these cones being preferentially more conical, opposed to more elongated, their eruptive points are presumed to be distanced. This does not exclude them from sharing the same magmatic conduit.

2) Volcanic centers in the central region are not as easily recognizable, but breach out as typical dissected cinder cones. Since volcanic centers erupting as more elongated and breached cones, their eruptive points suggest they are more clustered than the simple cones farther south. Though these cones are poorly developed, their spatial distribution to the center of the UVF strongly supports the suggestion for more clustered magmatic feed fractures. This does not relate these volcanic centers to sharing the same magmatic conduit but does suggest a closer relationship of conduits.

3) Magma migration follow a possible perpendicular path from fractures in a NE/SW alignment. Though difficult to determine and represent, in cases where strong tensional forces are distributed, volcanism typically follows weakened areas rather than obstacles through the substrate. Structural analysis suggest post-dated fault movements may further clarify alignment of faults and fractures.

4) These applications within the methodology are consistent with the inferred phenomenon for the magma-feed intrusions. The results from the aerial photos and structural analysis correlate with the structural and stratigraphic information. The results of this study do suggest the geometry of deep magmatic feed structures and displacements. However, the surface alignment

of fractures and the relationship of cones and dikes suggest a poorly developed deep magmatic plumbing system and how this system relates to proposed magma migration patterns. Therefore, combined structural patterns and magma-feed intrusions analysis allow interpretations of the shallow crustal channels that provided intrusive pathways for the development of the UVF.

These conclusions help distinguish and associate the development of the UVF to its proper tectonic regime. Since volcanoes are generally the product of regional tensional structures from extensional, strike-slip, and compression strains, their structural geometry can be utilized to quantify volcanic patterns (Adlyaman et al., 1998; Norini et al., 2015; and Tobisch and Cruden, 1995). Indications of the UVF volcanic vents being rooted from vertical tensional fractures are supported by the NW/SE fault patterns, the elongated cinder cones in the central area of the UVF, domal uplifting, and the linear volcanic cluster of smaller monogenic cones, located in the southern region of the UVF. Not only do the structural components reflect the local tectonic stress, but the addition of calc-alkaline and alkaline volcanism with extension has been described as the result of continental crust thinning related to subduction (Gülen, 1984). The geology, distribution, and shape of the volcanic centers are directly related the tectonic regime of southern New Mexico and similar volcanic fields, as shown by Chorowicz et al., (1994) and Corazzato and Tibaldi (2006). Since the alignment of volcanic centers is along a NE/SW trend, upper crustal fractures must coincide with the eruptive points. This evidence suggests that the alkaline-rich magmas that protruded through the continental substrate followed through crustal channels during extension and domal uplift allowing for perpendicular fault/volcanic center patterns to exist.

Oxygen Isotope Analysis of Volcanic Rocks in South-Central New Mexico

The results from of new oxygen isotope data in combination with published geochemical data from McMillan et al., (2000) and Davis et al., 1993; Davis and Hawkesworth 1994; 1995) suggest that upper crustal components were involved in assimilating in Eocene arc-magmatism of Rubio Peak Formation and Uvas basaltic andesites. However, Uvas lavas were more enriched with crustal input than those of Rubio Peak lavas. I find that proposed ideas of Uvas mantle sources did in fact assimilate lower and upper continental crust during Oligocene extension and magmatism. Rubio Peak andesites from lithospheric magmas have been interpreted to being congested from upper and crustal sources along with rift magmas, but new oxygen isotope data does not indicate trends to suggest this involvement.

Oxygen isotope analysis carried out from the UVF basaltic-andesite lava flow samples indicate various amounts of $\delta^{18}O$ values. Key $\delta^{18}O$ data from several mineral phases support that crustal contamination modified the lavas. These data values were composed during two different accumulation events; one trend having $\delta^{18}O$ values increasing in stratigraphically lower lavas, and the other trend having decreased $\delta^{18}O$ values below the normal-differential array in upper lavas. Accordingly, this suggest that crustal contamination was proceeded by initiation of tectonic rifting, and fractures allowing integration of low $\delta^{18}O$ groundwater to protrude into the evolving magmatic system, accounting for the decreasing $\delta^{18}O$ values below accepted mantle array values.

Though the UVF is a less familiar volcanic field compared to others in New Mexico it has a considerably significant geologic record that reflects the events of crustal contamination/assimilation. Primary mafic magmas from the subducted-lithospheric

mantle were contaminated by the addition of crustal rocks and by heated hydrothermal waters have left the the Uvas basaltic-andesites to have a wide range in $\delta^{18}O$ values.

The $\delta^{18}O$ values andesite lavas from the Rubio Peak Formation of the MDVF (4.88-5.4) plot along the normal differential array, indicating minimal crustal assimilation of the primary melt. This supports the idea that the Rubio Peak andesites were probably composed of parental melts that differentiated through fractional crystallization versus magma mixing or assimilation of an extensive crustal component. The debate surrounding the magmatic genesis of the Rubio Peak Formation raises the question of the relationship between the plutonic growth and the volcanism in the MDVF. I suggest the oxygen isotope data reveals that andesitic magma of the Rubio Peak was not dominated by magma mixing/crustal assimilation, but rather the consideration for mafic magma recharge. I suggest five key findings that provide insight into this relationship:

1) I observed an increase in δ18O values in mid-stratigraphic lava flows of the UVF followed by a decreasing trend for overlying lava flows. Increasing values above the normal mantle differential array reflect high δ18O magmas and voluminous crustal input. The increasing δ18O values after Rubio Peak and Kneeling Nun tuff suggest that crustal contamination increased in the Oligocene volcanism and rifting.

2) I observed that pyroxene mineral separates predominately followed a trend slightly below the “normal differential array”. I find confidence in that the pyroxene phases are quite representative of their mantle source.

3) I observed that δ18O values for Rubio Peak samples were linear with the “normal differential array” (4.88-5.4). Rubio peak samples show little crustal contamination, this data suggest that the Rubio Peak andesites were composed of melts that differentiated through fractional crystallization process versus the previous idea that the andesites were composed to mixing melts.

4) I observed that Kneeling Nun tuff and Cooney Canyon tuff samples represented nearly identical high δ18O values from their quartz and plagioclase phase. Both units are relatively close in age, and I find it that these results are a representative value for these rocks. In addition, I interpolate that their parental melts correspond with elevating δ18O values from the

exchanging and assimilation of crustal rocks. I believe at this significant eruption, the temporal trend from progressive arc-magmatism begins to shift and the Farallon Plate in being recycled back into the mantle.

5) Despite increasing δ18O values of plagioclase from Rubio Peak to the UVF there is question if all values correspond effectively to the trend. Alteration by meteoric waters may be the link for the diversity in these values.

References

Adıyaman, O., Chorowicz J., and Köse, O., 1998, Relationships between volcanic patterns and neotectonics in Eastern Anatolia analysis of satellite images and DEM: Journal of Volcanology Geothermal Research. v. 85, p.17–32.

Chorowicz, J., Collet, B., Bonavia, F.F., and Korme, T., 1994, Northwest to north-northwest extension direction in the Ethiopian Rift deduced from the orientation of extension structures and fault slip analysis: Geological Society of America Bulletin, v. 105, p. 1560-1570.

Corazzato, C., and Tibaldi, A., 2006, Fracture control on type, morphology and distribution of parasitic volcanic cones: An example from Mt. Etna, Italy. Journal of Volcanology and Geothermal Research, v. 158, p. 177-194, doi: 10.1016/j.volgeores.2006.04.018.

Davis, J.M., Elston, W.E., and Hawkesworth, C.J., 1993, Basic and intermediate volcanism of the Mogollon-Datil volcanic field: Implications for mid-Tertiary tectonic transitions in southwestern New Mexico, USA, in Prichard, H.M., Alabaster, T., Harris, N.B.W., and Neary C. R., eds., Magmatic processes and plate tectonics: Geological Society [London] Special Publication, v. 76, p. 469-488.

Davis, J.M., and C.J., Hawkesworth, 1994, Early calc-alkaline magmatism in the Mogollon-Datil Volcanic Field, New Mexico, USA: Journal of the Geological Society, v. 151 p. 825-843.

Davis, J.M., and C.J., Hawkesworth, 1995, Geochemical and tectonic transitions in the evolution of the Mogollon-Datil Volcanic Field, New-Mexico, USA: Chemical Geology, v. 119, p. 31-53.

Gülen L., 1984, Sr, Nd, Pd isotope and trace elements geochemistry of calc-alkaline and alkaline volcanics, eastern Turkey: PhD thesis, Massachussets Institute of Technology, Cambridge, MA, 229 p.

McMillan, N.J., Dickin, A.P., and Haag, D., 2000, Evolution of magma source regions in the Rio Grande rift, southern New Mexico: Geological Society of America Bulletin, v. 112, p. 1582-1593.

Norini, G., Groppelli, G., Sulppizio, R., Nunez, G.C., and De Franco, R., 2015, Structural analysis and thermal remote sensing of the Los Humeros Volcanic Complex: Implications for volcano structure and geothermal exploration: Journal of Volcanology and Geothermal Research, v. 301 p. 221-237.

Tobisch, O. T. and Cruden, A.R., 1995, Fracture-controlled magma conduits in an obliquely convergent continental magmatic arc: Geological Society of America Bulletin, v. 23, p. 941-944.